Probing Planetary Formation and Evolution: Transiting Planets and Occulting Disks

By

Joseph E. Rodriguez Jr.

Dissertation

Submitted to the Faculty of the

Graduate School of Vanderbilt University

in partial fulfillment of the requirements

for the degree of

DOCTOR OF PHILOSOPHY

in

Physics

May, 2016

Nashville, Tennessee

Approved:

Keivan G. Stassun, Ph.D.

Joshua Pepper, Ph.D.

David A. Weintraub, Ph.D.

Andreas A. Berlind, Ph.D.

David J. Ernst, Ph.D.

DEDICATION

This dissertation is dedicated to the many people who have advised me, supported me, and encouraged me to pursue my passion for research in the field of astrophysics. Specifically, I want to thank my Mom (Jeannie), Dad (Joe) and Sister (Jenny) for always supporting me and pushing me towards success. I also want to thank Swata Patel for always standing by my side and helping me make one of the best decisions of my life, transferring to Vanderbilt University.

My appreciation to Keivan G. Stassun and Joshua Pepper for giving me the opportunity to pursue my Ph.D. at Vanderbilt under their advisement. I will always be grateful for the time, effort, and support that has been critical to my success. In addition, I would like to thank rest of the members of my dissertation committee, David A. Weintraub, Andreas A. Berlind, and David J. Ernst for their time, advice, and expertise.

ACKNOWLEDGMENTS

KELT-South is hosted by the South African Astronomical Observatory and we are grateful for their ongoing support and assistance.

We acknowledge with thanks the variable star observations from the AAVSO International Database contributed by observers worldwide and used in this research. This research was made possible through the use of the AAVSO Photometric All-Sky Survey (APASS), funded by the Robert Martin Ayers Sciences Fund. This paper uses observations obtained with facilities of the Las Cumbres Observatory Global Telescope.

This publication makes use of data products from the Wide-field Infrared Survey Explorer, which is a joint project of the University of California, Los Angeles, and the Jet Propulsion Laboratory/California Institute of Technology, funded by the National Aeronautics and Space Administration. This publication makes use of data products from the Two Micron All Sky Survey, which is a joint project of the University of Massachusetts and the Infrared Processing and Analysis Center/California Institute of Technology, funded by the National Aeronautics and Space Administration and the National Science Foundation.

This work has made use of NASA's Astrophysics Data System and the SIMBAD database operated at CDS, Strasbourg, France.

This paper makes use of data from the first public release of the SuperWASP data [Butters et al., 2010] as provided by the SuperWASP consortium and services at the NASA Exoplanet Archive, which is operated by the California Institute of Technology, under contract with the National Aeronautics and Space Administration under the Exoplanet Exploration Program.

Support for CARMA construction was derived from the Gordon and Betty Moore Foundation, the Kenneth T. and Eileen L. Norris Foundation, the James S. McDonnell Foundation, the Associates of the California Institute of Technology, the University of Chicago, the states of California, Illinois, and Maryland, and the National Science Foundation. Ongoing

CARMA development and operations are supported by the National Science Foundation under a cooperative agreement, and by the CARMA partner universities.

We have used observational data from the ASAS photometric survey and we are thankful for the observations and data reduction performed.

The CSS survey is funded by the National Aeronautics and Space Administration under Grant No. NNG05GF22G issued through the Science Mission Directorate Near-Earth Objects Observations Program. The CRTS survey is supported by the U.S. National Science Foundation under grants AST-0909182 and AST-1313422.

The DASCH project at Harvard is grateful for partial support from NSF grants AST-0407380, AST-0909073, and AST-1313370.

Development of ASAS-SN has been supported by NSF grant AST-0908816 and CCAPP at the Ohio State University. ASAS-SN is supported by NSF grant AST-1515927, the Center for Cosmology and AstroParticle Physics (CCAPP) at OSU, the Mt. Cuba Astronomical Foundation, George Skestos, and the Robert Martin Ayers Sciences Fund.

TABLE OF CONTENTS

LIST OF TABLES

LIST OF FIGURES

Chapter 1

Introduction

1.1 Disk Eclipse Search with KELT (DESK) Survey

It is known that planets form from the gas and dust in the protoplanetary disks surrounding young stellar objects (YSOs). What is not clear is what governs the large diversity of planet types and of planetary system architectures that are now being discovered by the thousands. The circumstellar environment involves a variety of processes that lead to the evolution of the protoplanetary disk over time—processes including accretion onto the star, dispersion by stellar winds and radiation, magnetic fields, outflows, and in many cases stellar companions—and that can manifest as disk substructures, gradients, and other properties that could reveal the mechanisms that influence planet formation and diversity therein.

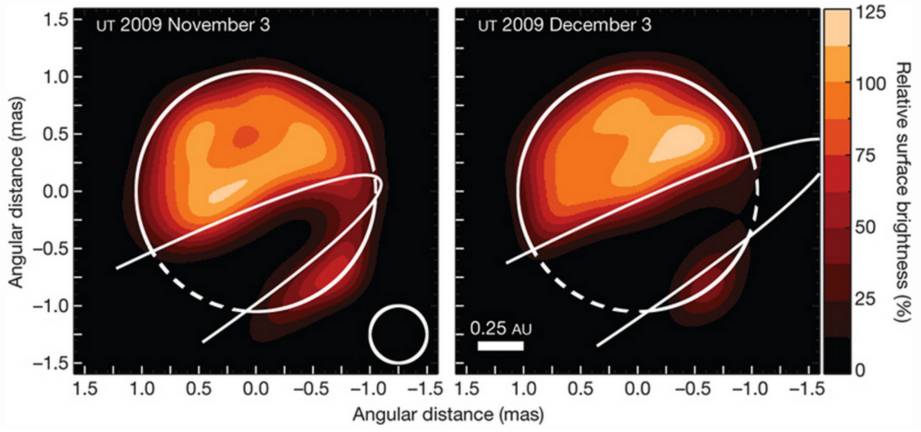

Figure 1.1: CHARA observations of ϵ Aurigae during the beginning of the most recent eclipse showing the disk of the companion crossing the face of the star. The white circle outlines the primary stars extent and the white lines are the model of the disk superimposed on the image. From Kloppenborg et al. [2010].

One method to constrain the planet-building properties of these disks is to observe them as they fortuitously eclipse their stars (Figure 1.1). Such events are very rare—only a few have been discovered. Fortunately, the advent of wide-field time domain surveys provides a ideal tool to search for rare eclipse events. The Kilodegree Extremely Little Telescope (KELT) survey in particular provides a unique combination of sky coverage, cadence, and baseline that is well-suited to search for these rare disk-eclipsing systems. Using the KELT survey I have been leading the Disk Eclipse Search with KELT (DESK) survey [Rodriguez et al., 2015a]. Using the data from KELT, we have been performing a search to find deep, long duration dimming events representing occultations of stars by circumstellar material. This survey was inspired by the discovery of J1407, the first circumplanetary disk system [Mamajek et al., 2012]. After searching through only ~50% of the available KELT data, the DESK survey has already discovered and analyzed four large dimming events around the young stars RW Aurigae, V409 Tau, AA Tau, and a ~69 year period eclipsing binary [Rodriguez et al., 2013, 2015b,c, 2016].

1.2 Transiting Exoplanets

With the success of the Kepler mission, the exoplanet field has shifted focus from pure discovery to a combination of discovery, demographic analysis, and detailed characterization, especially for exoplanet atmospheres. Unfortunately, a large portion of the discovered extra-solar planets are too faint to permit atmospheric characterization. The goal of the KELT survey is to discover transiting extrasolar planets around bright stars (V=8-11). The KELT survey is comprised of two telescopes, KELT-North and KELT-South, and together they are surveying over 70% of the sky with a ~20 minute cadence and up to a 10 year baseline [Pepper et al., 2007, 2012]. Such bright targets are optimal for subsequent characterization of a planet's atmosphere through a variety of techniques, including secondary eclipse observations and transmission spectroscopy. To date, the KELT Survey has discovered 16 transiting planets around bright stars with 10 in press [Siverd et al., 2012, Beatty

et al., 2012, Pepper et al., 2013, Collins et al., 2014, Bieryla et al., 2015, Fulton et al., 2015, Kuhn et al., 2015, Eastman et al., 2015, Rodriguez et al., 2015b]

An important aspect of the KELT survey is the ability to search for planets around hot host stars (T_{eff} > 6000K) that were previously avoided by other transit and radial velocity exoplanet surveys. These stars represent a very large part of parameter space for planets and their hosts that remains largely unexplored, and this includes importantly the not yet retired A stars. Of the 16 confirmed exoplanets by the KELT survey, 9 of them have a T_{eff} > 6000K. Hotter stars are rotating significantly faster (Vsini $\sim$ 100 km/s) causing the lines typically used for RV measurements to become weaker and broader making precise RV measurements difficult. With improved RV measurement techniques, photometric confirmation of the ephemeris, and measurements of the Rossiter-McLaughlin effect, confirmation of exoplanets around hot rapidly rotating stars is more feasible especially for larger, more massive planets. It has been proposed that hotter, more massive stars host a different population of planets than cooler, low mass stars [Winn et al., 2010]. The discoveries from the KELT survey provide a direct sample to test this hypothesis.

Chapter 2

Occultation of the T Tauri Star RW Aurigae A by its Tidally Disrupted Disk

2.1 Introduction

Classical T Tauri stars (CTTS) are a type of active pre-main sequence stars that show a large excess of infrared (IR) radiation and were first identified by the broad Hα emission line widths in their spectra. The large IR flux in the spectra of CTTS is normally attributed to thermal emission from their dusty circumstellar disks. A large excess of ultraviolet (UV) radiation is often observed and is believed to be a result of material in the disk being accreted onto the surface of the star, producing hot spots [Bertout et al., 1988]. Irregular photometric variability that is characteristic of CTTS has a typical amplitude of less than one magnitude and a time-scale of days to weeks [Herbst et al., 1994]. T Tauri stars are known to have significant magnetic activity which can produce cool star spots and enhanced chromospheric emission. Weak-line T Tauri stars (WTTS), which are typically found in the same star-forming clouds as CTTS, were first distinguished from CTTS by having very narrow Hα emission widths [Walter, 1986, Herbig and Bell, 1988]. They were then found to be bright x-ray emitters and show little to no UV or near-IR excess emission. These observational results are generally interpreted as indicating that WTTS are no longer accreting and are either diskless or have disks with very little mass in the form of small, hot dust grains [Haisch et al., 2001]. It is generally believed that CTTS evolve into WTTS when the disk is no longer a significant component of the system, as a result of accretion onto the star, planet formation, and dispersal.

From surveys, it appears that most nearby T Tauri stars are members of close binary systems [Ghez et al., 1993, Leinert et al., 1993, Richichi et al., 1994, Simon et al., 1995, Ghez et al., 1997b] . These companions can influence the stellar environment and affect the stellar properties determined for the primary star if not taken into account [Ghez et al.,

1997a]. Depending on the parameters of the companion star's orbit, the companion can significantly disrupt the primary star's circumstellar disk. Simulations show that a fly-by of a stellar companion can tidally disrupt the circumstellar disk around a star, leaving behind a truncated, more compact disk and a long tidal arm feature trailing out from the disrupted material [Clarke and Pringle, 1993].

Occultations of stars by their disks, though rare, provide a powerful tool for probing the structure of circumstellar disks. To date, only a few long-duration, deep eclipses of young stars have been discussed in the literature. Most such eclipses appear to be periodic, with the occultation attributed to a disk around a stellar companion or occultation of a star by its own disk. One well known example of this is ϵ Aur, an F0 giant that experiences long and deep eclipses every 27.1 years. The eclipse has a duration of almost two years and a depth of 0.8 - 1.0 magnitude [Carroll et al., 1991]. The eclipse is attributed to a companion star with its own circumstellar disk [Kloppenborg et al., 2010]. KH 15D is another system, discovered in 1995, which experiences complex eclipsing events with changing properties [Kearns and Herbst, 1998]. That system consists of a non-eclipsing binary star pair that is repeatedly occulted on the binary orbital period by the sharp edge of the circumbinary disk. Long-term secular changes in the occultations are caused by the slow precession of the circumbinary disk across our line of sight [Chiang and Murray-Clay, 2004, Winn et al., 2004]. There are a few other examples of periodically occulting systems (see, e.g. Bouvier et al. [2007], Plavchan et al. [2008], Grinin et al. [2008]).

Some young stars experience occultations that are not periodic (or at least not known to be). In 2007, a pre-main sequence star (2MASS J14074792-3945427) exhibited a long and extremely deep occultation [Mamajek et al., 2012]. This eclipse was observed by the SuperWASP photometric transit survey [Butters et al., 2010] and the ASAS photometric survey [Pojmanski, 2002]. The eclipse lasted ~54 days and had a ~4 mag maximum depth. The cause of the eclipse is thought to be a circumplanetary disk, in the process of formation, analogous to the rings around Saturn. Photometric variability was seen during the eclipse

and attributed to gaps in the large ring system around the hypothesized planet [Mamajek et al., 2012].

Such systems provide insight into the nature of proto-planetary and circumstellar environments and can be used as tools to probe the structure and composition of circumstellar disks. In this paper we present new observations of the bright system, RW Aur, indicating a long and deep occultation (Figure 2.1) somewhat similar to the one seen by Mamajek et al. [2012]. To our knowledge this paper is the first analysis of the event, which was first reported by Aleks Scholtz[1]. We interpret the event as an occultation of RW Aur A by a portion of its tidally disrupted disk.

The paper is organized as follows. We introduce the known characteristics of the RW Aurigae system in §2, illustrating the complex stellar environment. In §3, we describe the photometric observations, and then discuss the photometric properties of the data in §4. In §5, we present several interpretations of the light curve and discuss their plausibility. We summarize our results and conclusions in §6.

2.2 Characteristics of the RW Aur System

The RW Aur system (α = 05h 07m 49.566s, δ = +30° 24′ 05.18″) is at a distance of 142 ± 14 pc [Wichmann et al., 1998], and has a complex stellar environment. It is a binary system, comprising one CTTS (RW Aur B) orbiting another CTTS (RW Aur A) [Duchêne et al., 1999]. The primary component (RW Aur A) has a spectral type between K1 and K4 [Petrov et al., 2001], V ∼10.5 [White and Ghez, 2001] and an inferred mass of ∼1.3-1.4 $M_{\odot}$, determined by comparing broadband near IR observations to pre-main sequence models [Ghez et al., 1997a, Woitas et al., 2001]. The A component shows clear IR excess indicative of a circumstellar disk, with a mass of M_d ∼3×10^{-4} $M_{\odot}$[Williams and Andrews, 2006]. This disk radius is calculated to be ≤ 57 AU, making it one of the smallest detected around a T Tauri star [Cabrit et al., 2006]. RW Aur A exhibits some

[1] A huge eclipse in the young star RW Aur. http://dx.doi.org/10.6084/m9.figshare.92169

extreme features, including an accretion rate of 2-10 $\times$ 10^{-7} $M_{\odot}\mathrm{yr}^{-1}$, one of the highest known for a T Tauri star, [Hartigan et al., 1995] and also bright bipolar jets [Woitas et al., 2002]. López-Martín et al. [2003] determined that the bipolar jets coming from RW Aur A are inclined to our line of sight by 46° ± 3°, using the ratio of the proper motion and the radial velocities. These jets extend out at least 145″ from RW Aur A and contain knots of emission out to ∼100″ [Mundt and Eislöffel, 1998, Woitas et al., 2002]. Transverse velocity shifts have been detected for this jet, which indicate that it may be rotating and that the jet is originating from the disk surface within 1.6 AU from the star [Cabrit et al., 2006, Woitas et al., 2005]

RW Aur B is 1.5"(∼200 AU) [Duchêne et al., 1999, Cabrit et al., 2006] from RW Aur A and has an inferred mass of 0.7-0.9 $M_{\odot}$[Ghez et al., 1997a, Woitas et al., 2001]. It is a late K star (K6 ± 1 [White and Hillenbrand, 2004]) with V ∼13.7 [White and Ghez, 2001]. Ghez et al. [1993] found faint K-band emission 0.12" from RW Aur B and interpreted this to be a third stellar component to the system, RW Aur C. Other authors have also claimed the presence of a third component in the system, but clear evidence is lacking. Furthermore, later observations failed to confirm the third component [Ghez et al., 1997a].

The RW Aur system has been found to vary in many observational characteristics. Beck and Simon [2001] found that the RW Aur system showed peak-to-peak variations of 2-3 mag on timescales of months using Harvard photographic observations from 1899 to 1952 (See Figure 3 of Beck and Simon [2001]). The standard deviation of these variations is ∼0.7 mag. Petrov et al. [2001] observed periodic variability in the radial velocity of RW Aur A of 2.77 days as well as periodicity in the $U-V$ and $B-V$ colors of 2.64 days. The combined RW Aur system shows an overall non-periodic, photometric variability that Herbst et al. [1994] determined arises from the A component. The erratic variability has been attributed by different authors to the accretion of the disk onto the star or circumstellar extinction from strong disk winds [Herbst et al., 1994, Petrov and Kozack, 2007]. These are discussed in more detail in §4.1.

Cabrit et al. [2006] conducted millimeter observations of the RW Aur system using the IRAM Plateau de Bure Interferometer (1.3 mm, 2.66 mm). They find in the 1.3 mm observations that RW Aur A has an outer truncated circumstellar disk extending out 41 - 57 AU in radius, inclined by 45° - 60° to our line-of-sight, and what appears to be a large, tidally disrupted trailing "arm" that is wrapped around the star (see Figure 1.a from Cabrit et al. [2006]). This arm-like feature has a three-dimensional-length of ~600 AU, and is almost certainly the result of a recent stellar fly-by of RW Aur B [Cabrit et al., 2006]. This fly-by also caused the RW Aur A disk to be truncated near the periastron separation. While a large portion of the arm is redshifted, indicating it is wrapped around and behind the A component, there is a small portion that is connected to the northeast side of the RW Aur A disk which is blue-shifted by up to 3.1 km s^{-1} relative to the star. This feature resembles the destructive outcome of a coplanar eccentric fly-by similar to simulations from Clarke and Pringle [1993], where all material outside the periastron distance is fully disrupted and drawn out into a coherent tail in the direction of the companion's orbit. The RW Aur system therefore provides an excellent example of a T Tauri disk that has experienced a recent dynamical disruption.

2.3 **Photometric Observations**

Several photometric surveys have observed RW Aur over both short and long time scales going back to 1899. The light curve data are shown in Figures 2.1 and 2.3.

2.3.1 Archival Data

The Wide Angle Search for Planets (SuperWASP) is a wide field photometric survey designed to detect transiting extrasolar planets over a large fraction of the sky. SuperWASP observed RW Aur for one shortened season in 2004 and then two later seasons in 2006 and 2007. The SuperWASP public archive data is described in detail in Butters et al. [2010]. The SuperWASP observations have a cadence of a few minutes in the *V* band

and do not resolve the RW Aur system, thus the light curve incorporates light from all system components. The median error for SuperWASP is ~0.01 Mag.

The American Association of Variable Star Observers (AAVSO) is a non-profit organization dedicated to the goal of understanding variable stars. The AAVSO archive contains observations of RW Aur going back to 1937, with the observations increasing in cadence around 1954. The AAVSO data consist of V band and visual observations. Only some of the AAVSO data have corresponding uncertainties reported.

Wesleyan University's Van Vleck Observatory has monitored many known T Tauri stars with the 0.6 meter Perkin Telescope. The resulting observations are included in a public archive of $UBVRI$ photometry. RW Aur A was observed from January 1965 until October of 1994, with varying frequency. A detailed description of the archive is described in detail in Herbst et al. [1994].

The AC and AM photographic plate series at the Harvard College Observatory have observations of RW Aur from 1899 to 1952, resulting in 162 observations. The photographic observations were obtained using the 1.5 inch Cooke lens, corresponding to a plate scale of 600"/mm. The B band magnitudes were estimated by analyzing over 150 archival plates and comparing them to the known B magnitudes of nearby stars (Not shown in Figure 1, see Figure 3 of Beck and Simon [2001]).

2.3.2 KELT-North

The Kilodegree Extremely Little Telescope (KELT-North) is an ongoing survey, searching for transiting planets around bright stars (V = 8-10). KELT-North uses a Mamiya 645 80mm f/1.9 lens, and has a 42 mm aperture and a large field of view (26° × 26°) with a plate scale of 23"per pixel [Pepper et al., 2007].

RW Aur is located in KELT-North Field 04, which is centered on (α = 5hr 54m 14.466s, δ = +31° 44′ 37″). KELT-North observed this field from October 10, 2006 to September 23, 2012, obtaining 8,001 images. The data were reduced using a heavily modified version

of the ISIS software package, described further in §2 of Siverd et al. [2012][2]. The observations are in a broad *R*-band filter, with a ~15 minute cadence and the typical error is less than 0.04 Mag. The KELT-North observations also fail to resolve the RW Aur system. The KELT-North data is presented in Table 1.

Table 2.1: KELT-North photometric observations of RW Auriga

BJD_{TDB}	KELT *V* Mag[a]	Poisson Errors[b]
2454035.812879	10.326	0.008
2454035.817502	10.327	0.008
2454035.822123	10.324	0.008
2454035.826745	10.319	0.008
2454035.831367	10.311	0.008
2454035.835989	10.294	0.007
2454035.840612	10.286	0.007
2454035.845235	10.281	0.007
2454035.849855	10.286	0.007
2454035.854477	10.283	0.007

Notes. Table 1 is published in its entirety in the electronic edition of this paper. A portion is shown here for guidance regarding its form and content.
[a]Relative KELT Instrumental magnitude corrected to Johnson V-magnitude. Absolute accuracy to ~0.2 mag. Relative accuracy to ~0.04.
[b]Poisson errors to instrumental KELT magnitudes. True per-point magnitude errors must fold in 0.036 mag systematic errors.

2.4 Results: Variability Before and During the Dimming Event

Here we discuss the variability characteristics of the deep dimming event. We also describe the general photometric variability of RW Aur A. In Section 5 we discuss the dimming in the context of an interpretation in which the star has been occulted by a portion of its tidally disrupted disk.We focus our analysis on four data sets: KELT-North, AAVSO, SuperWASP, and Wesleyan (Van Vleck).

[2]Much of the software is publicly available at the following address: http://verdis.phy.vanderbilt.edu

2.4.1 Pre-Dimming Variability

CTTS can have erratic photometric variations on the time scale of a few days [Herbst et al., 1994]. The light curve for RW Aur shows this photometric variability and it is observed in all four data sets (Figure 2.1). The variability seen in the four data sets for RW Aur has a peak-to-peak amplitude of 1-2 mag, on the timescale of days to weeks, with a standard deviation of ~0.4 mag.

Two possible explanations for the non-coherent photometric variability are circumstellar extinction and varying accretion onto the surface of the star. Herbst et al. [1994] argued convincingly that the non-coherent variability is caused by irregular accretion onto the surface of RW Aur A, creating hot spots that rotate into and out of view. Herbst et al. [1994] performed an analysis of the $UBVRI$ photometric observations finding that the photometric variations are roughly divided evenly (with relatively large amplitude) between positive and negative excursions relative to a well defined median level. This is a defining characteristic of accretion-driven variability, as opposed to circumstellar obscuration-driven variability which tends to produce mainly dimming of the star, or flare driven-variability which tends to produce mainly brightening events. Importantly, the Hα flux appears to be correlated with the brightness of the star at all wavelengths [Herbst et al., 1982]. This is very strong evidence in favor of an interpretation in which the photometric variability of RW Aur A is principally connected to variations in its accretion rate. Petrov and Kozack [2007] and Grinin et al. [2004] suggest that the photometric variability is the result of a strong disk wind lifting material from the disk across the star causing circumstellar extinction. Such disk winds are a known feature of CTTS but at odds with the accretion variability interpretation of Herbst et al. [1994].

Some accreting stars can show periodic modulations in their light curves due to hot accretion spots on the stellar surface rotating in and out of view on the stellar period. To look for such periodicity we use a Lomb-Scargle periodogram as presented in Lomb [1976], Scargle [1982], Press and Rybicki [1989]. This Lomb-Scargle method performs

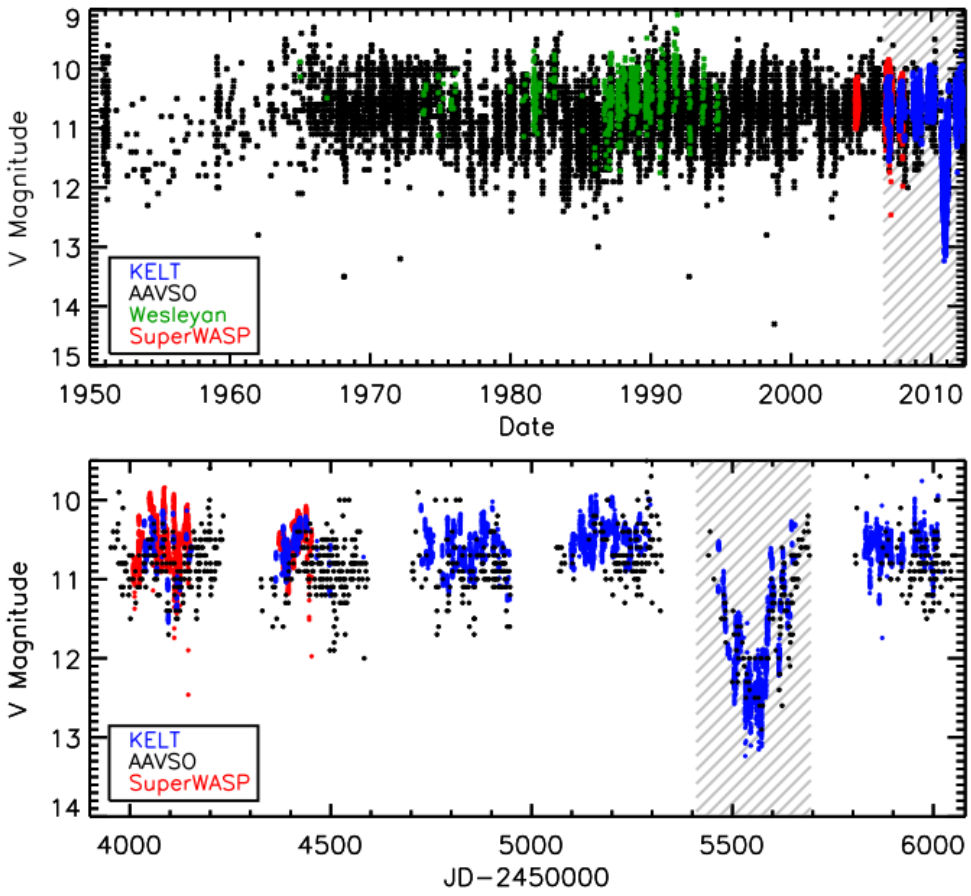

Figure 2.1: (Top) AAVSO (Black), KELT-North (Blue), SuperWASP (Red) and the Wesleyan Van Vleck (Green) light curves of RW Aur from 1950 to 2012. The KELT and SuperWASP light curves do not resolve the A and B components. The shaded region in the upper plot corresponds to the six KELT seasons which is shown in the bottom plot. (Bottom) The KELT-North, SuperWASP and AAVSO light curves plotted for the six KELT-North observing seasons. The dimming of the star is seen from late 2010 through early 2011 in the KELT-North and AAVSO light curves and is centered on early January of 2011. The median KELT and SuperWASP errors are ~0.01 Mag. For better visualization of the true nature of the data, the errors are not plotted. The shaded region in grey is the location of the main dimming event is seen in late 2010 through early 2011. A zoom in of this region is shown in Figure 2.3.

spectral analysis on unevenly sampled time series data and allows us to effectively identify weak periodic signals. We performed this analysis on the KELT, AAVSO, SuperWASP and Wesleyen photometric data.

We do not see any significant periodicity in the full KELT-North RW Aur light curve,

nor in the KELT-North light curve with the dimming in late 2010 removed aside from the 1 day diurnal sampling effect. The AAVSO and SuperWASP light curves also do not show any periodic signal. We do, however, confirm a ~2.7 day periodic variability seen by Petrov and Kozack [2007] in the Weslyan University $(B-V)$ and $(U-B)$ curves. The KELT and SuperWASP light curves each exhibits a small peak between 2.69 and 2.72 days. Though not individually statistically significant, their presence does lend additional credence to this signal. A periodicity at twice this value (~5.5 days) has been reported as the rotation period of the star [Petrov et al., 2001, Gahm et al., 1999]. We are unable to identify this periodicity in the individual U, B, or V Weslyan University light curves (Figure 2.2), which could be the result of the rotational modulation signal being masked by the stochastic accretion variability.

While the periodicity analysis does not shed much new light on the physical origin of the variability, the overall available evidence appears to favor an interpretation in which the photometric variability is tied to variations in the accretion rate. Spectroscopic monitoring observations obtained during the deep dimming event corroborate this interpretation also, as discussed in the next section.

2.4.2 2010-2011 Dimming

In late September 2010 the light curve of the RW Aur system became fainter, dropping from a median brightness of V = 10.4 to V = 12.5 mag (Figure 2.1). This decrease lasted for ~180 days, ending in late March 2011. A good deal of structure and variability, on similar time scales as the ingress and egress, 10-30 days, is apparent during the dimming (Figure 2.3). The peak-to-peak depth of the fading is ~4 mag and has a sustained duration of many months. Therefore, the dimming event has a much deeper and longer duration than the out of event stochastic variations that present a peak-to-peak amplitude of 1-2 mag and a standard deviation of ~0.4 mag on shorter timescales.

During the dimming, the system's brightness decreases to V ~12.5 (Figure 2.3). For

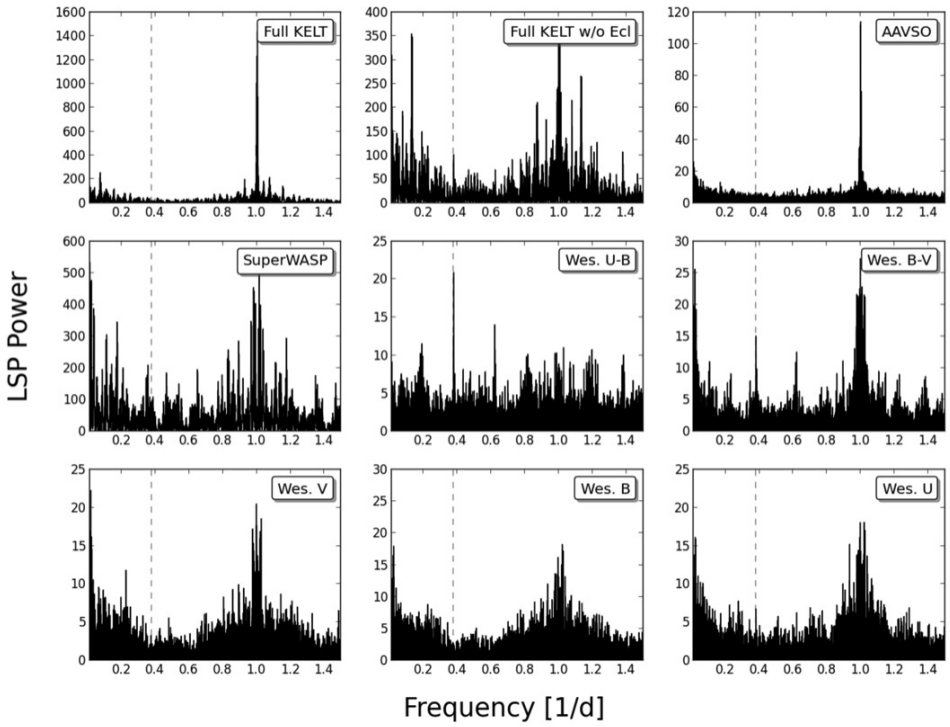

Figure 2.2: The resulting periodograms from the Lomb-Scargle analysis of the AAVSO, KELT-North, SuperWasp and Van Vleck photometric data. The vertical dashed line represents a 2.7 day periodicity that has been previously reported as half the rotation period of the star. We recover this period in the Wesleyan $U-B$ light curve data. The features seen at 1.0 c/d are the (high-frequency) aliases of long-term variation caused by diurnal sampling.

reference, the B component by itself was previously measured to be $V \sim 13.7$ [Ghez et al., 1997a]. Assuming the dimming is only due to a decrease in the brightness of the A component, we calculate that the V magnitude of the A component, during the dimming event, is ~ 12.9. That corresponds to a decrease in flux of the A component of 91%, making it ~ 1.5 times brighter than the B component during the 2010-2011 event. The large amplitude non-periodic short-timescale variability that is so ubiquitous outside the 2010-2011 dimming, appears to significantly diminish but is still present. This is expected if the short-term variability, originating from the A component, is subjected to significant dilution from the combined system with the B component during the dimming. This supports the interpretation that the A component is the source of the non-periodic variability. At the same

time, we do observe structure during the dimming, in particular a 1-1.5 mag brightening and then re-dimming toward the end which occurs with a characteristic timescale of ∼10 days, very similar to the main ingress timescale. Below we discuss the possibility that this structure during the dimming may imply substructure in the occulting body.

RW Aur A was serendipitously monitored spectroscopically during October through December of 2010 by Chou et al. [2013]. Although the authors were unaware of the 2010-2011 dimming, their spectroscopic observations by chance coincide precisely with the first half of the deep dimming event, including most of the ingress and the point of maximum depth. Their analysis of 14 different emission lines tracing accretion, infall and outflow, are broadly consistent with both the nature of the line profiles and with the short timescale variability observed by others many years before (see references in Chou et al. [2013]). In addition, their observed correlations between the various emission lines are consistent with a largely steady magnetospheric accretion model over the course of the observations. They do infer variations in the magnetospheric accretion of order 20 percent, comparable to previous accretion variability measurements for RW Aur A and with the accretion variability interpretation for the general photometric variability of the system [Herbst et al., 1994]. More fundamentally, these serendipitous spectroscopic observations suggest that the accretion behavior of RW Aur A was not connected with the source of the pronounced photometric dimming event.

It is clear that a dimming this large is not present prior to 2010 in the combined light curves from KELT-North, AAVSO, Van Vleck and SuperWASP. Although there is substantial variation seen in the full light curve across 60+ years (Figure 2.1), we observe no comparable events in duration or depth. We verify that by examining time spans in the full data set that might appear to represent similar eclipses, but a detailed look shows that those events clearly do not resemble the deep long and coherent event in 2010 to 2011. Since we can place a lower limit on the duration of the fading to be ∼180 days from the KELT and AAVSO light curves, we searched for a gap in the combined light curve, large enough,

that a similar previous event may have occurred but have been missed. We examine the RW Aur light curve, using all four data sets, and find no gap in the observations greater than 180 days since 1961. Prior to 1961, the only photometric observations of this target are the Harvard photographic observations and a much sparser set of AAVSO observations. Those data span the years 1899 to 1961, with frequent gaps of 200+ days. We can therefore conclude, that if the 2010 to 2011 event repeats it would have a minimum period of ~50 years.

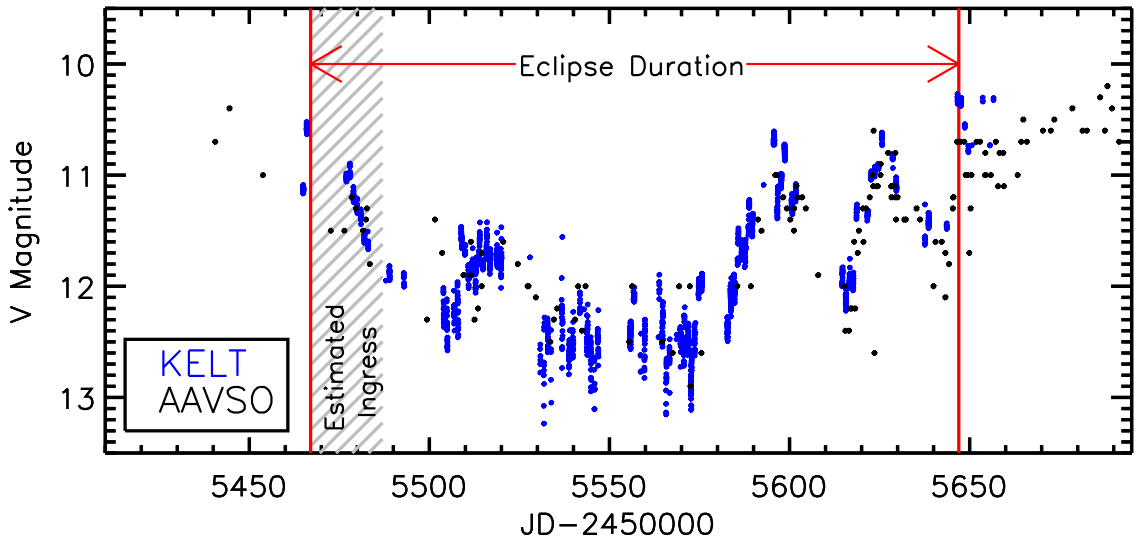

Figure 2.3: KELT-North (blue) and AAVSO (black) light curves zoomed in on the eclipse. In grey dashed highlights is the estimated ingress of 20 days and the two red vertical lines mark the estimated eclipse duration. The KELT observation have an error of 0.04 Mag while the most AAVSO data do not have reported errors. The faintest points observed during the dimming are near the observational limit of KELT.

2.5 Interpretation and Discussion

2.5.1 Favored Interpretation: Occultation by the RW Aur A Tidally Disrupted Disk

In this section we present what we regard as the most plausible interpretation of the 2010-2011 dimming event, namely an occultation of RW Aur A by a fragment of the tidal arm that resulted from its disrupted circumstellar disk. This known feature of the circum-

stellar environment provides the necessary ingredients of a large opaque body, with a sharp edge moving perpendicular to the line of sight, to be able to naturally explain many of the features of the observations. We explore alternate interpretations in §5.2, but here we investigate the necessary properties of the occulting body and discuss how well these properties agree with those observed for RW Aur A's tidally stripped arm.

We calculate the key characteristics of the occulter by modeling the dimming as an occultation of RW Aur A by a large body which possesses a sharp edge that is oriented perpendicular to the direction of motion. From the photometric observations, we are able to determine three important features about the occulter: transverse velocity, semi-major axis and width. From the light curves, we estimate the ingress to be between 10-30 days and the total duration to be about 180 days. As a result of the cadence and gaps in observing between the KELT-North data and AAVSO, the values determined for these two parameters are based on a visual inspection of the light curves. We choose to define the end of the dimming event to be after the two large variations at ~5600 and ~5640 (JD- 2450000) (Figure 2.3) since this type of variability is not seen anywhere in the light curve outside the dimming event and thus can be attributed to the mechanism responsible for the event. We also observe that the variations during the dimming (including the substructure near the end of the event), all share the same characteristic timescale of the ingress/egress (10-30 days).

Using the known mass and age of RW Aur A (1.3-1.4 $M_{\odot}$, 4.5-6.2 Myr [Ghez et al., 1997a, Woitas et al., 2001]), we refer to the Dartmouth Stellar Evolution Program's (DSEP) young stellar models to find that the radius should be between 1.5-1.7 $R_{\odot}$[Dotter et al., 2008]. These specific models give a $\log(T_{\rm eff})$ of 3.67-3.70 that is consistent with the effective temperature determined for RW Aur A by Liu and Shang [2012]. For our calculations, we adopt a mass of 1.35 ± 0.135 $M_{\odot}$(error estimate for isochrone fitting) and a stellar radius of 1.6 ± 0.32 $R_{\odot}$(conservative error estimate for the stellar evolution models).

We use the stellar radius and the minimum timescale of the ingress and characteristic

variation seen during the occultation (10 days) to calculate the maximum transverse velocity of the occulter to be $2(1.6\ R_{\odot})/10$ days = 2.58 ± 0.52 km s^{-1}. Furthermore the calculated velocity of the occulter and the total observed duration of the occultation yields a physical width of the occulting body of 2.58 km s^{-1} $\times$ 180 days = 0.27 ± 0.05 AU. Assuming Keplerian motion and a circular orbit, a velocity of 2.58 km s^{-1} implies a semi-major axis of 180.5 ± 28.9 AU:

$$\frac{1.35\,M_{\odot}G(10\,\mathrm{days})^2}{4(1.6\,R_{\odot})^2} \sim 180.5\mathrm{AU}. \tag{2.1}$$

Using instead the estimated maximum ingress timescale (30 days) we calculate a minimum transverse velocity of 0.86 ± 0.17 km s^{-1}, semi-major axis of 1624.7 ± 260.1 AU and a occulter width of 0.089 ± 0.02 AU. At 180 AU, the occulter would be more than three times as far from RW Aur A as the maximum estimated extent of the circumstellar disk (57 AU, see §2). Unless the occulter is moving at an extremely oblique angle, these values should be roughly accurate to within a factor of a few.

Cabrit et al. [2006] conducted millimeter observations of the RW Aur system and found that the system appears to have undergone a complex interaction with its companion, RW Aur B, that resulted in a short truncated circumstellar disk around RW Aur A (inclined by 45° - 60°) and a large (600 AU along the spine) tidally disrupted arm that wraps around behind the A component (see §2). The arm is believed to be mostly wrapped behind the A component, although a small portion appears to be in front. The portion of the arm in front of the A component has a blue shifted velocity relative to RW Aur A of ≤ 3.1 km s^{-1} which is similar to our calculation of the occulter's transverse velocity. The 0.86 km s^{-1} velocity, for the 30 day ingress calculation, is also consistent since Cabrit et al. [2006] measured a range of blue shifted velocities in their millimeter observations.

The observations of the tidal feature are consistent with the simulations of a coplanar stellar interaction conducted by Clarke and Pringle [1993]. There is no indication that the orbit and disk plane are not in the same plane, which is the most probable configuration.

Bisikalo et al. [2012] found that the orbit of the binary is retrograde to the orbit of the circumstellar disk around RW Aur A. The simulations by Clarke and Pringle [1993] for a co-planar, retrograde interaction, not only produce a tidal arm, but also show that the interaction disrupts a significant amount of material out of the disk plane (see Figure 7 from Clarke and Pringle [1993]). Therefore it is plausible that material was disrupted out of the disk plane into our line-of-sight even though the system is significantly inclined.

Although the distance between RW Aur A and the arm is unknown, simulations by Clarke and Pringle [1993] show that in an eccentric stellar interaction, the disrupted arm spirals outward from the primary component and its closest point would be outside the extent of the disk. Thus our calculated semi-major axis of ~180 AU (or larger for 30 day ingress) is consistent with simulations of the hypothesized interaction. Without more information about the system configuration during the flyby, we have no definitive knowledge of the full three-dimensional direction of movement for the blueshifted component of the arm. We therefore expect that it is unlikely that the velocity vector is extremely oblique. Thus, we expect that the transverse velocity we calculate is within a factor of a few of the true velocity. Since our calculated velocity is quite similar to the radial velocity seen in the Cabrit et al. [2006] observations, that congruence supports the conclusion that the disrupted arm (likely a fragment of the full arm) and the occulter are the same body.

The occultation displays a large maximum depth (~2 mag) and a long duration (180-210 days), with some substructure occurring on a timescale similar to the ingress, 10-30 days (Fig 2.3). There are large amplitude variations observed near the end of the dimming (5590 - 5650 JD UTC-2450000). These features appear to repeatedly brighten from the maximum dimming depth to the median out of occultation magnitude suggesting that the occulter has substructure and potentially gaps. The faintest points during the occultation are near the edge of KELT's detectability, compromising our ability to characterize any short period variability during the dimming. Within this interpretation, the brightness variations seen during the occultation are due to the substructure of the tidal arm fragment.

Having made several simple assumptions (sharp leading edge, Keplerian motion, etc.), our calculated properties of the occulter are consistent with the observed properties of the tidal arm from Cabrit et al. [2006]. The distance between RW Aur A and the occulting body derived in this section (~180 AU) is comparable to the separation between the RW Aur A and RW Aur B components (~200 AU). This location implies that the occulting body cannot be a circumbinary object and is probably a fragment of one of the components of the system. Therefore we believe that the best explanation for the occultation mechanism, producing the 2010-2011 occultation, is that a fragment of the tidally disrupted arm crossed in front of RW Aur A.

2.5.2 **Alternate Explanations**

We have presented evidence for an interpretation in which the deep, long duration dimming of RW Aur A is due to occultation by its tidally disrupted circumstellar disk. We now explore alternate explanations for these observations.

2.5.2.1 Occultation by Stellar Companion

We can rule out the possibility that the occulter is comparable in size to RW Aur A because the combined ingress/egress timescale would need to be similar to the entire duration of the dimming. If the cause of this event was the result of an eclipse of the A component by a large unseen stellar companion, this would require the companion to have extreme stellar parameters. We can model the system as a large stellar disc passing in front of a smaller one (RW Aur A). This allows us to use the same calculations as in §5 for the velocity, semi-major axis and diameter (projected width) of the occulting star. The same calculations apply because the eclipsing star's leading edge would be perpendicular to is tangential motion. The occulting star would thus need to be moving ~2.5 km s^{-1} and have a diameter of ~0.27 AU, corresponding to a radius ~58 $R_{\odot}$, a giant star. The star would also need to be dark and cause the large variations at the end of the dimming (Figure 2.3).

From these observed and calculated characteristics, we are confident the occulter is not an unseen stellar companion.

2.5.2.2 Alternate Stellar Parameters of RW Aur A

We address the assumptions in our calculations of the occulter distance from from RW Aur A. In §5 we determined that the occulting body must be more than three times as far from the star as the outer edge of the known circumstellar disk. Since that calculation is based on our determination of the linear velocity of the occulter, which in turn depends on the radius of the star, we ask whether our stellar radius estimate (1.6 $R_{\odot}$) could be incorrect. Given the observed maximum extent of the disk of 57 AU [Cabrit et al., 2006] and assuming Keplerian motion, we calculate that RW Aur A would need a radius of at least ~2.75 $R_{\odot}$for the occulter to be located at the edge of the disk.

However, a star with a radius 2.75 $R_{\odot}$would be much more intrinsically luminous. A star with a radius of 2.75 $R_{\odot}$, $\log(T_{\rm eff})$ of 3.684, and an apparent magnitude of V = 10.4, would be at a distance of ~218 parsecs, which is much larger than the measured distance to RW Aur of ~140 pc [Wichmann et al., 1998]. Furthermore, according to the Dotter et al. [2008] stellar models, a radius of 2.75 $R_{\odot}$implies a stellar age of ~9.5×10^5 years. RW Aur is part of the Taurus-Auriga association, where star formation is thought to have first occurred on the outer edge and progressed inward. The youngest estimated age for the Taurus-Auriga stellar association is ~1 Myr for the center of the association; however, RW Aur is located on the outer edge of the region, where star formation is believed to have occurred much earlier and corresponds to an age closer to 10 Myr [Palla and Stahler, 2002]. Since a radius of 2.75 $R_{\odot}$is not consistent with either the apparent magnitude or age of RW Aur A, it is not likely that the estimated radius is incorrect.

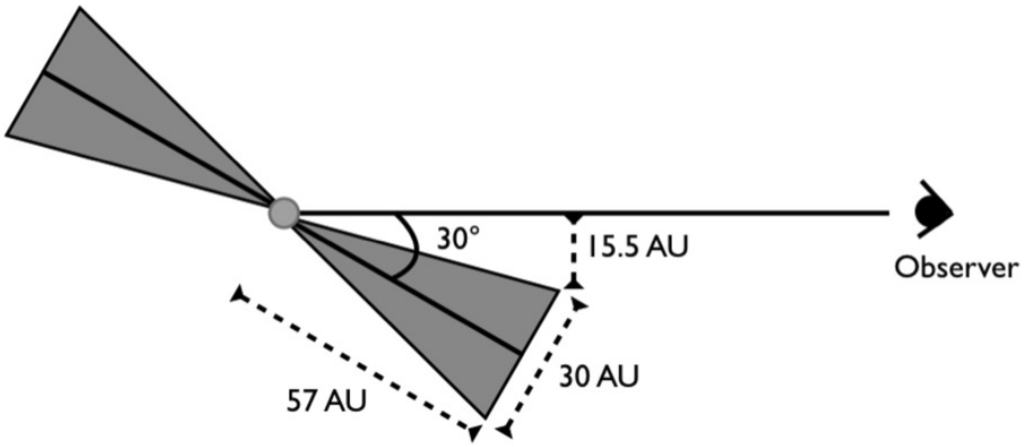

Figure 2.4: Schematic of the RW Aur A disk geometry, showing to scale, the height required for a feature at the edge of the disk to cause the observed occultation.

2.5.2.3 Occultation from Outer Edge of RW Aur A's Circumstellar Disk

We explore the possibility that a large feature at the edge of the circumstellar disk around RW Aur A has occulted the star. Even though the disk is inclined to our line of sight, pre-transitional disks are not uniformly flat, and tend to flare as a function of semi-major axis. An example of this is clearly seen in Espaillat et al. [2010] which shows that the height of the disk is 13.8 AU at a semi major axis of 71 AU but only 0.009 AU at 0.1 AU from the star.

To determine the plausibility of a a feature at the edge of the RW Aur A circumstellar disk causing the occultation seen in late 2010, we model the feature to be in a Keplerian orbit, at the farthest estimated extent of the disk (57 AU) and calculate the additional height required to cross the face of the star. For our model, we consider a conservative disk inclination from Cabrit et al. [2006] for RW Aur A of 60° and a flared disk height of 15 AU above the mid-plane at the outer edge. We assume that the disk flares out linearly to 15 AU. The flared disk height we use is an extreme example of what is seen in other disks [Espaillat et al., 2010]. Using geometric arguments, we calculate that the necessary increase in height for a feature at the disk edge to occult the star is 15.5 AU in addition to the extreme flaring

already assumed for the disk (Figure 2.4).

Using instead the argument of Keplerian motion, a feature at the edge of the disk would have an orbital velocity of ~4.66 km s^{-1}, corresponding to a width of ~0.49 AU. This results in the postulated feature with a projected height and width of ~15 AU and ~0.5 AU respectively. A feature with these dimensions would be so tall and thin as to be highly implausible.

2.5.2.4 A Warp in the Inner Circumstellar Disk

RW Aur A appears to have undergone a close interaction with its companion, RW Aur B, in the recent past. Here we consider the plausibility that a warp in the inner part of the RW Aur A disk, caused by the flyby, could cause the dimming seen in 2010-2011. The models by Clarke and Pringle [1993] for a retrograde, co-planar orbit show that even though all disk material outside periastron is fully disrupted, the interaction has little effect on the disk interior to this. Therefore, the Clarke and Pringle [1993] simulations predict that an interaction of this type would not warp or twist the innermost part of the disk. Other mechanisms such as a misaligned magnetic field, stellar radiation, or planetary companions could cause a warp. The longevity of a warped circumstellar disk is dependent on the mechanism that causes it.

A misaligned magnetic field, where disk material is funneled onto the stellar surface, would show variations on the timescale of days to a few weeks (e.g., AA Tau; Bouvier et al. [2003]) because this is the Keplerian timescale in the disk at a distance of a few stellar radii, which is the extent of the star-disk magnetic interaction. The magnetic misalignment effect, such as is seen around AA Tau, could not result in the 180 day dimming of RW Aur A.

If the warp is caused by the presence of planetary companions, the stability of the warp should be related to the stability of the planets' orbit and therefore the warp should last many orbital periods [Burrows et al., 1995, Mouillet et al., 1997]. Armitage and Pringle [1997] showed that radiation-induced warping is possible in high luminosity stars ($L_* \gtrsim$

$10\,L_{\odot}$) as long as the central star's intrinsic luminosity is much higher than what is created by accretion from the disk. This was an alternate explanation for the warp seen in the disk around β Pictoris [Armitage and Pringle, 1997].

To explore the possibility that the occultation is caused by a warp, we adjust our interpretation from §5.1 and now model the occulter as an opaque body with a sharp leading edge moving across the face of the star at an oblique angle. The obliquity of the leading edge allows the occulter to move at a higher velocity, thus potentially placing it closer to the star. To determine whether a warp is plausible or not, we must determine two key characteristics, the additional height required to cross into our line-of-sight and width of the warp. As we place a warp closer to the star, the orbital velocity increases, which as a result would increase the calculated occulter width (Figure 2.5). For a warp to be plausible, it would likely need a larger width then height. Assuming the same scenario as in the previous sub-section, where the disk flares out linearly to a height of 15 AU, we determine through geometric arguments that the only location where the calculated width of the occulter is larger than the line-of-sight height is at a distance from the star of $\leq$11 AU.

This would require the leading edge of the occulter to cross at a highly oblique angle, $\leq 15^{\circ}$ angle relative to the direction of motion. This semi-major axis for the feature corresponds to an orbital period of $\leq$31 years, well within our window of observations and so we should have observed it to repeat. It does not seem plausible that the presence of planets could create and dissipate a warp in less then one orbital period, especially since a planet-induced warp should be stable for longer than its orbital period.

The accretion rate is too high and luminosity of RW Aur is too low for it to cause a radiation induced warp in its inner disk. Also, the stability of the warp by induced radiation would be very long and should have been observed more than once in 50+ years of constant observation. In both potential disk warping mechanisms (planetary companions and stellar radiation), the lifetime of the warp would be much longer then the orbital timescale and would have been observed more than once. Therefore, we do not believe that a warp is a

likely interpretation of the 2010-2011 dimming.

Finally, we examine the possibility that the circumstellar disk around RW Aur A has eclipsed the star once due to a large precession of the disk. From our calculations, we are confident that the occulter is not located inside the disk around RW Aur A (minimum semi-major axis ~180 AU compared to the maximum radius of the disk, 57 AU [Cabrit et al., 2006]). We have determined that due to the inclination of the disk, any warp would need to be extremely large to cross our line of sight. This would also require an extreme precession of the circumstellar disk to force it into our line of sight. Thus precession is not a plausible explanation.

Given the extreme disk distortions required by these scenarios, we can conclude that the circumstellar disk around RW Aur A is not a likely explanation for the 2010-2011 dimming.

2.5.2.5 UXor Variation

UX Orionis stars are a class of pre-main sequence stars, typically Herbig Ae/Be objects, that experience large dimming events, sometimes described as Agol-type minima, in the *V* band of up to 3 mag, lasting on timescales of days to months. These events manifest as sudden drops in the visual brightness followed by a slow recovery. The minima events are aperiodic but recurring and not known as one-time phenomena. During these minima events, as the light decreases, the star becomes redder, then bluer, and the polarization increases. High dust column densities cause the initial dimming and reddening of light, while the bluing during minima and polarization is caused by an increase in the scattered light [Grinin et al., 1998, Waters and Waelkens, 1998].

Some UXor stars such as SV Cep show long term periodicities in their light curves on the timescale of years [Rostopchina et al., 1999]. Even though UXor stars are usually early type, there are a few known late type stars that display UXor variations, such as the late K stars UY Aurigae [Ménard and Bastien, 1987], AA Tau [Bouvier et al., 1999] and the

M2 star DF Tau [Chelli et al., 1999]. Also, even though one of the explanations for the deep minima in UXor stars requires the disk to be edge on, the variations typically occur in pre-main sequence stars that are surrounded by circumstellar disks at an inclination of 45° - 68° [Natta and Whitney, 2000].

RW Aur A would be one of the rare late-type stars showing UXor variability. There are some apparent similarities in the long term light curve of the UXor star SV Cep when compared with our observations of RW Aur A. Both SV Cep and RW Aur A show minima lasting 100-400 days and long term changes in the median base line [Rostopchina et al., 1999]. Even in the extreme case of SV Cep, which experiences rare deep minima, it still shows 3 events in 36 years [Rostopchina et al., 1999]. We have examined the entire 50+ year light curve of RW Aur and find nothing resembling the depth and duration of the 2010-2011 dimming. Thus if RW Aur A is a UXor star, it would have the longest time lapse between minima known.

An explanation of UXor minima is that they are the result of hydrodynamical fluctuations in either the inner rim or outer edge of the star's circumstellar disk [Dullemond et al., 2003]. Taking a conservative disk inclination for RW Aur A of 60° (See figure 2.4), we determined in section §5.2.3 that a feature at the edge of the RW Aur A disk, even with an extremely flared disk, would have to protrude an additional 15.5 AU from the disk to cross the star. A 15.5 AU protrusion is far larger then any known hydrodynamical fluctuations of a circumstellar disk. Therefore we explore the possibility that the disk of RW Aur A has a puffed-up inner rim causing the occultation. Dullemond et al. [2003] determined that the height of the inner rim would be $H_{rim} \sim 0.2\ R_{rim}$ with a hydrodynamical fluctuation of $\sim 0.1\ R_{rim}$. We use the conservative inner radius of the RW Aur A disk of 0.103±0.005 AU from Eisner et al. [2007]. This results in a maximum puffed-up inner rim height of 0.031 AU. Using the same inclination of the RW Aur disk, this would result in a relative height of 0.027 AU to our line of sight. At 0.103 AU from the star, in a disk inclined by 60° , the height necessary to cross our line-of-sight is 0.0555 AU. Even using the most conservative

values, the required height to cause extinction is still twice the maximum puffed-up height of the inner rim for the RW Aur A disk. Moreover, this puffing would need to have occurred only once for some unknown reason. However, the accretion rate onto the star during the occultation did not change appreciably (See §4.2). Thus, it is unlikely that the dimming observed is the result of circumstellar extinction from a hydrodynamically puffed-up inner disk rim.

Unfortunately, we do not have any color or polarization observations of the system during the large dimming event and therefore cannot look for the reddening during the beginning of the dimming or color reversal and increased polarization of the light at the maximum depth. These types of observations would allow us to definitively determine if the 2010-2011 event is a UXor minimum. However, when comparing our observations to known UXor stars, if the 2010-2011 dimming was a UXor minima, it should have occurred more than once in the 50+ years of consistent observations. Also, RW Aur A does not fit the typical profile of a UXor star and therefore, we do not believe it to be a new UX Orionis star.

2.6 **Summary and Conclusions**

The new observations of the RW Aur system from KELT-North show that a long (~180 days) deep (~2 magnitude) dimming occurred in late 2010 to early 2011. The event is also visible in the AAVSO archive which contains photometric observations of RW Aur.

We have determined that the most plausible explanation for this event is that a fragment of the arm from the tidally disrupted circumstellar disk, thought to be caused by a recent fly-by of the B component, crossed the face of the A component. The observations from Cabrit et al. [2006] show a tidally disrupted "arm" feature, 600 AU long, that is connected at the Northeast position of the A component and wraps around behind the star towards the B component. We calculate a maximum linear velocity of the occulter of 2.58 km s^{-1}, consistent with the maximum blue-shifted velocity, relative to RW Aur A, of the tidally

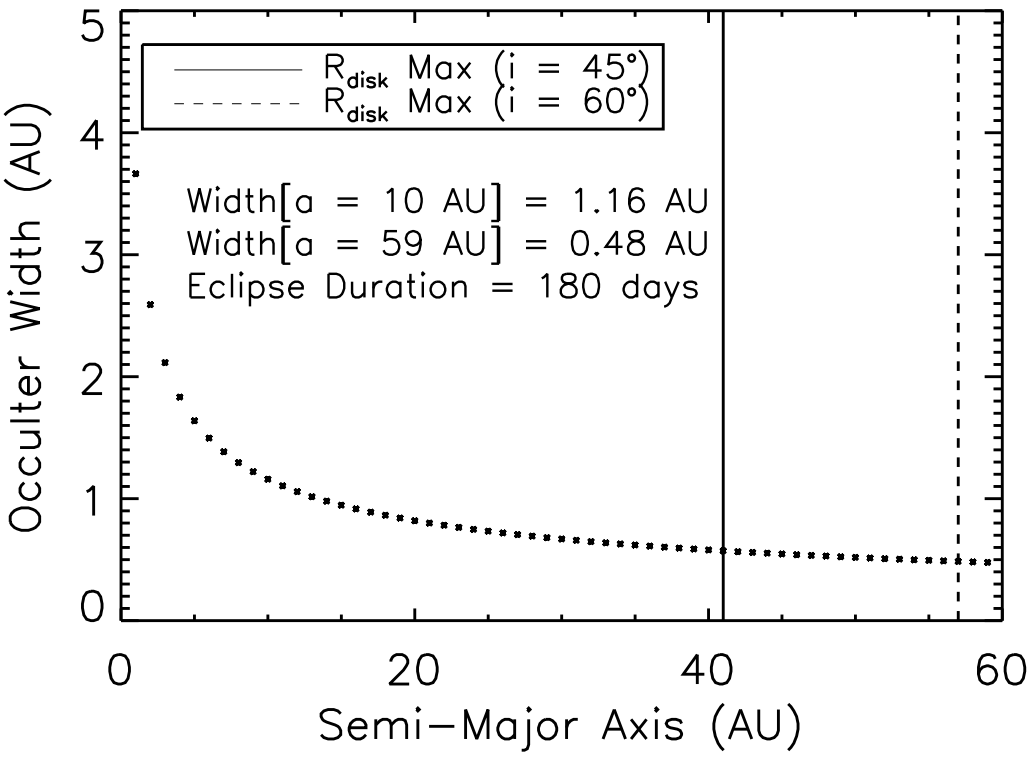

Figure 2.5: Calculated width of the occulting body as a function of semi-major axis for the given observed occultation duration of ~180 days, assuming Keplerian motion. The vertical lines correspond to the maximum disk radius of 41 to 57 AU, based on the two possible inclinations that Cabrit et al. [2006] estimated for the disk (45° and 60°).

disrupted arm, ~3.1 km s^{-1} [Cabrit et al., 2006]. Assuming Keplerian motion, the occulter is located at a distance of ~180 AU from RW Aur A, which is over twice the maximum radius of the observed circumstellar disk, but could still be located in this tidal feature.

The simulations performed by Clarke and Pringle [1993] predict that the tidally disrupted arm, produced from a close stellar fly-by of a companion, would have a relative width of 0.05 the periastron distance. Cabrit et al. [2006] calculated that the periastron distance, during the stellar fly-by of RW Aur B, would have been 100-140 AU. From our maximum linear velocity, we calculate the thickness of the arm fragment to be 0.27 AU (~0.003 the periastron distance). Evidently the tidal arm has remained fairly coherent despite the tidal disruption event. These observations may indicate that we are witnessing the leading edge of the tidally disrupted arm occulting the star, and that future occultations

may arise from other portions of the tidal arm. Therefore, we encourage observers to obtain multi-filter photometric observations of RW Aur in hopes of better characterizing future obscurations of the star. These results also motivate additional detailed simulations to extend the early work of Clarke and Pringle [1993] along with a reexamining of the spectra taken by Chou et al. [2013] that coincide with the first half of the dimming event, including the point of maximum depth. Since the authors of Chou et al. [2013] were unaware of the dimming event, a comparison of their results with out-of-occultation observations may show spectroscopic signatures of the occulting body. This rare observation provides insight into the dynamics of proto-planetary environments in binary star systems.

Chapter 3

Recurring Occultations of RW Aurigae by Coagulated Dust in the Tidally Disrupted Circumstellar Disk

3.1 Introduction

The circumstellar environment of young stars of a few Myrs old (T Tauri stars) involves complex dynamical interactions between dust and gas that directly influences the formation of planets. Past studies have shown that binarity is a common property of T Tauri stars (Ghez et al. 1993, Leinert et al. 1993, Richichi et al. 1994, Simon et al. 1995, Ghez et al. 1997). The process of planetary formation can be significantly altered when the circumstellar disk is gravitationally influenced by a stellar companion [Clarke and Pringle, 1993, Dai et al., 2015]. Specifically, strong binary interactions with disks are also likely to influence planetary core formation and chemical composition by stirring up and heating materials, enhancing planetesimal collisions. The prototype example of this type of system is RW Aurigae, a binary system of two Classical T Tauri Stars (CTTS), RW Aur A and B [Duchêne et al., 1999]. Detailed millimeter mapping by Cabrit et al. [2006] showed evidence of a recent close stellar fly-by of RW Aur B which disrupted the circumstellar material around RW Aur A, leaving a short truncated circumstellar disk and a large ∼600 AU long tidal arm extending from RW Aur A.

The system parameters are comprehensively described in §2 of Rodriguez et al. [2013]. Briefly, the RW Aur system is comprised of at least two components (RW Aur A and B) separated by ∼1.5”(∼200 AU) [Cabrit et al., 2006]. Bisikalo et al. [2012] measured that the separation of RW Aur A and B over ∼70 years has increased by ∼0.002”yr^{-1}. At the angular separation and 140 pc distance, the Keplerian orbital period would be > 1500 years [Bisikalo et al., 2012]. It is likely that the orbit is likely coplaner, prograde, and either unbound or highly eccentric [Dai et al., 2015]. This suggests that the orbit of RW Aur A

and B is inclined to our line-of-sight, like the disk around RW Aur A, at 45°–60° [Cabrit et al., 2006].

In 2010 the RW Aur system dimmed by ∼2 mags for a period of ∼180 days, marking the first event of this kind observed in this system dating back to the late 1890's [Beck and Simon, 2001]. Rodriguez et al. [2013] (hereafter Paper I) interpreted that dimming as an occultation of RW Aur A by disrupted circumstellar material from the close fly-by encounter of the two stars RW Aur A and B. Using simple kinematic arguments, Paper I determined that the occulting object, likely a clump of circumstellar material, was ∼0.3 AU in width, moving at a few km/s. If in a Keplerian orbit, it would be ∼180 AU from RW Aur A . Using simple geometric and kinematic arguments, it was determined that the occulting feature could not be located in the circumstellar disk around RW Aur A and therefore may not be in Keplerian orbit.

Recent hydrodynamical simulations by Dai et al. [2015] support the interpretation that a star-disk tidal encounter during a fly-by of RW Aur B could explain the unusual morphology of the RW Aur system. They found a strong agreement between their simulations and the millimeter observations by Cabrit et al. [2006], which first proposed the star-disk fly-by scenario. The model predicts that the line of sight to RW Aur A currently intersects a bridge of stripped-off material between the two stars. Dai et al. [2015] argue that the bridge structure may have small clumps of dense material that could occult the primary star. These simulations support the original hypothesis presented in Paper I and predict the possible occurrence of additional dimming events. In addition, numerical simulations of eccentric binary interactions of classical T Tauri stars suggest that the interaction can create accretion streams of inner disk material onto the stellar photosphere. These streams would be created near apastron and eventially form into "ring-like" structures around each star [Sytov et al., 2011, Gómez de Castro et al., 2013].

In this paper, we present new high-cadence photometry of the RW Aur system showing a shallow dimming in 2012-2013 and a second, larger dimming event in 2014-2015. The

Table 3.1: List of observations

Filter	Exposure Time (s)	Number of Exposures
B	25	587
V	15	602
R	15	631
I	15	604

2014-2015 event was first reported by Petrov et al. [2015] and resembles the dimming observed in late 2010 (Paper I). We apply similar geometric and kinematic arguments as we did for the 2010 event to show that the new dimmings are consistent with another clump of material from the tidally disrupted disk.

3.2 **Photometric Observations**

Several photometric surveys have observed RW Aur over both short and long timescales going back to 1899. Here we describe the observations used in our analysis.

3.2.1 KELT-North

Starting in 2003, the Kilodegree Extremely Little Telescope (KELT)-North survey has been continuously observing the entire sky between a declination of +18 and +44, searching for transiting Hot Jupiters around bright stars ($8<V<10$). Each KELT-North field spans $26^\circ \times 26^\circ$ with 23"per pixel. All observations are in a broad *R*-band filter with a ∼15 min cadence [Pepper et al., 2007, 2012]. RW Aur is located in KELT-North Field 04, which is centered on α = 5hr 54m 14.466s, $\delta = +31^\circ\ 44'\ 37''$ J2000. We obtained 9619 images of field 04 from UT 2006 October 27 to UT 2014 December 31. The data acquisition and reduction is described in detail in §2 of Siverd et al. [2012]. The KELT-North observations do not resolve individual stars in the RW Aur system.

3.2.2 Kutztown University Observatory

RW Aur was observed in *BVRI* using the 0.61 m Ritchey-Chrétien optical telescope at the Kutztown University Observatory (KUO) in Kutztown, Pennsylvania. A total of 2305 data images were obtained, as listed in Table 3.1, over 43 nights between UT 2014 February 25 and UT 2015 March 30.

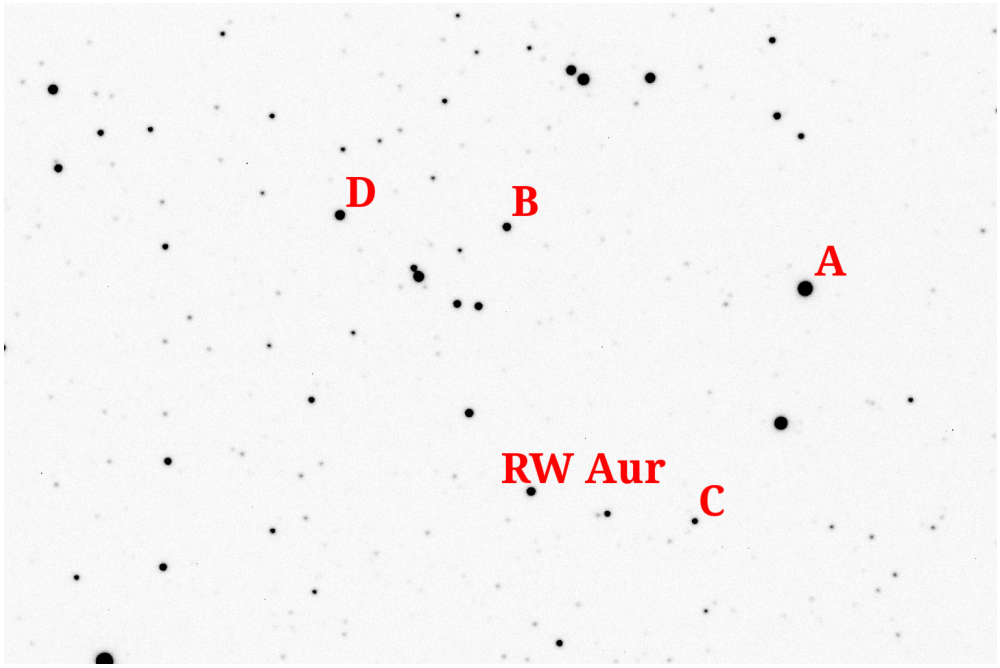

Figure 3.1: The KUO field-of-view for RW Aur. The standard reference stars are labeled as A, B, C, and D.

The telescope's f/8 focal ratio, coupled with the camera's array of 3072 × 2048 (9 μm) pixels, yields a field of view of 19′.5 × 13′.0. The CCD was kept at an operating temperature of -15°C and dark, flat, and bias calibration frames were applied to all data images in the usual way. A sample data image is given in Figure 3.1, labeling RW Aur and four standard reference stars. The known magnitudes of the reference stars are listed in Table 3.2. A standard method of aperture photometry was employed, and the instrumental magnitudes were color-corrected using several Landolt standard fields. The KUO observations

do not resolve the RW Aurigae system.

The observed *BVRI* light curves are displayed in Figure 3.5 and the $B-V$ color curve is shown in Figure 3.6.

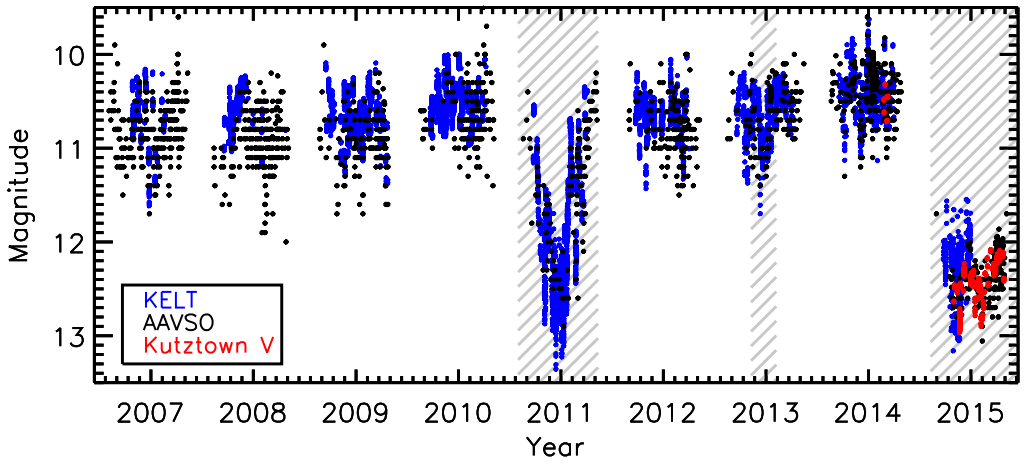

Figure 3.2: The KELT-North (Blue) and AAVSO (Black) observations plotted for the 9 KELT-North seasons. The three gray-shaded regions correspond to the 2010-2011, 2012-2013 and 2014-2015 large dimming events. The AAVSO and KUO data are in Visual and V-band magnitudes while the KELT-North observations are in instrumental magnitudes, that we approximate to the V-band but no attempt has been made to place all the data on the same absolute scale.

3.2.3 American Association of Variable Star Observers (AAVSO)

AAVSO is a dedicated, non-profit orginization with the primary goal of understanding all types of variable stars. The archive consists of data from astronomers, both amateur and professional, around the world. Reported observations for RW Aur begin in 1937 and the data used in this work are either in the *V* band or visual observations. The AAVSO observations do not resolve the RW Aur system.

3.3 Results

In this section we review the results from the 2010-2011 eclipse and present new observations from the KELT-North Survey showing two additional dimming events in 2012-2013

Table 3.2: The properties of the reference stars. The quoted apparent magnitudes were obtained from the AAVSO Variable Star Database (A. A. Henden 2010, private communication). The cited sources are as follows: †APASS, ††Tycho-2, †††TASS.

	Reference Star Label			
	A	B	C	D
Tycho-ID	TYC 2389-936-1	TYC 2389-589-1	N/A	TYC 2389-630-1
R.A. (J2000)	05:07:24.62	05:07:50.55	05:07:35.27	5:08:05.17
DEC. (J2000)	30:20:28.1	30:19:02.5	30:24:47.0	30:18:40.6
B	10.135 (±0.064)††	12.571 (±0.050)†	13.286 (±0.048)†	12.226 (±0.043)†
V	9.617 (±0.040)††	12.046 (±0.012)†	12.901 (±0.017)†	11.437 (±0.011)†
R	—	11.665 (±0.072)†	12.582 (±0.069)†	10.980 (±0.050)†
I	8.942 (±0.092)†††	11.307 (±0.101)†	12.281 (±0.096)†	10.552 (±0.071)†
$(B-V)$	0.518 (±0.075)	0.525 (±0.051)	0.385 (±0.051)	0.789 (±0.044)

and the 2014-2015 dimming event first announced by Petrov et al. [2015].

3.3.1 2010-2011 Dimming

Photometric analysis of the RW Aur system by the KELT-North and AAVSO surveys showed that in late 2010 the RW Aur system dimmed from $V \sim 10.4$ to $V \sim 12$ for ~180 days. Since RW Aur B is too faint ($V \sim 13.7$) to affect the total brightness of the system ($V \sim 10.4$), we assumed the entire dimming was caused by a decrease in flux from RW Aur A. This corresponded to an 86% reduction in the star's flux. Spectroscopic observations by Chou et al. [2013], which coincided with the first half of the 2010-2011 dimming, suggest that the accretion behavior of RW Aur A was consistent with previous observations prior to the large dimming. This provides evidence that the dimming is independent of the close-in star-disk accretion process. Paper I modeled the dimming as an occultation of RW Aur A by a large body which possessed a sharp leading edge perpendicular to its direction of motion. Combining this model with kinematic and geometric arguments, Paper I argued that RW Aur A was occulted by a large (~0.3 AU wide) body moving at a maximum velocity of ~2.6 km s^{-1} and if in Keplerian orbit, would be located ~180 AU from the star. Since the known short disk (57 AU, Cabrit et al. [2006] around RW Aur A is quite inclined to our

line of sight (> 30°), in Paper I we argued that the occulting body could not lie within the disk plane.

3.3.2 2012-2013 Small Dimming

In the two seasons following the 2010-2011 dimming, the median brightness of the RW Aur system was slightly fainter then the median brightness of the season prior to the dimming ($V \sim 10.5$). In early December of 2012, the brightness of the RW Aurigae system dimmed from a median brightness of $V = 10.5$ to $V = 11.2$ mag for ~40 days (See Figure 3.3). As with the 2010 eclipse, if we assume the entire event is the result of only RW Aur A dimming, then RW Aur A dimmed by ~50%. Although our ability to estimate the ingress timescale is hindered by the known short-timescale photometric variability, we can constrain the ingress duration to be 10-20 days. We also estimate the egress to be similar in duration to the ingress. This event is about a third of the depth of the 2010-2011 event and significantly shorter in duration. However, the 10-20 day ingress timescale is similar to the ingress timescale of the 2010-2011 event. We adopt the same occultation model as in §5.1 of Paper I, that is a large body with a sharp leading edge perpendicular to its direction of motion passing in front of RW Aur A. Since the ingress/egress timescale is similar to what was determined for the 2010-2011 event, this implies that the occulting bodies that caused the 2010-2011 and 2012-2013 dimmings are moving at a similar velocity and are located at a similar semi-major axis (that are 2.6 km s-1 and 180 AU, respectively). The duration of the 2012-2013 event is only ~40 days, which implies that the occulting body is 2.6 km $s^{-1} \times 40$ days = 0.06 AU in width (as compared to the ~0.3 AU width estimated for the occulting body of the 2010-2011 event).

3.3.3 2014-2015 Dimming

As first reported by Petrov et al. [2015], after the seasonal observing gap in mid-2014 the RW Aur system appeared significantly dimmer then in the previous observing season.

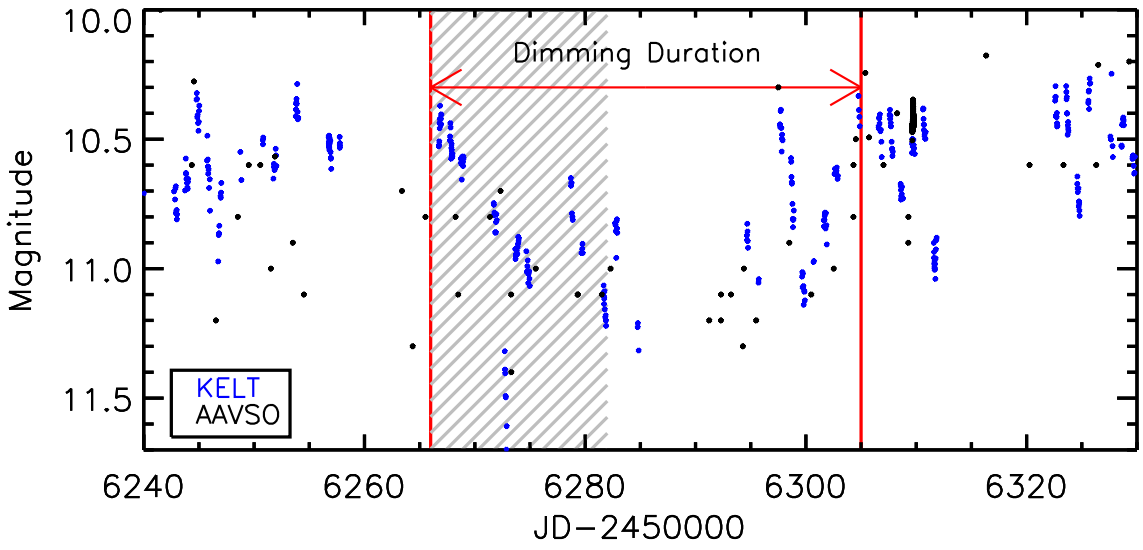

Figure 3.3: A zoom-in of Figure 3.2 in late 2012 to early 2013 showing a small dimming of the RW Aur system. The shaded region is the estimated ingress (the period of time for the dimming).

From analyzing the Hα and He I line at 5875Åbefore and during the 2014 dimming, they find no evidence that the known high accretion rate of RW Aur A has changed during the time of the dimming. This suggests that the dimmings are unrelated to the accretion process which takes place close to the star. Their observations of the Na I D lines and the Ca II K line provide evidence that the stellar winds of RW Aur A have changed significantly and propose that the increased wind velocity is pushing dust from the disk across our line of sight. Resolved *UBVRI* photometric observations of the RW Aur system during the 2014-2015 dimming indicated that RW Aur A was dimmer by >2 magnitudes in all bands and was actually fainter than its companion RW Aur B on UT 2014 November 14 (V~13.7) [Antipin et al., 2015]. X-ray observations during RW Aur's bright state and during the 2014-2015 dimming show that the absorbing column density increased during the dim state and was consistent with the interstellar medium's gas-to-dust ratio [Schneider et al., 2015]. Moreover, the resolved photometry by Antipin et al. [2015] suggests that the dimming resulted from foreground grey extinction and also provides evidence that all three dimming events are the result of only RW Aur A becoming dimmer while the brightness of RW Aur

B remained constant.

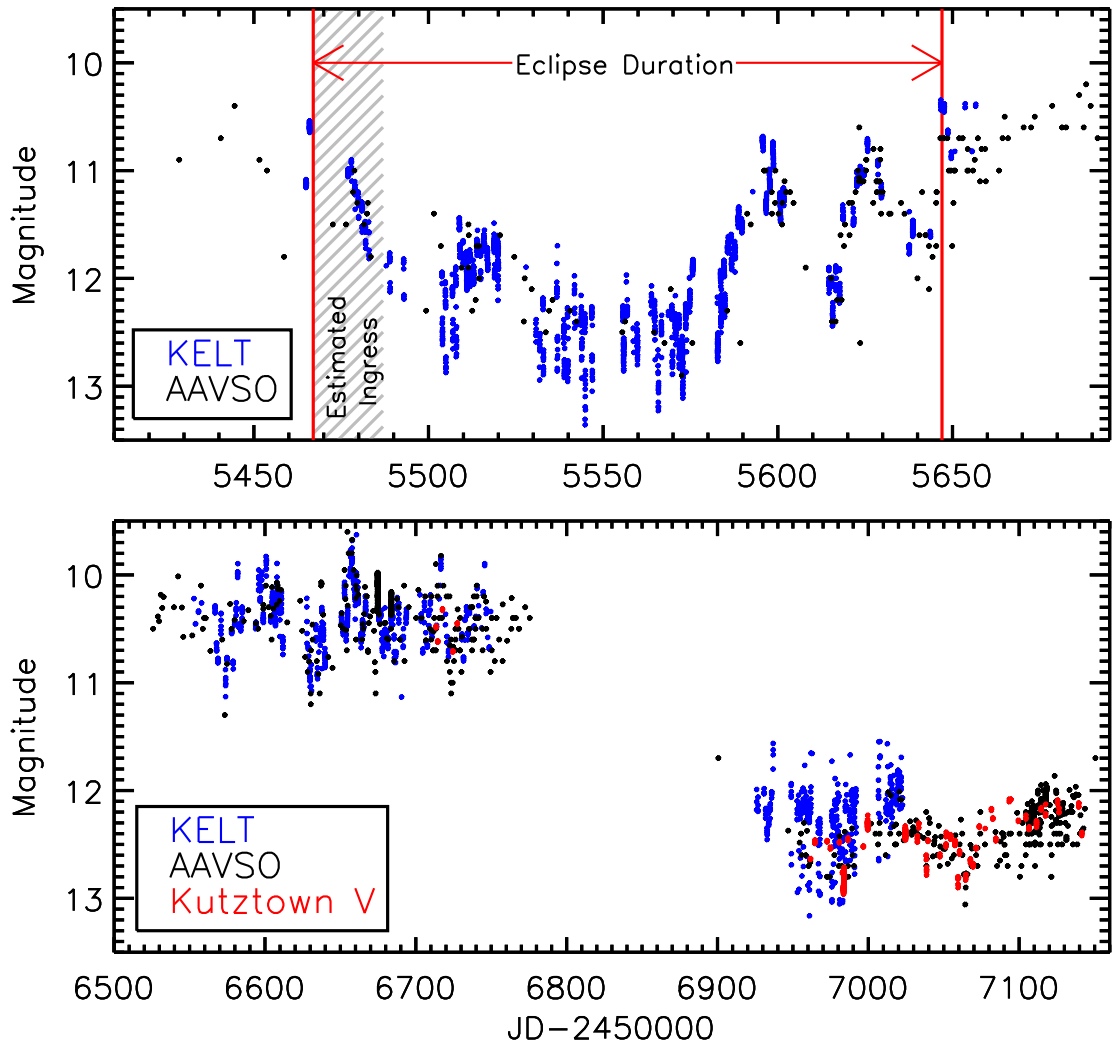

Figure 3.4: (Top) Recreation of Figure 3 from Paper I showing the 2010-2011 large dimming event. (Bottom) Zoom in of the last two KELT-North seasons showing the 2014-2015 dimming.

Combining the KELT, AAVSO and KUO observations, we find that the combined RW Aur system dimmed by ~2 mag in the KELT-North observations (Broad *R* Band), similar in depth to the 2010-2011 dimming (See Figure 3.2). Similar to the season prior to the 2010-2011 dimming, the RW Aur system was slightly brighter at a $V \sim 10.4$ prior to the 2014-2015 dimming. Using KUO, we conducted multi-band (*BVRI*) photometric monitoring of the entire RW Aur system prior to and during the 2014-2015 dimming. We find that

the depth is ∼2.3 mag in B, ∼2.0 mag in V, ∼1.75 mag in R and ∼1.5 mag in I. Antipin et al. [2015] showed that during the beginning of the 2014-2015 dimming, RW Aur A had dimmed by ∼3 mag and was actually fainter then RW Aur B in all bands in which we observed in ($BVRI$). Therefore, since our observations do not resolve the system, this depth difference is likely a result of the fact that the light from RW Aur B is included in our measurement. In §4.2 we discuss that in fact it appears the dimming evolved with time, steadily becoming more grey.

Similar to the 2010-2011 dimming, the short-term non-periodic photometric variability that is so prominent outside the 2010-2011 dimming and prior to the 2014-2015 dimming is still apparent during the new event but has diminished significantly in amplitude. During the 2010-2011 dimming, a few large 1-1.5 mag brightening and re-dimming features were observed and attibruted to sub-structure in the occulting body (Paper I). In the AAVSO and KUO observations of the 2014-2015 dimming, we observe a ∼0.5 mag peak-to-peak amplitude brightening and then dimming event over an ∼80 day period beginning at JD-2450000 of ∼6970. Interestingly, this is similar in depth and duration to the entire event seen in 2012-2013. Observations at the end of the 2014-2015 observing season from KUO and AAVSO appear to suggest that the RW Aur system may have begun to return to its original median brightness.

As with the previous two dimming events, we model the 2014-2015 dimming as an occultation of RW Aur A by a large body with a sharp leading edge perpendicular to its direction of motion. Unfortunately, the potential ingress and egress of this dimming appear to have occurred in the 2014 and 2015 seasonal observing gaps. Therefore, without an estimate of the ingress or egress timescale, we cannot calculate a transverse velocity of the occulting body. However, from the 2010-2011 and 2012-2013 dimming events, we calculated that the ingress timescale was between 10 and 30 days, which corresponds to a transverse velocity of 0.8-2.6 km s^{-1}. From the KELT-North, AAVSO, and KUO observations, the 2014-2015 dimming lasted at least the entire duration of the observing season,

~250 days. Using this duration and adopting the calculated transverse velocity from the analysis of the 2010-2011 dimming suggests that the minimum width of the occulter is at least 2.6 km s^{-1} × 250 days = 0.38 AU (0.8 km s^{-1} × 250 days = 0.12 AU) since our total duration is only a lower estimate.

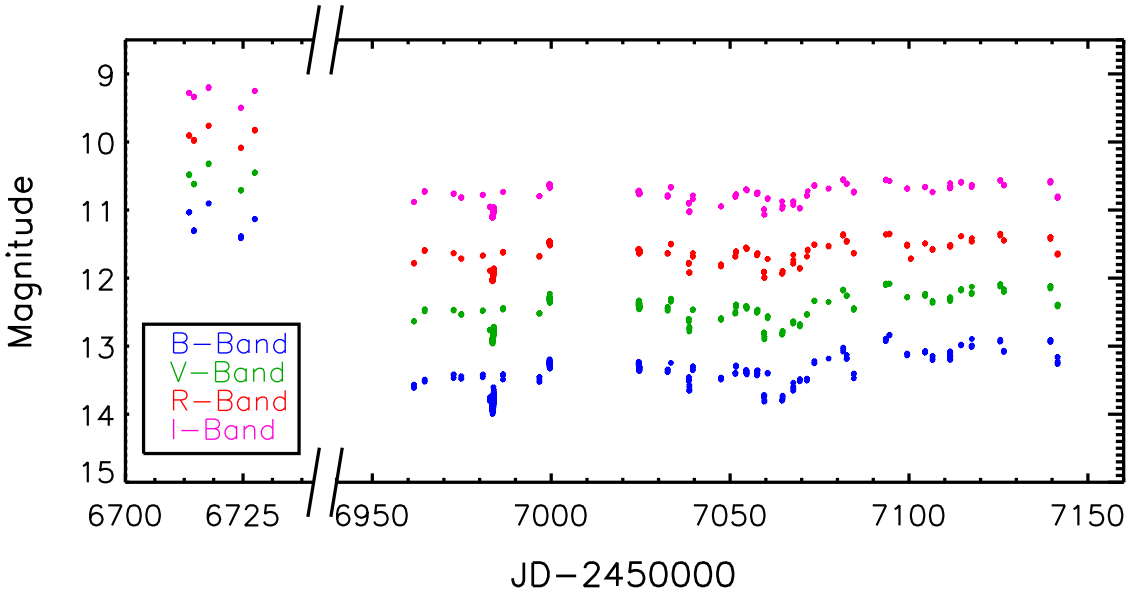

Figure 3.5: The KUO *BVRI* light curves of RW Aur covering the 2014-2015 large dimming event. These observations do not resolve the RW Aur system.

3.4 **Discussion**

In Paper I, we argued that the 2010-2011 dimming was caused by a consolidation of tidally disrupted material occulting RW Aur A. "In this section, we argue that the recent dimming events observed here, and first mentioned by Petrov et al. [2015], support this interpretation. We also discuss the possiblity of grain growth in the disrupted material.

3.4.1 Interpretation: Occultation by the RW Aur A Tidally Disrupted Disk Material

Using the IRAM Plateau de Bure Interferometer, the RW Aurigae system was mapped in ^{12}CO and dust continuum [Cabrit et al., 2006]. Their observations showed a long tidal arm wrapped around RW Aur A. Through comparison with numerical simulations

by Clarke and Pringle [1993], they proposed that RW Aur A recently experienced a fly-by from RW Aur B. This interaction would have significantly disrupted the disk originally around RW Aur A, resulting in the truncated disk and the large tidal arm. Also, the spectroscopic observations during the eclipse show that the accretion rate of RW Aur A did not change during the dimming [Chou et al., 2013]. Based on the millimeter and spectroscopic observations, Paper I proposed that the 2010-2011 dimming was caused by an occultation of the primary star, RW Aur A, by tidally disrupted material. This hypothesis has been supported by the hydrodynamical simulations by Dai et al. [2015] which suggest the occulting body to be a bridge of disrupted material connecting RW Aur A and B. The simulations also predict the possibility of additional dimming events.

Photometric monitoring of the RW Aur system from KELT-North, KUO and AAVSO show two additional dimming events that occurred after the 2010-2011 dimming event. From the 2012-2013 dimming, we estimate a similar ingress timescale as we did for the 2010-2011 event. We do not have coverage of ingress/egress for the 2014-2015 event due to the seasonal observing gaps. The similarities in the initial dimming duration for the 2010-2011 and 2012-2013 events suggest that the occulting bodies for both events are moving at similar velocities and likely at similar distances from RW Aur A (if we assume the occulting material to be in a Keplerian orbit). Therefore, it is likely that the cause of both (and possibly all three) dimming events are related.

In this work and in Paper I, we made some simple assumptions (sharp leading edge and Keplerian motion) to determine some characteristics of the occulting bodies that caused the three dimming events observed. Our calculated transverse velocity from the 2010-2011 and 2012-2013 dimmings are consistent with the measured velocities of the tidally disrupted material from the millimeter observations by Cabrit et al. [2006]. This velocity suggests a semi-major axis of ~180 AU, which is less than the projected separation of RW Aur A and B (~200 AU) but larger then the estimated extent of the known disk around RW Aur A (57 AU, Cabrit et al. [2006]). The hydrodynamical simulation by Dai et al. [2015] of the RW

Aur eccentric fly-by nicely replicates the millimeter observations by Cabrit et al. [2006] and support the interpretation that the 2010-2011 occultation was caused by an occultation of RW Aur A by tidally disrupted material. The simulations also suggest the possibility of additional dimming events in the future. Our observations and analysis of the 2012-2013 and 2014-2015 dimmings are consistent with the simulations and interpretation first proposed in Paper I.

Since no other dimming event was observed for ~50 years prior to 2010 (Paper I) and two more dimmings have occurred since, it is probable that the 2010-2011 event was the leading front of tidally disrupted material and more dimming are likely to occur. From the hydrodynamical simulations, Dai et al. [2015] suggested that the occulting mechanism may be a bridge of material connecting RW Aur A and B. Although this structure is poorly resolved in the simulations, they estimate it to be ~100 AU wide (~0.7″ in the plane of the sky). If the 2010-2011 dimming was caused by the leading edge of this bridge of material, and is moving 0.8-2.6 km s^{-1} as our calculations have shown, it will take 180-600 years for the trailing edge of the bridge to fully cross our line of sight. In ~5 years, we have observed 3 separate dimming events with 3 different durations. Therefore, it is possible that >50 more dimmings of RW Aur could occur over the next century.

Young stellar objects have also been seen to eject blobs of gas with very high velocities. An example of this is HH 30, a young system in which gas blobs with sizes similar to our solar system being ejected from the star at ~220 km s^{-1} [Burrows et al., 1996]. These blobs are mesured to be ~0.4″ in width (or ~56 AU wide using the ~140 parsec distance to the Taurus molecular cloud) [Burrows et al., 1996, Elias, 1978]. If we assume that the cause of the RW Aur dimmings is caused by similarly sized gas blobs, the time required for one blob to cross our line of size at the observed velocity for the HH 30 gas blobs would be ~1.2 years. This duration is similar to the duration of the 2010-2011 and 2014-2015 dimming events of RW Aur. Therefore, it is possible that the occulting body could be an ejected blob of gas from RW Aur A. This would also cause the spectroscopic signatures of gas in the

line of sight that have been observed by Petrov et al. [2015] for the 2014-2015 dimming. However, we emphasize again that spectroscopic accretions signatures have been found to not correlate in time with the occultation events [Chou et al., 2013], which suggests that the occulting material is not directly related to accretion phenomena which are generally believed to drive outflows and ejections.

Paper I investigated a series of other possible explanations for the 2010-2011 dimming event that are also ruled out for the additional two dimmings presented in this work. However, spectroscopic observations prior to and during the 2014-2015 dimming event show evidence that the stellar wind of RW Aur A has changed. Therefore, an alternative explanation for the 2014-2015 dimming is that enhanced stellar winds ejected large dust grains from the RW Aur A disk causing the occultation [Petrov et al., 2015]. We do not rule this interpretation out but suggest that the consistency between the millimeter observations of the disrupted material by Cabrit et al. [2006], our observed and calculated properties of the occulting bodies, and the agreement with the hydrodynamical simulations by Dai et al. [2015] of the eccentric star-disk encounter, favor the tidally disrupted disk explantion as the cause of all three dimming events. Since there is no evidence of prior occultations for the last 50+ years (Paper I), and now we have several such events within the last few years, it is likely that we are observing the leading edge of the bridge structure, and the successive occultations presented here and in Paper I represent smaller coherent structures within it.

3.4.2 Evidence for Grain Growth in the Tidally Disrupted Disk

Although our color observations do not resolve the RW Aur system, observations by Antipin et al. [2015] show that RW Aur B has remained constant during the 2014-2015 dimming, indicating that the color changes observed are likely not due to RW Aur B. Using the measure *BVR* magnitudes for RW Aur B (14.5, 13.8 and 12.92 respectively, [Antipin et al., 2015]), we subtract the brightness of RW Aur B from the KUO *BVR* observations to create the $B-V$ an $V-R$ color plots seen in Figure 3.6. The $B-V$ color of RW Aur

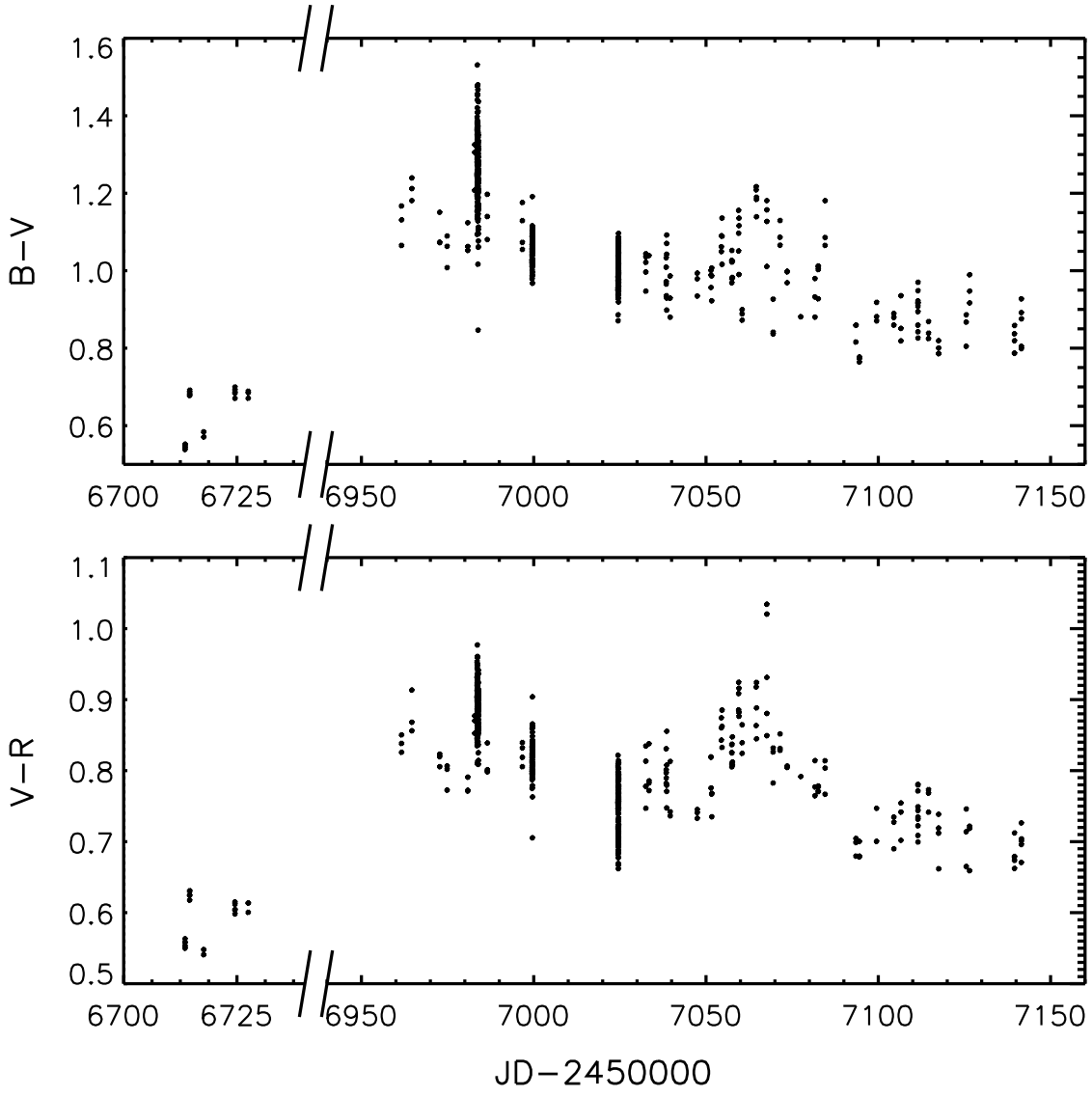

Figure 3.6: The KUO $B-V$(top) and $V-R$ (bottom) color curve of RW Aur A during the 2014-2015 dimming. The *BVR* brightness of RW Aur B [Antipin et al., 2015] has been subtracted from the KUO observations

increased from a quiescent value of ~ 0.6 prior to the dimming, to ~1.2 early in the 2014-2015 dimming, and then monotonically declined back toward the original value except for a brief reversal (JD-2450000 ~ 7060) suggesting some inhomogeneity in the dust grain size distribution within the occulting material (see Figure 3.6). Meanwhile, the *V* mag of the star during the middle of the dimming remained roughly constant, dimmed by ~2.0 mag (see Figure 3.5). That the total extinction is roughly constant but the color of the extinction

is changing indicates that the total absorption column is roughly constant throughout the occultation but that the ratio of total-to-selective extinction changes. The initial change in $B-V$ from 0.6 to 1.0 indicates a $B-V$ color excess, E$(B-V)$ = 0.4. With A_V = 2.0, we have a ratio of total-to-selective extinction, $R(V) = A_V/E(B-V)$ = 2.0/0.4 = 5. This is the standard value typically adopted for dust grains in molecular clouds and star forming regions, which suggests the presence of dust grains, and not just molecular material, in the environment of this young system. The E$(B-V)$ value then drops steadily to ~0.2 and perhaps less, giving $R(V) > 2.0/0.2 > 10$. In other words, the occulting material becomes steadily more grey. Rather, the shift in observed $R(V)$ indicates that the dust grains at the leading edge of the occulting feature are relatively small and representative of dust in star forming regions, whereas the material deeper into the occulter is likely comprised of larger grains, which could be dust grains onto which ice mantles have developed, and/or larger coagulated grains or pebbles (assuming the extinction is optically thin). Another possibility is that the steadily greyer extinction is caused by having a larger fraction of the occulting material be optically thick as the dimming progressed. Antipin et al. [2015] find that the RW Aur A spectral energy distribution changes during the 2014-2015 occultation and they suggest both a grey extinction and a selective extinction, similar to our results here. We do not know whether this evolved protoplanetary material existed prior to the tidal disruption event, or if the growth of the dust grains was aided by the disruption event. The evidence suggests that the building blocks of planetary material can exist in the space between binary stars, perhaps through fly-by interactions such as that seems to have occurred in the RW Aur system.

3.5 **Summary and Conclusions**

With the deep dimming event observed in 2010-2011 (Paper I), the intrigue surrounding the RW Aur system has dramatically increased. New photometric observations from KELT, AAVSO and KUO show two additional dimming events in 2012-2013 and 2014-2015 (the

2014-2015 dimming was first announced by Petrov et al. [2015]). From our analysis, the observations of the additional dimming events are consistent with an occultation of RW Aur A by tidally disrupted material lying far outside the extent and plane of its short circumstellar disk. This interpretation has been supported by hydrodynamical simulations of the proposed RW Aur star-disk interaction [Dai et al., 2015].

Multiband photometric observations during the 2014-2015 dimming showed that the occulting material became steadily more grey as the dimming progressed. This suggests that the outer portion of the occulting body consists of small dust grains while the core is primarily made up of (either or all three) large dust grains, dust enveloped in ice or is optically thick. Either way, the observations are consistent with evolved protoplanetary material and the evolution of this material may have been expedited by the tidal interaction. The recurring dimmings of RW Aur A will continue to increase the interest surrounding this unique system. Continued monitoring of RW Aur will provide insight into the effect the tidal interaction will have on the evolution of planetesimals from the disrupted material. Future high spatial resolution observations of this system would be of great value in clarifying the nature of the circumstellar environment.

Chapter 4

V409 Tau As Another AA Tau: Photometric Observations of Stellar Occultations by the Circumstellar Disk

4.1 Introduction

The circumstellar environments of young stellar objects (YSOs) involve complex dynamical interactions between dust and gas that directly influence the formation of planets. UX Orionis stars (UXors), which are one specific category of YSOs, are a class of pre-main sequence stars that have circumstellar disks and experience large aperiodic photometric dimming events. These events range in depth and duration but can be up to 3 magnitudes in the V-band on timescales of days to months. Most UXor stars exhibit infrared excesses in their spectral energy distributions (SEDs) that are generally interpreted as being due to emission from circumstellar disks. Some UXor stars show minima lasting months to years with long-term (decade) changes in median base line brightness [Rostopchina et al., 1999]. During the minima, a color reversal from red to blue is normally observed together with an increase in polarization. The initial dimming and reddening of light is thought to originate from high column densities of dust, while the bluing during minima and the polarization are caused by an increase in the scattered light [Bibo and The, 1991, Grinin et al., 1991, 1998, Waters and Waelkens, 1998].

Hydrodynamical fluctuations in the stars' circumtellar disks have been suggested to explain the large dimming events seen in UXor stars [Dullemond et al., 2003]. Occultations of the host star by dust clumps in their circumstellar disk has also been proposed as another explanation. [Wenzel, 1969, Grinin, 1988, Voshchinnikov, 1989, Grinin et al., 1998, Grady et al., 2000]. If the dimmings are caused by features in a geometrically thin disk, then the disk would need to be seen very nearly edge-on [Grinin et al., 1991, Grinin and Rostopchina, 1996, Herbst and Shevchenko, 1999, Bertout, 2000]. However, the UXor

Table 4.1: CTTS that are candidate UXor stars (G or later)

Target	Spectral Type	Reference
CO Ori	G5	Eaton and Herbst [1995]
RY Tau	F8-K1	Eaton and Herbst [1995]
RY Lupi	G0	Eaton and Herbst [1995]
DK Tau	K6	Oudmaijer et al. [2001]
CB 34V	G5	Tackett et al. [2003]
SU Aur	G2	Unruh et al. [2004]
UY Aur	G5	Berdnikov et al. [2010]
AA Tau	K7	Bouvier et al. [2013]
V409 Tau	M1.5	This work

Notes. The spectral types listed here are from SIMBAD except for AA Tau and V409, the references for which are provided in §2.

variations described above typically occur in optically visible pre-main sequence stars that are surrounded by circumstellar disks viewed at less edge-on inclinations of 45° - 68°, indicating the disks must be flared and/or possess warps or large-scale features with large vertical scale heights [Natta and Whitney, 2000]. Even though UXor stars are usually early type Herbig Ae and Be stars, a few are Classical T Tauri Stars (CTTS) that display similar photometric variability, such as the late K star AA Tau [Bouvier et al., 1999]. It has been found that about 10% of late type CTTS display the UXor photometric dimming variability, perhaps reflecting the required geometric and line-of-sight orientation [Bertout, 2000]. A list of CTTS that are candidate UXors is provided in Table 1.

One way to better understand the structure and evolution of circumstellar disks is to observe a star being occulted by circumstellar material. AA Tau is one of the most best-studied stellar systems displaying both short and long term photometric variability, a common characteristic of T Tauri stars [Vrba et al., 1993, Bouvier et al., 1999, 2003, 2007]. Based on long-term monitoring, AA Tau had remained at a constant brightness from 1978 until 2011 [Grankin et al., 2007, Bouvier et al., 2013]. In 2011, AA Tau dimmed by ~2 mag [Bouvier et al., 2013] and has not returned to its normal brightness as of UT 2013 December 9 (The end of our data set). Bouvier et al. [2013] concluded that the dimming is likely the result of a density increase in the occulting region of the circumstellar disk that is

located at least 8 AU from the host star, assuming the occulter is in a Keplerian orbit. Based on the 2 years of constant brightness, Bouvier et al. [2013] conclude that the azimuthal extent of the occulter is at least 30°. During this dimming, the system experiences a color reversal from red to blue, a known characteristic of UXor stars [Bouvier et al., 2013].

Another example of a young star being occulted by circumstellar material is the well-studied system RW Aurigae. In late 2010, the known T Tauri system RW Aurigae, which contains at least two stellar components (RW Aurigae A and B), experienced a ∼2 magnitude dimming event for ∼180 days [Rodriguez et al., 2013]. The RW Aurigae system has been photometrically observed since the late 1890's [Beck and Simon, 2001], but no event of similar depth and duration had ever been seen prior to 2010. Detailed investigations of the system suggest that there was a recent close fly-by of RW Aur A by RW Aur B, tidally disrupting the outer portions of the circumstellar disk of RW Aur A [Cabrit et al., 2006]. The dimming was attributed to a portion of the tidally disrupted circumstellar disk occulting the primary component, RW Aur A. Subsequent modeling of the star-disk encounter by Dai et al. [2015] supports this interpretation. This system shows that binary star interactions can sculpt circumstellar disks. There are other systems in the literature that display both periodic and non-periodic large dimming events, which as of yet are unexplained, that may also be caused by circumstellar material [Carroll et al., 1991, Kearns and Herbst, 1998, Chiang and Murray-Clay, 2004, Winn et al., 2004, Bouvier et al., 2007, Grinin et al., 2008, Plavchan et al., 2008, Kloppenborg et al., 2010, Mamajek et al., 2012, Rattenbury et al., 2014].

Objects like AA Tau and RW Aur, that display large photometric dimming events caused by their circumstellar disks, give us opportunities for studying the evolution of the circumstellar environments of young stars and perhaps even embryonic planets in disks. In this paper, we present new photometric observations of the 2011 dimming of AA Tau. The observations of the sudden dimming of AA Tau support the previous interpretation by Bouvier et al. [2013] that the dimming is caused by a region of enhanced density in the

circumstellar disk. We also present new photometric observations of V409 Tau that show that it underwent two separate dimming events. In the observations of V409 Tau we present below, we see two clear dimming events that are separated by a short period of time and are similar to the dimming event of AA Tau. Our observations of V409 Tau prior to the two dimming events are much sparser in cadence but appear consistent with the typical short-term variability associated with late type T Tauri stars. We interpret the dimming of V409 Tau, analogously to the dimming event of AA Tau, as likely due to photometric variability resulting from density variations in the disk of V409 Tau.[1] These long dimming events are known characteristics of UXor stars, and thus we can add V409 Tau to the short list of late-type stars showing this behavior.

The paper is organized as follows. We introduce the known characteristics of the V409 Tau system in §2, illustrating the complex stellar environment. In §3, we describe the photometric observations, and then discuss the photometric properties of the data in §4. In §5, we present several interpretations of the light curve and discuss their plausibility. We summarize our results and conclusions in §6.

4.2 **Known Characteristics**

In this section, we present a review of the known physical and observational parameters of the stars V409 Tau and AA Tau.

4.2.1 **V409 Tau**

V409 Tau (α = 04h 18m 10.785s, δ = +25° 19′ 57.39″; V∼13.34 [Zacharias et al., 2012]) was determined by Kenyon et al. [1994] to be a member of the Taurus-Auriga association using IRAS observations. Spectroscopic observations by Luhman et al. [2009]

[1]Throughout this paper, we refer to the reductions of brightness of V409 as "dimmings", and not "eclipses". Although we propose that the observed dimmings are caused by eclipses of the star by intervening material, we avoid the term "eclipse" when referring to the observations to maintain generality in the descriptions of the data.

show V409 Tau to be a M1.5 star, with $T_{\rm eff}$ = 3632 K, and provide strong evidence confirming it as a member of the Taurus-Auriga association. Gorynja [1968] first classified V409 Tau as a variable star. Using the Trans-atlantic Exoplanet Survey (TrES), Xiao et al. [2012] measured periodic photometric variability of 4.754 days with an amplitude of 0.3 mag. Andrews et al. [2013] estimated the age of V409 Tau to be variously 1.86 Myr, 5.012 Myr, and 3.47 Myr using three separate pre-main sequence stellar models [D'Antona and Mazzitelli, 1997, Baraffe et al., 1998, Siess et al., 2000]. From these models, the stellar mass was estimated to be ~0.40 $M_{\odot}$, ~0.63 $M_{\odot}$and ~0.43 $M_{\odot}$respectively.

4.2.2 **AA Tau**

AA Tau is a low-mass, photometrically variable, system in the Taurus-Auriga association that has been previously classified as a UXor star. It has a spectral type of ~K7, V~12.2, $T_{\rm eff}$ = 4030K, radius of 1.85 $R_{\odot}$and a mass of 0.85 $M_{\odot}$[Bouvier et al., 1999]. Both photometric and spectroscopic monitoring provide evidence that the system is experiencing magnetospheric accretion [Bouvier et al., 2003]. The outer portion of the AA Tau disk has an inclination of $\sim 71^{\circ}$ while the inner part of the disk is warped and misaligned with respect to the outer disk [Cox et al., 2013]. Bouvier et al. [1999] observed a ~8.5 days, ~1.4 mag quasi-periodic variability in the $UBVRI$ filters where the $B-V$ color only showed a 0.1 mag change on the timescale of weeks. This ~8 day photometric periodicity, first reported by Vrba et al. [1993], has been attributed to the magnetically warped inner disk periodically occulting the host star [Bouvier et al., 2007]. These eclipses have presented with varying depths, which provides evidence that the occulter is changing size or opacity on the timescale of days. It is likely that the inner warp and the accretion streams from the disk onto the stellar surface are at similar locations in the inner disk, orbiting with a period of ~8 days. The accretion is likely varying, directly affecting the warp, and likely causing the change in the eclipse depth [Bouvier et al., 2007]. In a study of > 500 variables in the Orion Nebula Cluster, Rice et al. [2015] identify 73 young stars that show AA Tau

like short quasi periodic dimming events.

In 2011, AA Tau dimmed by ~2 mag. Bouvier et al. [2013] claim that the near-IR colors during AA Tau's dimmed state and an observed bluer slope in the red/NIR spectrum from XSHOOTER [D'Odorico et al., 2006, Vernet et al., 2011] suggest that the system is experiencing 3-4 mags of visual extinction compared to its normal bright state. Bouvier et al. [2013] argue this because they required a much higher extinction ($A_v > 3$) to match the red and near-IR wavelength regimes in the XSHOOTER spectrum. They argue that the reason the system only shows ~2 mag depth event in the V band (and not a 3-4 mag event) is that the system experiences a color reversal becoming bluer at optical wavelengths during the dimming. This color reversal is a common feature of UXor stars.

Importantly, while the ~8 day quasi-periodic variability was not observed during the initial stage of the 2011 dimming event [Bouvier et al., 2013], it was seen during a later stage of the dimming event in late 2012/2013, for a 3 month period by Bouvier et al. [2013]. This indicates that the source of the long timescale dimming is likely situated outside the inner disk region that is the likely source of the short-timescale accretion variability. Indeed, on the basis of Keplerian arguments, Bouvier et al. [2013] suggested that the obscuring material must be situated at ~8 AU from the star.

4.3 **Photometric Observations**

V409 Tau and AA Tau have been observed in several photometric surveys over the past two decades. We present new photometric data for both targets in Figure 4.1.

4.3.1 Archival Data

The All Sky Automated Survey (ASAS) is a photometric survey with the goal of observing as much of the southern sky as possible in order to study any and all kinds of photometric variability in the *I*-band. Pojmanski [1997] describes the data acquisition and reduction techniques. ASAS observed V409 Tau from UT 2002 December 13 to UT 2009

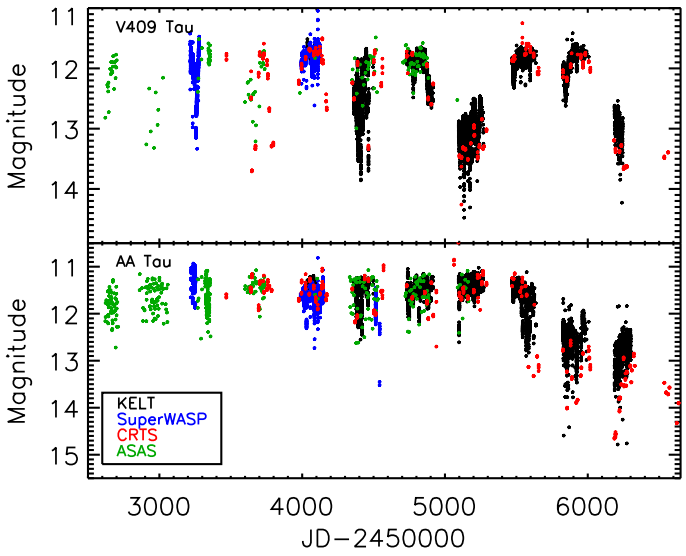

Figure 4.1: KELT-North (Black), SuperWASP (Blue), CRTS (Red) and the ASAS (Green) light curves of V409 Tau (Top) and AA Tau (Bottom) from 2004 to 2013. A vertical offset has been applied to the KELT, SuperWASP and ASAS data to match pre-dimming magnitudes of AA Tau to the *V* band observation by CRTS. The same vertical offset has been applied to the V409 Tau observations. Only the CRTS data are in *V*-band magnitudes whereas the other observations are in very broad band magnitudes that we approximate to *V*-band but no attempt has been made to place all the data on the same absolute scale.

September 12, obtaining 153 observations. ASAS also observed AA Tau from UT 2002 December 13 to UT 2009 November 30, collecting 376 observations.

The Catalina Real-time Transient Survey (CRTS) is a wide-field photometric survey designed to detect variable sources on the time scale of minutes to years using a *V*-band filter. The data used in the work described here were from Catalina Survey Data Release 2[2]. More information on the CRTS observations and data reduction can be found in Drake et al. [2009]. CRTS observed V409 Tau from UT 2005 April 9 to UT 2013 September 27, acquiring 350 observations. CRTS observed AA Tau from UT 2005 April 8 to UT 2013 December 9, obtaining 429 observations.

The Wide Angle Search for Planets (SuperWASP) is a photometric survey for transiting extrasolar planets with a cadence of a few minutes in broad filter centered on 550nm. SuperWASP observed V409 Tau, first in 2004 from July 29 to September 30 and then again

[2]http://nesssi.cacr.caltech.edu/DataRelease/

from UT 2006 September 17 to UT 2007 January 24, for a total of 3695 images of V409 Tau. SuperWASP observed AA Tau in 3 separate seasons: UT 2004 August 2 to UT 2004 September 4, UT 2006 September 11 to UT 2007 February 15 and UT 2008 February 18 to UT 2008 March 17, acquiring 2744 observations. The SuperWASP public archive is described in Butters et al. [2010].

Using the 40/50/100 cm Schmidt telescope at Asiago, Romano [1975] obtained 24 non-filtered observations of V409 Tau from UT 1962 October 22, until UT 1964 July 13. The observations showed a brightening from 1962 to 1964. This data is not publicly available and therefore we do not include it in our light curve analysis. We refer back to these observations when interpreting our results to understand the V409 Tau system in §5.2.

Table 4.2: KELT-North Table of Observing Seasons

Season	UT Start Date	UT End Date
1	2006 October 26	2007 January 17
2	2007 September 19	2008 February 2
3	2008 September 24	2009 March 26
4	2009 September 22	2010 March 16
5	2010 October 2	2011 March 17
6	2011 September 22	2012 March 21
7	2012 September 17	2013 January 9th

4.3.2 KELT-North

The Kilodegree Extremely Little Telescope (KELT-North) project is an ongoing, wide-field ($26^\circ \times 26^\circ$) survey for transiting planets around bright stars (V = 8-10). The survey uses two telescopes, KELT-South (Sutherland, South Africa) and KELT-North (Sonita, Arizona), and observe in a broad R-band filter, with a ~15 minute cadence and a typical photometric precision for stars of $V \sim 11$ of ~ 0.04 mag [Pepper et al., 2007, 2012]. The KELT data are reduced using a heavily modified version of the ISIS software package [Alard and Lupton, 1998, Alard, 2000], described further in §2 of Siverd et al. [2012][3]. V409 Tau

[3]Much of the reduction software is publicly available: http://verdis.phy.vanderbilt.edu

and AA Tau are both located in KELT-North Field 03, which is centered on α = 3h 58m 12s, δ = 59° 32′ 24″. For the work presented in this paper, all of the KELT observations come from the KELT-North telescope. KELT-North observed this field for 7 seasons from UT 2006 October 26 to UT 2013 January 9, obtaining ~9100 images. All data shown has a relative photometric error less than 20% RMS. Table 2 shows the start and end date for each KELT-North season. A portion of the KELT-North photometric data set is shown in table 3.

Table 4.3: KELT-North photometric observations of V409 Tau and AA Tau

JD_{TT}	V409 Tau Relative Mag[a]	V409 Tau Photometric Errors[b]	AA Tau Relative Mag[a]	AA Tau Photometric Errors*b*
2454034.731241	-0.181	0.054	0.084	0.044
2454034.735862	-0.209	0.053	0.026	0.041
2454034.740481	-0.205	0.046	0.109	0.044
2454034.745101	-0.195	0.052	0.081	0.044
2454034.758962	-0.209	0.049	0.138	0.064
2454034.763581	-0.239	0.047	0.030	0.039
2454034.768202	-0.205	0.048	0.082	0.043
2454034.772822	-0.228	0.044	0.096	0.0439
2454034.791297	-0.235	0.047	0.094	0.044
2454034.795917	-0.158	0.051	0.135	0.044

Notes. The data shown in Table 3 is published in its entirety in the electronic edition of this paper for both V409 Tau and AA Tau.
[a]Relative KELT-North Instrumental magnitude. The median of the KELT-North Instrumental magnitude has been subtracted off.
[b]Photometric errors for instrumental KELT-North magnitudes. True per-point magnitude errors must fold in 0.036 mag systematic errors.

4.3.3 CARMA 3mm

We observed the V409 Tau system using the Combined Array for Research in Millimeter Astronomy (CARMA) for ~3.5 hours in the 3mm continuum. Specifically, we used the CARMA 15 E configuration consisting of nine 6.1m and six 10.4m antennas. All observations were taken on UT 2014 August 8. Along with observing V409 Tau, we observed Uranus, 3C84 and 0510+180 as the flux, passband and gain calibrators, respectively. The

observations and flux value presented in this paper were reduced and measured using the MIRIAD software program, described in detail by Sault et al. [1995].

4.4 Analysis and Results

Here we present and discuss the photometric properties of AA Tau and V409 Tau (data shown in Figure 4.1). Our analysis focuses on the SuperWASP, ASAS, CRTS and KELT-North photometric data.

4.4.1 **AA Tau**

AA Tau has been classified previously as a UXor star, displaying both short term quasi-periodic variability and non-periodic large dimming events. The KELT-North photometric data confirm known characteristics of the AA Tau system presented in the literature.

First, after a long quiescent period, AA Tau decreased in brightness by ~2 mag in 2011 [Grankin et al., 2007, Bouvier et al., 2013]. Second, the pre-dimming obervations of AA Tau in all data sets show a ~1.0 mag amplitude variability that is common to most classical T Tauri stars, as first shown by Herbst et al. [1994]. YSOs will display both periodic and non-periodic variability, typically on the timescales of days to weeks. We use the Lomb-Scargle (LS) period search in the VARTOOLS analysis package to search for periodic variability [Hartman, 2012]. The Lomb-Scargle (LS) periodicity analysis is designed to search for small sinusoidal periodic signals in unevenly sampled time-series data [Lomb, 1976, Scargle, 1982, Press and Rybicki, 1989]. The goal of our LS analysis was to recover the previously known ~8 day period for AA Tau. Our LS analysis of the first KELT-North season of AA Tau shows a periodicity of ~8.2 days (Figure 4.2). The phased light curve of AA Tau at a period of 8.21 days is shown in Figure 4.3. This is similar to the periodicity found by Vrba et al. [1993], Bouvier et al. [1999] and is interpreted as the magnetically warped inner disk occulting the host star at a semi-major axis of a few stellar radii. The large peaks at 1.0 and 2.0 cycles/day in all periodograms is a diurnal alias of the

long period variability. Finally, the pre-dimming observations of AA Tau in all data sets show variability of up to 1.0 mag amplitude that is common characteristic of most classical T Tauri stars, as first shown by Herbst et al. [1994].

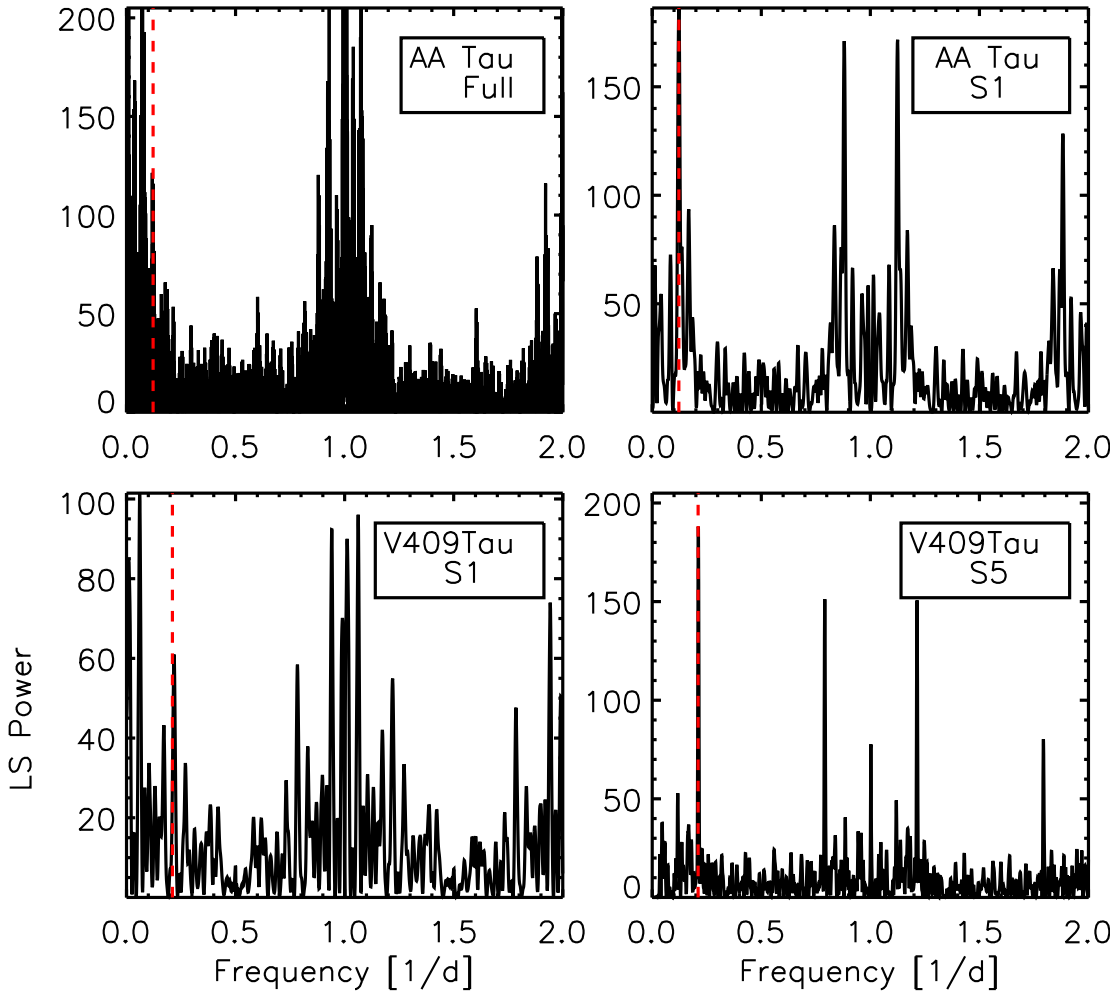

Figure 4.2: LS periodicity analysis of the KELT-North photometric data. Top Row: LS periodogram of for the Full KELT-North AA Tau data set (Left) and KELT-North season 1 (right). The vertical red dashed line corresponds to the 8.2 day period found by Vrba et al. [1993]. Bottom Row: KELT-North season 1 V409 Tau data set (Left) and KELT-North season 5 (Right). The vertical red dashed line is the 4.574 day period found by Xiao et al. [2012]. The large peak at 1.0 and 2.0 cycles/day in all periodograms is a diurnal alias of the long period variability.

We confirm the previous dimming event in KELT-North survey data. The KELT-North and CRTS observations of AA Tau show that the dimming event began in late November of 2010 and has remained consistently fainter through the end of our photometric observa-

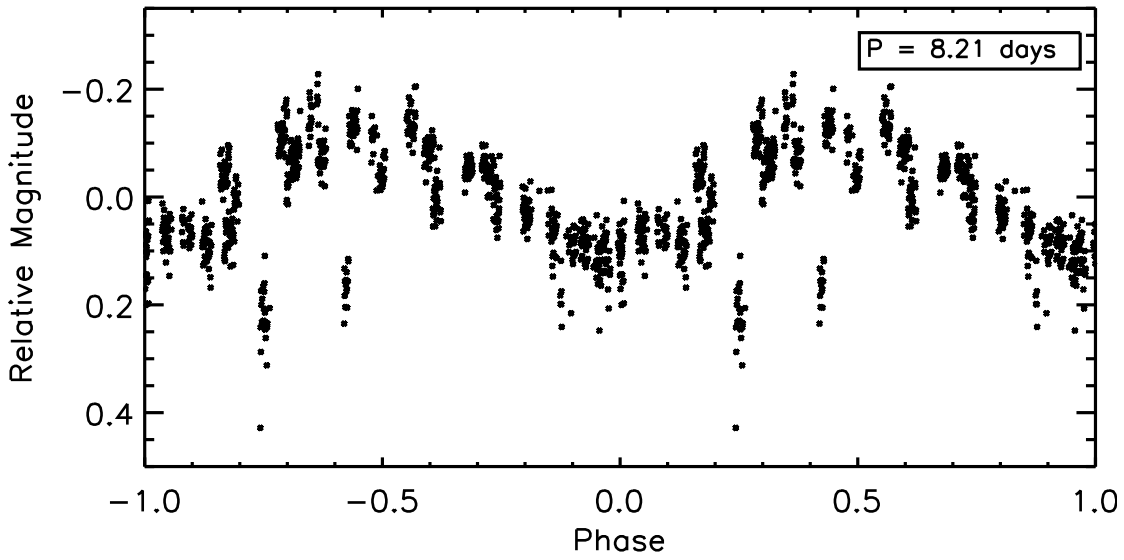

Figure 4.3: KELT-North Season 1 light curve of AA Tau phased to an 8.21 day period recovered from LS analysis.

tions, December 2013 (see Figure 4.4). This means the sudden dimming event has lasted ∼3 years and is likely still occurring.

During the dimming, we do not recover the ∼8 day periodicity. During the dimming event, AA Tau is near the sensitivity limit of KELT-North. Therefore, we cannot conclusively rule out the possibility of a periodicity during the dimming. However, the ∼1 mag variability that is characteristic of T Tauri stars, is clearly observed in both the KELT-North and CRTS data sets. Moreover, Bouvier et al. [2013] did clearly observe the ∼8 day quasi-periodic variability during a 3 month period in 2012/2013. They suggest the reason that the 8-day periodicity is not observed throughout the 2011 dimming is that the observed light has become dominated by scattered light originating from high latitudes on the star. Consequently, the 8-day modulation of the equatorial latitudes by the magnetically warped inner disk seen during AA Tau bright state is not continuously observed, even though the 8-day periodicity does in fact continue [Bouvier et al., 2013].

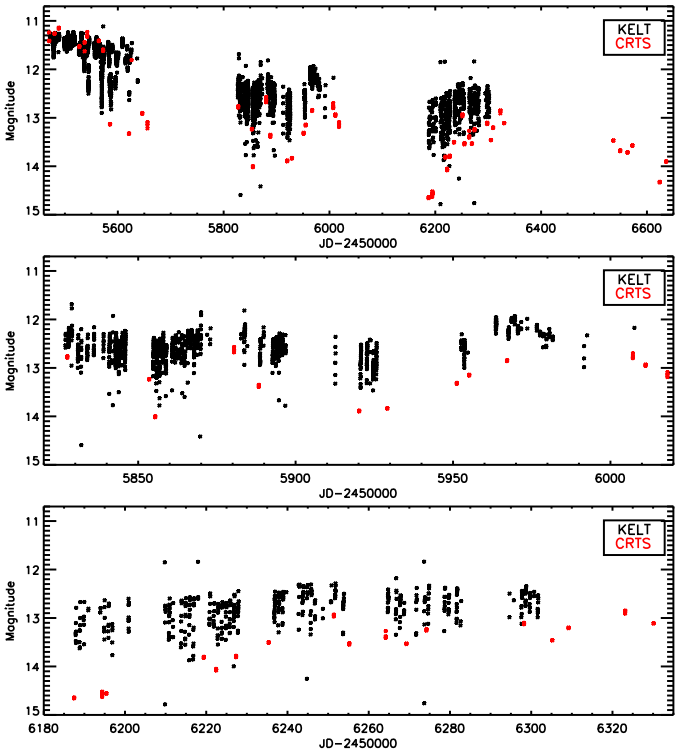

Figure 4.4: (Top) KELT-North (Black) and CRTS (Red) light curves of AA Tau during the 2011 sudden dimming event. (Middle) A zoom-in of the first full KELT-North season during the dimming. (Bottom) A zoom-in of the second full KELT-North season during the dimming.

4.4.2 **V409 Tau**

In the KELT-North and CRTS data, we observe two separate instances where V409 Tau has clearly dimmed below the known brightness level for an extended period of time. In this section, we discuss the observational characteristics of these events. We also analyze the general photometric variability seen both during and outside the two prominent dimming events.

4.4.2.1 Out-of-Dimming Variability

Young stars tend to display both periodic and aperiodic photometric variability, both of which can be caused by circumstellar extinction and accretion of material onto the star's surface [Herbst et al., 1994, Grinin et al., 2004, Petrov and Kozack, 2007]. Xiao et al.

[2012] found a 4.754 day, 0.3 mag amplitude periodicity in TrES photometric observations of V409 Tau [Alonso et al., 2007]. The goal of our LS analysis was to recover the previously known period for V409 Tau. Using LS analysis to search for periodicities of less than or equal to 1000 days, we do not find any evidence of a significant periodicity in the combined KELT, SuperWASP, CRTS, and ASAS photometric data sets. However, using only the KELT-North season 1 data we recover a 4.5 day period and using only KELT-North season 5, we recover a 4.7 day period (see Figure 4.2). We fit a Fourier series, with 5 harmonics, to remove long term trends in season 5 of KELT. A phased plot (4.737 day period) of the KELT-North season 5 data (with the long term trends removed) is shown in Figure 4.5. These periods are similar to the period seen by Xiao et al. [2012].

Prior to the dimming events seen in 2009 and 2012, V409 Tau appears to display some photometric variability with amplitude varying from 0.5-2 mags. This variability is also seen during both dimming events. Unfortunately, we have not found any archival photometric observations of V409 Tau prior to 2002, which hinders our ability to determine the longevity of the variability we present here. There are reported observations from UT 1962 October 22 until UT 1964 July 13 by Romano [1975]. These observations display a light curve that begins at a magnitude of ∼15 and ends at ∼13.5. Interestingly, this feature has similar properties to the dimming events seen by the KELT-North and CRTS data.

The V409 Tau light curves do show dimming features of much shallower depths and shorter duration in the KELT, SuperWASP, CRTS, and ASAS from 2002 to 2007. The data sampling is much sparser during this period, which hinders our ability to determine if these are true variations or if they are just artifacts of the data quality and sampling. Between the 2010 and 2013 events, for about ∼500 days, V409 Tau brightened back to its normal V mag of ∼12. During this period, the typical chaotic variability is clearly observed.

4.4.2.2 2009-2010 Dimming Event

In late January 2009, V409 Tau dimmed significantly from a pre-dimming brightness of $V \sim 11.8$ down to $V \sim 13.2$ (Figure 4.6a). In the KELT-North and CRTS data, this dimming begins at a JD~2454850 (Terrestrial Time (TT)). It is clear, however, that this dimming event has a peak depth below the long-term median of ~1.4 mag and that it sustained for over a year. Since there is no known companion to V409 Tau, we assume the entire dimming is caused by a decrease in the brightness of the host star, corresponding to a decrease in flux of 72%.

After the ~200 day long observing gap beginning at JD~2454900 (TT), V409 Tau is clearly fainter by ~1.4 mag and stays fainter through the extent of the observing season (until JD~2455300 (TT)). Over the course of this observing season (KELT-North observing season 4), where V409 Tau is in a dim state, the brightness of the system increases by a few tenths of a magnitude. After the following seasonal observing gap, V409 Tau is back at its nominal pre-dimming brightness level of V~11.7, the median brightness of KELT-North observing season 3. Due to the end of the seasonal observing gap, we cannot determine exactly when the dimming event of V409 Tau ended and can only place an upper limit on the duration of the event.

If the event began at JD~2454850 (TT), then the maximum duration we estimate is ~630 days (the red vertical lines in Figure 4.6), however this is necessarily an upper limit on the dimming duration. We estimate the ingress of this event to be ~240 days (grey shaded region in Figure 4.6) but this is not well constrained due to the seasonal observing gaps, and could have been much shorter.

A significant amount of structure can be seen during the dimming. Unfortunately, during the dimming event, the star's brightness is quite low, nearly consistent with zero flux for KELT-North, thus complicating the analysis. The CRTS observations appear to show a slightly deeper event then seen in KELT-North. This is likely attributed to the CRTS data being in the V filter while the KELT-North observations are in a broad R filter. How-

ever, there is a short-term variability in the KELT-North and CRTS data starting around JD~2455170 (TT) and ending at JD~2455289 (TT), and that is similar in amplitude to that seen outside of the dimming. This variability may continue for a longer but the KELT-North and CRTS data sets ended due to the seasonal observing window. In any case, there is evidence for continuing variability during the dimming, as in AA Tau, and that is similar in nature to the short timescale variations seen outside of the dimming event.

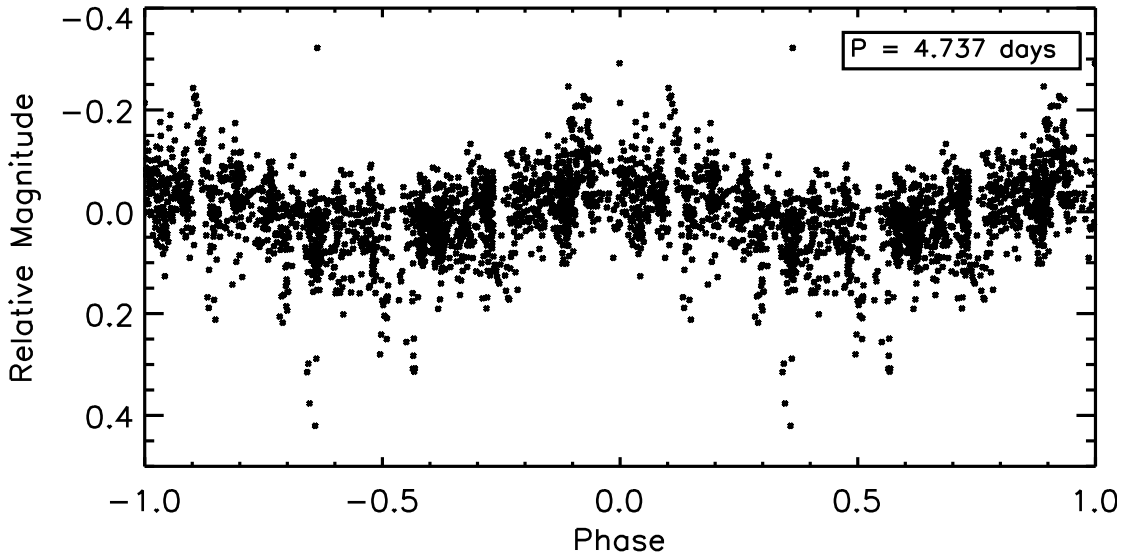

Figure 4.5: KELT-North Season 5 light curve of V409 Tau phased to a 4.723 day period recovered from our LS analysis. A 5 harmonic Fourier series was fit to the data to remove long term trends.

4.4.2.3 2012-2013 Dimming Event

In May 2012, V409 Tau experienced another large dimming event, from a pre-dimming brightness of $V \sim 11.8$ down to $V \sim 13.2$ (Figure 4.6b). This event is quite similar to the 2010 event discussed in the previous subsection. We estimate the ingress of this event to be ~275 days, slightly longer than the 2009 event, but again this parameter is not well constrained. This event lasted through the extent of the KELT-North and CRTS data sets. Similar to the 2009-2010 dimming, the CRTS observations appear to show a slightly deeper event then seen in KELT-North. For this dimming event, both the ingress and potential egress

appear to be located in the seasonal observing gaps for V409 Tau, hindering our ability to determine key characteristics such as the duration ingress and egress. Thus, we cannot determine whether this dimming event was of a similar duration to the 2010 event, which were separated by ~1000 days. We can rule out the possibility that this specific ~600 day long, 1.4 mag depth dimming event is periodic because we should have detected another event around JD~2454200(TT). Although there is a gap in the combined photometric coverage from all data sets around this time, it is not large enough to completely miss another event similar in duration to what was seen in 2010 and possibly 2012. However, a ~1.5 mag brightening event was observed from 1962 till 1964 by Romano [1975] using observations from the 40/50/100 cm Schmidt telescope at Asiago. It is possible that Romano [1975] measured the recovery of another dimming even and this type of dimming is periodic in V409 Tau. However, with the lack of photometric coverage between the early 1960's and the start of our photometric data set (2002), it difficult to be conclusive.

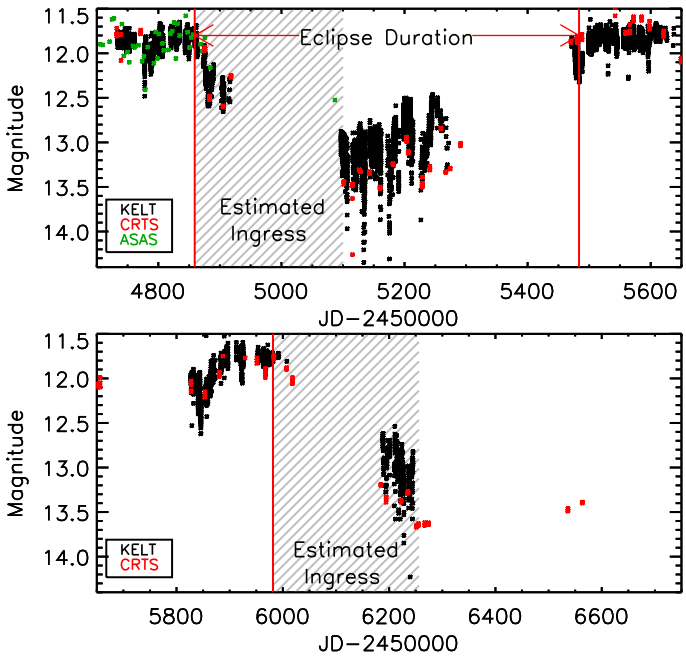

Figure 4.6: KELT-North (Black), CRTS (red) and the ASAS (green) light curves of V409 Tau during the first (top) and second (bottom) dimming events. The shaded region corresponds to the estimated duration of the events ingress.

4.4.2.4 Spectral Energy Distribution Analysis

We assembled the available broadband flux measurements of V409 Tau (not observed during one of the large dimming events) from the literature and also measured a new flux at 3 mm using the CARMA array (see Table 5.1). We fit these fluxes using the star+disk spectral energy distribution (SED) model grid of Robitaille et al. [2006a, 2007], based on the radiation transfer code of Whitney et al. [2003b,a]. Briefly, these SED models represent young stars with disks and/or envelopes for physical parameters spanning a large range of stellar masses, temperatures, and luminosities, and for disk parameters spanning a large range of sizes, structures, accretion rates, and inclinations on the plane of the sky. Additional free parameters include the line-of-sight extinction and distance to the system.

Figure 4.7 shows the observed SED and the family of best-fit models satisfying a goodness-of-fit criterion of $\Delta\chi^2/\chi^2_{\rm min} < 3$ per data point [see, e.g., Robitaille et al., 2007, for discussion of this statistical criterion]. Note that the SED models included in the Robitaille et al. [2006a] grid extend only to λ = 1mm so Figure 4.7 extends only to 1 mm. The SED models in gray represent the various star+disk parameter combinations that are formally consistent with the data according to the above χ^2 criteria.

To further narrow the range of possible SED models, we additionally required the model SED parameters to include a stellar $T_{\rm eff}$ within 300 K of that determined by Luhman et al. [2009], a total line-of-sight extinction within 0.3 mag of the A_J = 1.3 also determined by Luhman et al. [2009], and a distance of 140±40 pc (i.e., within 40 pc of the nominal Taurus-Auriga association distance). Applying these additional constraints significantly reduces the SED models that can fit the data to within the χ^2 goodness-of-fit criterion above, leading to a single model in the Robitaille et al. [2006a] grid (solid black SED in Figure 4.7). This model has a disk that is inclined at an angle of 81°, i.e., nearly edge-on. We take this as suggestive that the V409 Tau disk is fully consistent with being nearly, but not precisely, edge-on while satisfying the other observed constraints for the system. The new CARMA observation at 3 mm is not included in the fit but is consistent with a simple

Table 4.4: Archival flux measurements of V409 Tau used in the SED analysis.

Band	Flux[a]	Error[b]	Reference
NUV	0.030	0.021	GALEX
u'	17.5	1.0	SDSS
g'	15.5	0.7	SDSS
r'	13.0	0.7	SDSS
i'	12.0	0.7	SDSS
z	11.7	0.7	SDSS
J	10.7	0.5	2MASS
H	9.6	0.5	2MASS
K_S	9.0	0.5	2MASS
WISE1	8.3	0.3	WISE
WISE2	8.0	0.3	WISE
WISE3	5.6	0.3	WISE
WISE4	3.8	0.3	WISE
IRAC1	8.1	0.3	Spitzer
IRAC2	7.8	0.3	Spitzer
IRAC3	7.3	0.3	Spitzer
IRAC4	6.3	0.3	Spitzer
MIPS1	4.4	0.3	Spitzer
MIPS2	1.7	0.3	Spitzer
MIPS3	−1.45	Upper limit	Spitzer
0.89 mm	48.8 mJy	22.2 mJy	Luhman et al. [2009]
1.3 mm	18.7 mJy	1.4 mJy	Luhman et al. [2009]
3 mm	2.87 mJy	0.28 mJy	this work

[a]Magnitudes unless otherwise indicated.
[b]Single-epoch errors have been inflated to reflect time variability of the source.

extrapolation of the best-fit model.

4.5 **Interpretation**

In this section we present the most plausible interpretation of both the sudden dimming event of AA Tau and the dimming events seen from V409 Tau. For AA Tau, we concur with the previous observations and interpretations by Bouvier et al. [2013] that the dimming is likely caused by an occultation of the host star by a higher density region of the circumstellar disk. For V409 Tau, we also interpret the dimming events to be caused by an occultation of the host star by a one or more features in the circumstellar disk, predicted

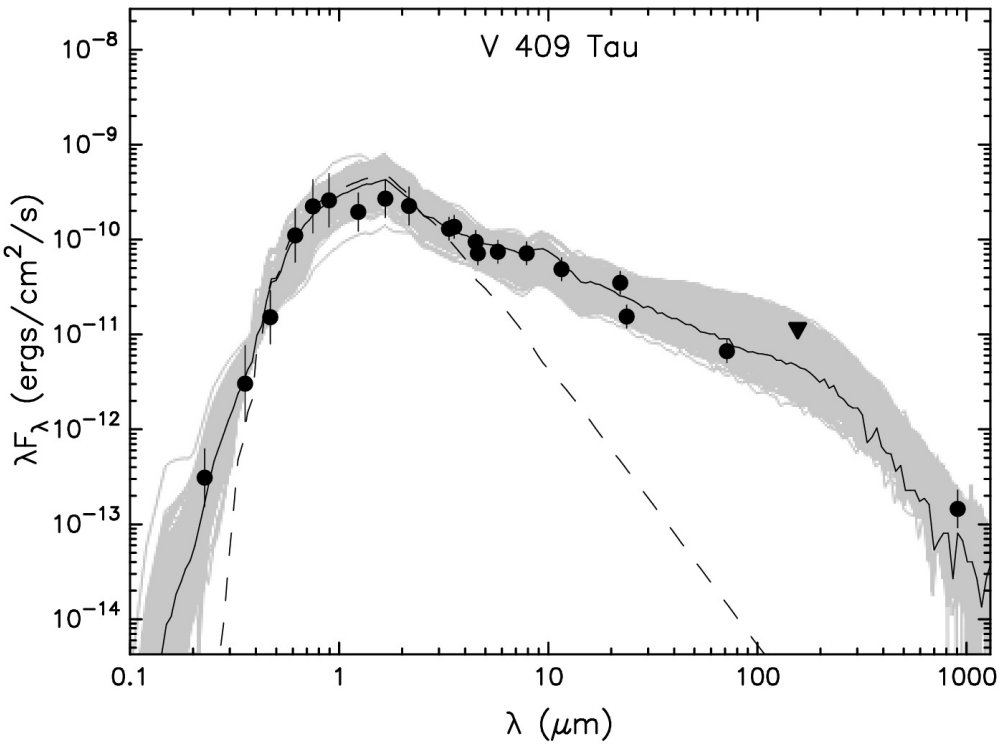

Figure 4.7: Spectral Energy Distribution fit for the V409 Tau system. Symbols with error bars represent flux measurements with uncertainties, and inverted triangles represent 3σ upper limits (see Table 4.4). The dashed curve represents the photosphere while the gray curves represent all of the star+disk models that are consistent with the data to application of the $T_{\rm eff}$, A_J, and distance criteria. The solid curve represents the final best-fit SED including all observational constraints (see the text).

from our SED analysis. Below we explore the involvement of each system's circumstellar disk in the large dimming events observed.

4.5.1 **AA Tau**

Bouvier et al. [2013] suggests that the deep and sudden dimming of AA Tau is likely due to an increase in extinction from an overdense region in the known circumstellar disk on a Keplerian timescale. In this section, we calculate the parameters of this feature from the KELT-North and CRTS data, assuming the feature is located in the disk plane. We compare our results with the work done by Bouvier et al. [2013].

Using observations from the Crimean Astrophysical Observatory (CrAO), Bouvier et al.

[2013] determined that AA Tau took ~200 days to reach minimum brightness. From the KELT-North and CRTS data, we visually estimate the ingress of the AA Tau dimming to be ~300 days long, beginning in late November or early December of 2010. Since AA Tau was in a consistently bright state for 24 years and the host star is ~0.8 $M_{\odot}$, Bouvier et al. [2013] determined that the occulter would have a semi-major axis ≥ 7.7 AU. Given the known inclination of the circumstellar disk around AA Tau, we can estimate the height of the feature that caused the dimming, assuming it is located in the disk plane. Using a semi-major axis of 7.7 AU and a disk inclination of ~ 71°, this would require a scale height of ~7.3 AU for the occulter to cross the line of sight. The duration of the event is ~800 days and it has not begun to recover to its pre-dimming median brightness through the extent of our data set. Using a stellar mass of 0.85 $M_{\odot}$and a semi-major axis of 7.7 AU, this would require the azimuthal extent of the feature to be over 46°, or > 6 AU.

Given the measured and calculated parameters of the occulting feature, we can model the dimming event as an occultation of the host star by a large body in a Keplerian orbit. This body cannot have a leading edge perpendicular to its direction of motion because it would be moving too slowly to be located within the body of the circumstellar disk. Rather, we model the occulting object to have a leading edge that is slightly inclined from its direction of motion, i.e., "wedge" shaped. Assuming the feature causing the dimming is located within the estimated radius of the AA Tau disk, i.e., within 215 AU [Kitamura et al., 2002], and assuming an ingress timescale of 200 days, this would require the leading edge of the feature to be <4.6° (<3.2° for ingress of 300 days), close to parallel with its direction of motion. Using an ingress duration of 200 days and a wedge angle of 5°, the transverse velocity of the occulter would be $2(1.84\,R_{\odot})/(T_{ingress}\sin\theta)$ ~1.7 km s^{-1}. Assuming Keplerian motion, this would place the occulting object near the edge of the circumstellar disk. For the body to be located at 7.7 AU, the minimum semi-major axis determined by Bouvier et al. [2013], the leading edge of the occulter would need to have a wedge angle of <1°. The long duration of the AA Tau dimming can be interpreted in

multiple ways, including a wedge, a fuzzy edge, and/or scattered light. Since we can't definitively determine which of these is correct, we adopt the wedge model presented above as a way of developing an illustrative model that is representative of the timescales and spatial scales involved.

4.5.2 **V409 Tau**

From the SED analysis, we have shown that V409 Tau has an infrared excess indicative of a circumstellar disk, specifically one that is nearly edge-on. We interpret the dimming events as occultations of the host star by one or more features in the circumstellar disk. This interpretation is supported by our observations since the ~1 magnitude variability, seen prior to the dimming events, is apparent during the dimming. We believe the short-term variability arises on or near the stellar surface. Therefore, an occultation by material much farther away in the disk would have no effect on the fractional amplitude of the short term variability.

Through simple kinematic and geometric arguments, we are able to estimate certain parameters of the occulting body. One key parameter necessary for calculating the properties of the occulting body is the radius of V409 Tau. Using prior observables of Log(T_{eff}) = 3.56 ± 0.02, Log(L/$L_{\odot}$) = -0.59± 0.08 and [Fe/H] = -0.01 ± 0.05 for V409 Tau [Andrews et al., 2013, D'Orazi et al., 2011], we use the Dartmouth Stellar Evolution Programs young stellar models within a Markov Chain Monte Carlo (MCMC) to derive posterior distributions for the mass, age and radius of V409 Tau (see Figure 4.8) and the most probable parameters (with 68% confidence interval uncertainties) [Dotter et al., 2008]. From this analysis, we determine an age of $2.78^{+6.10}_{-0.42}$ Myr, a mass of $0.57^{+0.16}_{-0.13}$ $M_{\odot}$and a radius of $1.11^{+0.20}_{-0.07}$ $R_{\odot}$.

We can repeat the same kind of model calculations for V409 Tau as we did for AA Tau. That is an occultation of the host star by a large body in a Keplerian orbit, possessing a slightly inclined wedge-shaped leading edge. Beginning with the 2009 dimming, we

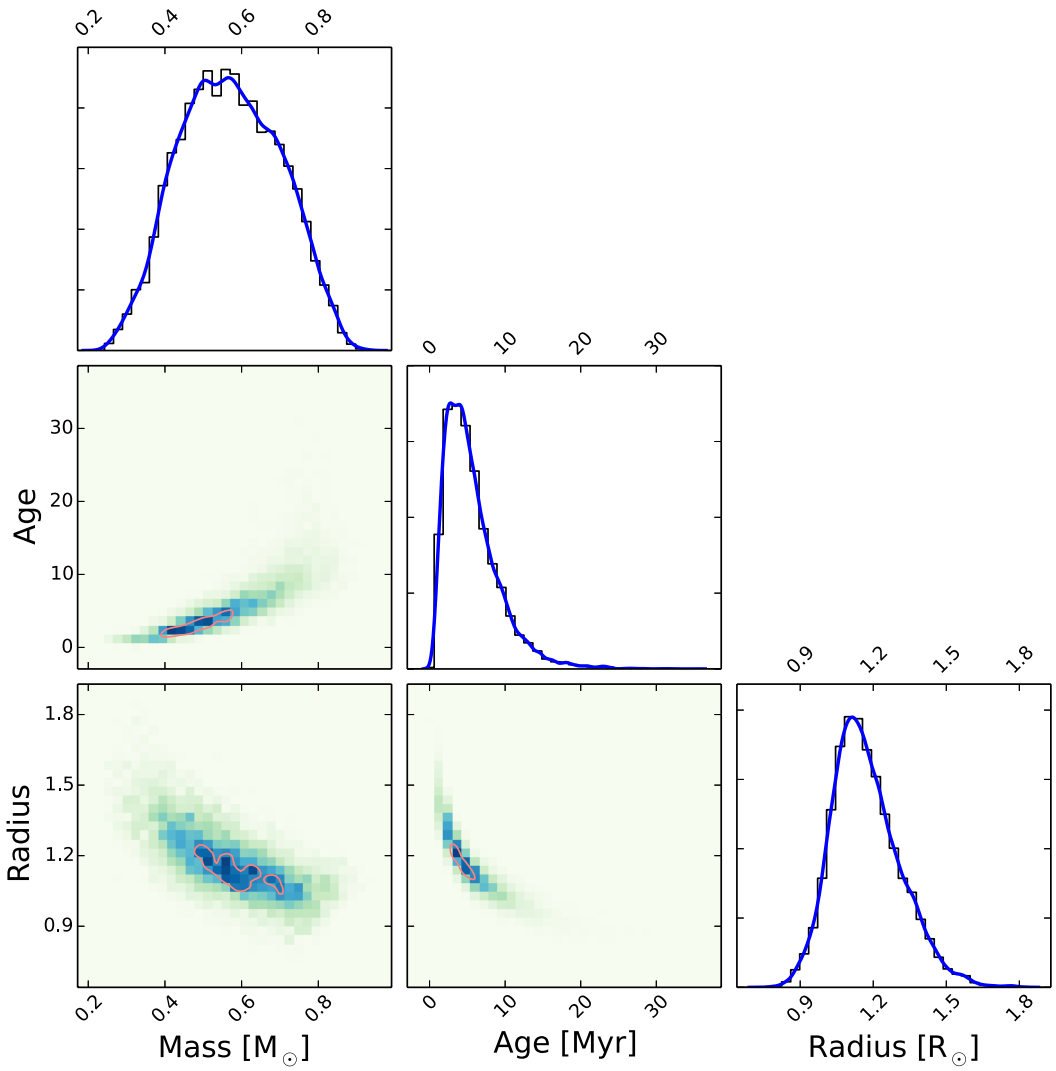

Figure 4.8: The posterior distributions of mass, age, and radius, and our determined parameters (w/ 68% confidence interval uncertainties)

estimate the ingress timescale to be ~240 days. Since we do not have an estimate of the outer disk radius for V409 Tau, we constrain the feature to the known radius of the AA Tau circumstellar disk, ~215 AU [Kitamura et al., 2002]. At 215 AU, this would require the leading edge of the occulter to have a wedge angle $< 2.8°$ for an ingress of 240 days (see §4.2.2). We estimate the ingress of the 2012 event to be close to 275 days (see §4.2.3) which constrains the leading edge wedge angle to be $< 2.5°$. Both of these estimated leading-edge wedge angles correspond to the feature being located at the outer edge of the circumstellar

disk.

Observations by Romano [1975] show a brightening of V409 Tau from a visual magnitude of 15 to ~13.5 over the time-span of 630 days. From their data, it is possible that they observed the end of another dimming event. If they did observe another dimming event, then the full duration would likely be longer than the 2009 and 2012 events seen in the KELT-North and CRTS data. Without other photometric observations between our data and the observations in the 1960's by Romano [1975], we are unable to better constrain a potential periodicity. There is just over 46 years between the end of the 1962 brightening event and the end of the 2009 event. Since there are two consecutive potential occultations of V409 Tau in our data and one from the 1960's data by Romano [1975], if we assume they are all related, we can interpret them in two ways: 1) They are caused by two separate features orbiting in similar locations of the circumstellar disk. 2) A single feature is responsible for all three events.

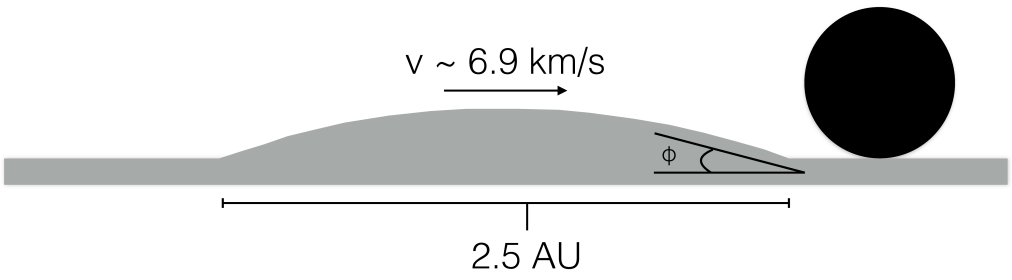

Figure 4.9: A diagram displaying the theoretical warp or "wedge-shaped" feature in the V409 Tau disk that has a shallow leading edge or "wedge angle". Not to scale. Φ corresponds to the leading edge angle or wedge angle.

If the 2009 and 2012 events are from two separate features within the circumstellar disk with a minimum period of ~46.25 years (the time between the 1962 and 2009 events),

assuming Keplerian motion and using our derived parameters for the stellar mass of V409 Tau, this would require the semi-major axis of the occulting feature to be >10.7 AU. At this distance from the star, the feature would have a very shallow "wedge-shaped" leading-edge angle of ~0.6° corresponding to a transverse velocity of $2(1.11R_{\odot})/(T_{ingress}\sin\theta)$ ~6.9 km s^{-1}. Using the full estimated maximum duration of the 2009-2010 dimming, ~630 days, this would require the feature to have a width of ~2.5 AU (see Figure 4.9. The beginning of the 2012 dimming is ~1130 days after the 2009 one. Using the same assumptions as above and that the second feature is orbiting with a period ~1130 days longer than the first, this would require a semi-major axis of >11.1 AU, velocity ~6.8 km s^{-1} and a leading edge wedge angle of ~0.5°. We interpret this feature as two separate warps or perturbations in the circumstellar disk that have crossed our line of sight. Another possibility is that we are seeing two separate dust clumps (or high density regions), located in a similar location of the disk. Simulations show that dust clumps can form in groups and then combine in the disk over time, which could be the beginning processes of planetary formation [Fromang, 2005].

The second interpretation is that a single feature caused all three dimming events observed. Assuming this scenario would imply a periodicity of ~1130 days, the time between the 2009 and 2012 events. This would place the occulting feature ~1.7 AU from the star. This would also imply that the duration and depth is changing on a dynamical timescale, since we should have observed two more dimming events in 2006 and 2002. Examining the KELT-North observations around those dates, there is a hint of potential dimming events, but the behavior is more consistent with the ~1 mag short period photometric variability that are commonly known for T Tauri stars [Herbst et al., 1994]. However, since the circumstellar disk around V409 Tau is likely close to being edge-on (from our SED analysis), any small fluctuation or change in the thickness of the disk would strongly affect the optical brightness. Nelson et al. [2000] showed that heating and cooling of the inner disk (inside 10 AU from the host star) would show fluctuations in the spatial distribution of the grains

on the timescale < 10 years. Since both observed dimming events have durations estimated to be shorter than 10 years, they are consistent with heating and cooling timescales in the disk.

From our SED analysis (see §4.2.4), our best fit model has a disk inclination of ~81°. Again, this is only suggestive and we only conclude that the disk is likely close to but not exactly edge-on. From our analysis, we estimate that the feature would be >10.7 AU from the host star if we interpret the events in our data to be caused by different features in the disk, but related to the event seen in the early 1960s. If we interpret the events to be caused by one feature, the estimated semi-major axis of the feature would be 2 AU. Adopting the the disk inclination of 81° at a semi-major axis of 10.7 AU and 2 AU, the required height of the warp would only need to be 2 AU and 0.3 AU respectively. Therefore, it would only take a relatively small perturbation to cross our line of sight. Also, we estimate from kinematics the width of the feature to be 2.5 AU from kinematics. We would expect that a warp would be wider than tall which is possible in this scenario. These estimates dont consider that the disk could flare out as a function of radius, which has been seen in many other disks [Espaillat et al., 2010].

4.6 **Conclusions**

The study of stars being occulted by circumstellar material can provide useful information about the environments and dynamics of YSOs. This information may be of great value for our understanding of how planetary systems evolve. New observations of AA Tau from the KELT-North survey allow us to expand on the analysis performed by Bouvier et al. [2013]. The sudden dimming that began in late 2010 appears to still be occurring without any signs of recovery. We are able to use the data to constrain proprieties of the occulting feature, assuming Keplerian motion.

New observations of V409 Tau from the KELT-North survey show that the system experienced two separate, ≥630 day long ~1.4 mag dimming events in early 2009 and mid-2012.

Our observations also show a photometric variability on the timescale of days to weeks occurring before and during the events. Both of these characteristics are a common behavior of UXor stars. The events were confirmed independently by the Catalina Real-time Transient Survey. A brightening of V409 Tau was seen in the early 1960's by Romano [1975]. It is possible that this event was another dimming followed by a brightening. Our SED analysis models the V409 Tau system to have a nearly edge-on disk. Using KELT-North photometric observations of AA Tau as a direct comparison, we interpret the V409 Tau dimming events as occultations of the host star by one or more features in the nearly edge-on circumstellar disk. We see that both stars display both the short period (days to weeks) variability and long term dimming events (months to years) that are commonly associated with T Tauri and UXor stars.

The timescales of the two dimming events in V409 Tau are consistent with a fluctuation in the disk's thickness, but it is also possible that they are caused by an occultation of the host star by a warp or perturbation in the circumstellar disk. The short period chaotic variability, presumably due to spots and/or accretion on the stellar surface, is also apparent during the dimming events of V409 Tau, further supporting the occultation scenario by circumstellar disk structures far from the inner disk where the short-timescale variations presumably arise.

These results motivate additional observations to monitor the V409 Tau system for another dimming event. Like AA Tau, V409 Tau should serve as a valuable laboratory for detailed studies of the structure of protoplanetary environments around low-mass pre-main-sequence stars. The use of photometric surveys like KELT to discover and characterize the occulation of young stars by their circumstellar disks will be applicable to future surveys such as the Large Synoptic Survey Telescope (LSST). With LSST, we will be able to significantly increase the sample size of these rare and valuable systems.

Chapter 5

An Extreme Analogue of ϵ Aurigae: An M-giant Eclipsed Every 69 Years by a Large Opaque Disk Surrounding a Small Hot Source

5.1 Introduction

One of the most well studied eclipsing binaries (EB) is ϵ Aurigae (HD 31964). At $V \sim 3$ and having the longest known orbital period for an EB (~27.1 yr), this unique system has become a prime target for extensive characterization. The primary eclipse has a depth of 0.8–1.0 mag (visual) and lasts for ~2 yr. The primary star is an evolved F0 giant first proposed as being eclipsed by a very large faint companion Carroll et al. [1991]. The Spectral Energy Distribution (SED) of ϵ Aur was reproduced using 2 components: a 2.2 $M_{\odot}$post-asymptotic giant branch F star, and a 5.9 $M_{\odot}$B5V star with a thick semi-transparent disk [Hoard et al., 2010]. Using the CHARA array to obtain interferometric images during the 2009-2011 eclipse, Kloppenborg et al. [2010] confirmed the eclipse to be caused by a dark companion with a tilted disk.

In this work, we present the analysis of TYC 2505-672-1, a system similar to ϵ Aur, but with an even longer period of ~69.1 yr, making it now the EB with the longest known period. We use catalog photometry fortuitously obtained both during and prior to eclipse for an analysis of the system spectral energy distribution (SED), and we use extensive photometric observations from the Kilodegree Extremely Little Telescope (KELT) together with archival observations spanning 120 yr. The primary component of the system is an M-type red giant that over the past century has shown two very deep, multi-year-long dimming events, most recently noted in Astronomer Telegrams by the MASTER Global Robotic Net [Lipunov et al., 2010]. It has been suggested that the dimmings are caused by either R Coronae Borealis (RCB) events of the M-giant [Denisenko et al., 2013] or by a very long-period eclipse of the M-giant by a large, faint companion as in ϵ Aur [Tang et al., 2013].

From our SED and light curve analysis, we interpret the dimmings to be caused by a small, hot companion surrounded by a large opaque disk eclipsing the M-giant primary star every ∼69 yr. However, as we discuss, the evolutionary status of this hot companion is unclear, but may be a rare example of a low-mass, recently "stripped red giant" destined to become a Helium white dwarf, such as that reported by Maxted et al. [2014].

5.2 Characteristics of the TYC 2505-672-1 System

The known properties of the TYC 2505-672-1 (2MASS J09531000+3353527) system (α = 09h 53m 10.0043s, δ = +33° 53′ 52.734″; V∼10.71) are a bit sparse [Hog et al., 1998, Høg et al., 2000]. Afanasiev et al. [2013] observed the optical spectra of TYC 2505-672-1 during the dim state and found it to be consistent with an M1 III red giant. They did observe H-alpha emission in the spectra and suggest that the M-giant might be entering an RCB phase. Pickles and Depagne [2010] found from spectral template fitting a best-fit spectral type of M2 III; in order to be as conservative as possible in estimating the stellar and system parameters, we adopt a very broad range of spectral types (M0-8IIIe) for the primary star in the analysis that follows.

5.3 Data

Over the past century, multiple surveys have observed TYC 2505-672-1 at a variety of cadences (see Figure 5.1). Note that over the ∼120 yr time span of the data there have been two apparent eclipses, one recently in 2011–2015, and one sparsely sampled around 1942–1945. We next describe these photometric light curves, and the available catalog broadband absolute photometric data, in turn.

5.3.1 KELT-North

The Kilodegree Extremely Little Telescope (KELT-North) is an ongoing photometric survey searching for transiting planets around bright (V = 8-11) stars. KELT-North uses a Mamiya 645-series wide-angle lens with a 42mm aperture and a 80mm focal length (f/1.9), corresponding to a large field of view (26° × 26°) with a plate scale of 23″ per pixel. The telescope has a non-standard filter, comparable to an extra-broad R-band, with a typical photometric RMS precision of <1% for bright stars, but varies substantially across the KELT field. The survey observes a predefined set of fields with a ∼15 minute cadence through the entire season of visibility of each field [Pepper et al., 2007]. TYC 2505-672-1 is located in KELT-North Field 06, which is centered on (α = 09hr 46m 33.752s, δ = +31° 39′ 24.11″). KELT-North observed this field from UT 2006 October 27 to UT 2014 December 21, obtaining 9,320 images. The data were reduced using a heavily modified version of the ISIS software package, described further in §2 of Siverd et al. [2012]. The photometric scatter (outside the eclipse) of the KELT-North light curve for TYC 2505-672-1 is ∼2%, roughly consistent with the expected scatter for a target of this brightness located at its position in the KELT-North field. Observations during the eclipse are at the observational limit of KELT-North. Therefore, we do not trust the observed in-eclipse variability from the KELT-North data.

5.3.2 American Association of Variable Star Observers (AAVSO)

The Association of Variable Star Observers (AAVSO) is a worldwide network of amateur and professional astronomers dedicated to the understanding of variable stars. AAVSO monitored TYC 2505-672-1 from UT 2013 February 08 until UT 2015 September 22, obtaining 246 observations in V band (and visual observations). The observations presented in this work were taken by 18 different observers from the AAVSO network. Many of the AAVSO members use an web interface photometry tool on the AAVSO website called

Variable star PHOtometry Tools (VPHOT). The average error from all observers is 0.02 mag with a standard deviation of 0.35 mag.

5.3.3 Digital Access to a Sky Century at Harvard (DASCH)

The Digital Access to a Sky Century at Harvard (DASCH) survey is a digitized version of the Harvard astronomical photographic plate collection. These observations allow the astronomical study of objects on the century-long time scale. To date, they have scanned over 100,000 plates corresponding to over 7 billion measured magnitudes. The DASCH observations are in the B bandpass and have limiting magnitude of 15 (this value does vary). The DASCH data release 4 represents observations from 1885 to 1992 (see Grindlay et al. [2012] for an overview of the survey). The DASCH survey observed TYC 2505-672-1 from UT 1890 March 08 until UT 1989 December 01, obtaining 1432 observations. Only some of the observations have listed errors. The average of the listed errors is 0.1 mag with a standard deviation of 0.03 mag.

5.3.4 Catalina Real-time Transient Survey (CRTS)

The Catalina Real-time Transient Survey (CRTS) is a wide photometric survey consisting of 3 telescopes covering 33,000 Deg^2 to find rare transient objects. All transient objects are openly published within minutes of the observations. See Drake et al. [2009] for information about the survey and data reduction process. CRTS observed TYC 2505-672-1 from UT 2006 February 22 until 2013 June 05, resulting in 78 measurements. The photometric values are determined using the SExtractor software package [Bertin and Arnouts, 1996]. The average error for the CRTS observations is 0.055 mag with a standard deviation of 0.005 mag.

5.3.5 All-Sky Automated Survey for SuperNovae (ASAS-SN)

The All-Sky Automated Survey for SuperNovae (ASAS-SN or "Assassin"; Shappee et al. [2014]) is a long-term project to monitor the whole sky down to a limiting magnitude of $V \sim 17$ mag with the highest cadence possible using a global network of telescopes with a modular design. The focus of the survey is to find nearby supernovae (SNe) and other bright transient sources. Currently, ASAS-SN consists of two fully robotic units on Mount Haleakala in Hawaii and Cerro Tololo in Chile. Each unit has four telescopes on a common mount and is hosted by Las Cumbres Observatory Global Telescope Network. Each telescope consists of a 14-cm aperture Nikon telephoto lens and a 2k $\times$ 2k thinned CCD, giving a 4.5×4.5 degree field-of-view and a 7.8"pixel scale. These 8 telescopes allow ASAS-SN to survey 20,000 deg^2 per night, covering the entire visible sky every two days. The pipeline is fully automatic and discoveries are announced within hours of the data being taken. ASAS-SN has observed the field containing TYC 2505-672-1 141 times since UT 2012 January 23. For the ASAS-SN data, we remove epochs affected by clouds and performed aperture photometry using the IRAF `apphot` package and calibrated the results using the AAVSO Photometric All-Sky Survey (APASS; Henden et al., 2015). The average ASAS-SN error for TYC 2505-672-1 is 0.022 mag with a standard deviation of 0.021 mag.

5.3.6 Broadband Photometry from the Literature for Spectral Energy Distribution Modeling

In order to ascertain the physical nature of the system, and in particular to help constrain the properties of the occulting body, we assembled all of the available photometry from the literature, which we then use in Section 5.4.1 to model the spectral energy distribution (SED) of the system. All the broadband measurements are listed in Table 5.1, and they are organized for convenience according to whether the available measurements happened to

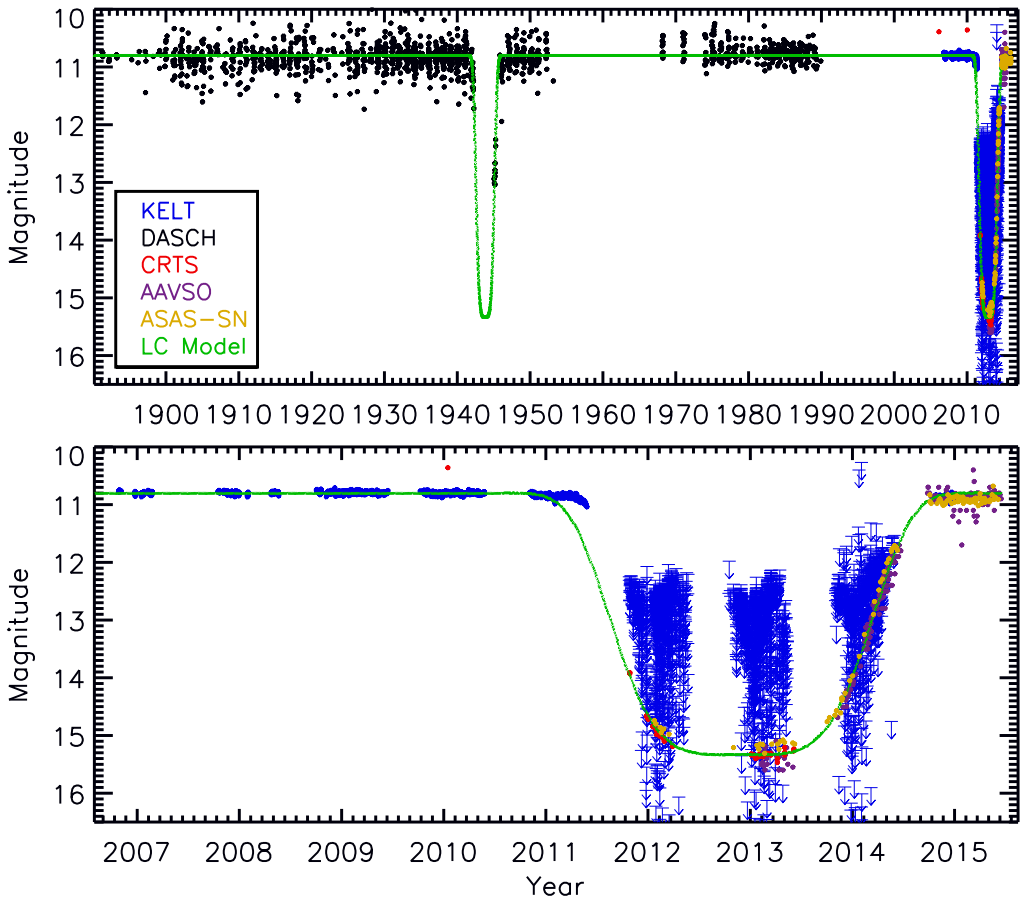

Figure 5.1: (Top) The KELT-North (Blue), DASCH (Black), CRTS (Red), AAVSO (Violet), and ASAS-SN (Yellow) observations plotted from 1890 to 2015. The green line represents a LC model of the combined photometric data. (Bottom) The photometric observations covering the most recent eclipse. The KELT-North observations during the eclipse are below the faintness limit of KELT and are therefore only upper limits. Only the AAVSO, CRTS, and ASAS-SN data are in the Visual and V-band magnitudes. We approximate the all observations to the AAVSO V-band to match the quiescent magnitude of the AAVSO data but no attempt has been made to place all the data on the same absolute scale.

be obtained during occultation or not.

Table 5.1: Archival flux measurements of TYC 2505-672-1 used in the SED analysis.

Band	Magnitude	Error[a]	Source	Reference
FUV	21.07	0.29	GALEX	Bianchi et al. [2011]
NUV	19.476	0.1	GALEX	Bianchi et al. [2011]
u'	14.778	0.05	SDSS	Pickles and Depagne [2010]
g'	11.501	0.05	SDSS	Pickles and Depagne [2010]
r'	10.181	0.05	SDSS	Pickles and Depagne [2010]
z'	9.575	0.05	SDSS	Pickles and Depagne [2010]
BT	13.128	0.279	Tycho-2	Høg et al. [2000]
VT	10.938	0.061	Tycho-2	Høg et al. [2000]
J	7.614	0.05	2MASS	Cutri et al. [2003]
H	6.781	0.05	2MASS	Cutri et al. [2003]
K	6.567	0.05	2MASS	Cutri et al. [2003]
WISE1	9.179	0.065	WISE	Cutri and et al. [2014]
WISE2	9.859	0.05	WISE	Cutri and et al. [2014]
WISE3	11.559	0.1	WISE	Cutri and et al. [2014]
WISE4	12.386	0.05	WISE	Cutri and et al. [2014]
In-Eclipse				
B	16.382	0.05	APASS	Henden et al. [2015]
V	15.032	0.052	APASS	Henden et al. [2015]
g'	15.711	0.05	APASS	Henden et al. [2015]
r'	14.544	0.197	APASS	Henden et al. [2015]
i'	13.755	0.201	APASS	Henden et al. [2015]

NOTES
[a]Single-epoch errors have been inflated to reflect time variability of the source.

5.4 Results

5.4.1 SED Analysis and Implications

As shown in Table 5.1, we are fortunate to have broadband photometry from the literature both outside of occultation and during occultation, at wavelengths from the GALEX FUV band (0.15μm) to the WISE4 band (20μm), providing a rich dataset for modeling the underlying component(s) of the system. As we discuss in Section 5.5, our modeling of the SED conclusively shows that there is a small hot star in the system (possibly a white dwarf), and that this small hot star is likely to be surrounded by a large cool disk.

We fit three separate Kurucz atmosphere models to the available data. First, we fit a

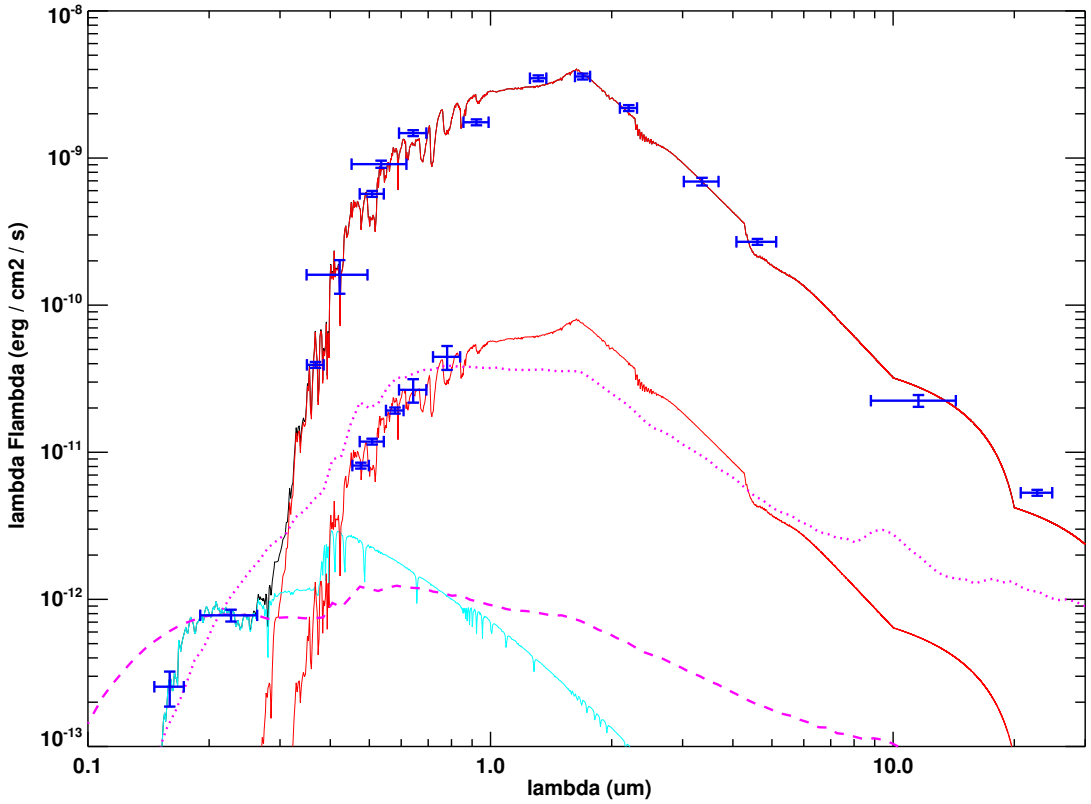

Figure 5.2: Spectral Energy Distribution fit for TYC 2505-672-1. The upper red curve has $T_{\rm eff}$ = 3600 K while lower red curve is the same model but scaled down by a factor of 50. The blue curve is the best fit to the GALEX fluxes; it has $T_{\rm eff}$ = 8000 K. The magenta dashed curve is a low-mass M-dwarf with an accretion rate of 10^{-6} $M_\odot$ yr^{-1}. The dotted magenta curve shows what it would take for a cool star with a low accretion rate to match the GALEX points (a solar-type star accreting at 3×10^{-8} $M_\odot$ yr^{-1}).

cool, low gravity model ($\log g$ = 2.5, as appropriate for a modestly-evolved red giant) to the data obtained outside of eclipse, excepting the GALEX fluxes. Second, we fit the same model to the data obtained during eclipse. Third, we fit a hot source to the GALEX fluxes, with the additional constraint that the sum of this hot source and that of the first step are consistent with the SDSS u-band measurement. In each model fit, the fit parameters were the effective temperature, the extinction, and a normalization. Note that according to the Galactic dust maps of Schlegel et al. [1998], the maximum extinction for this line of sight is A_V = 0.04 mag, therefore the precise extinction value is of minor importance. We adopted solar metallicity for simplicity; these broadband fits are not strongly sensitive to the choice

of metallicity.

The resulting best SED fits are shown in Figure 5.2. The upper red curve has $T_{\rm eff}$ = 3600 K as appropriate for a red giant, and consistent with the spectral class of M2 III found by Pickles and Depagne [2010]. The lower red curve is the same model but scaled down by a factor of 50. The blue curve is the best fit to the GALEX fluxes and to the u-band flux; it has $T_{\rm eff}$ = 8000 K, such as for a cool white dwarf.

It is possible that the small excess apparent in the SED at 20 μm is due to thermal infrared emission from the disk around the companion star. It is beyond the scope of this paper to model such a disk, given the lack of observational constraints on the disk emission. However, if the disk emits strongly as a nearly "flat-spectrum" source then its emission at 20 μm would be on the order of $\sim 10^{-12}$ erg cm^{-2} s^{-1} (based on the peak emission of the companion), which at 20 μm is $\sim$20% of the red giant's photospheric emission and thus could plausibly account for the modest excess emission observed at that wavelength. Observations in the near- to mid-IR during eclipse of the red giant primary would definitively test this possibility.

Our SED analysis provides the following results and interpretations:

(1) UV fluxes. The fact that the system is detected in both the GALEX NUV and FUV bands clearly indicates the presence of a hot component in the system; an M star alone cannot explain this UV excess emission. As can be seen from the SED fit, a secondary star with $T_{\rm eff}$ = 8000 K fits the two GALEX fluxes nicely. It is possible that the UV flux is arising from something other than a stellar photosphere. Specifically, if accretion is occurring in the disk around the companion, this could cause a UV flux from photons inside the disk being scattered and escaping. If the observed UV flux is from accretion onto a cool star, then the photospheric emission of the star will be lower than that of the hot component shown in our SED fit, which would then require a very high accretion rate to reproduce the observed UV flux. Utilizing the SED models of low mass stars with accreting disks from Robitaille et al. [2006b], we attempted to fit the GALEX fluxes with

a low-mass star that is actively accreting from a disk. While a comprehensive search of all possible parameters is beyond the scope of this paper, in general we found that it is not possible to simultaneously fit both GALEX fluxes with such a model and a reasonably low accretion rate. A stellar photosphere with a low accretion rate fitting the GALEX fluxes would require the peak of the photospheric SED to rise far above the blue curve in Figure 5.2 (the magenta dotted line represents a solar-type star accreting at 3×10^{-8} $M_\odot$ yr^{-1}), which would then be inconsistent with the observed SED in eclipse. In order to keep the peak of the photospheric SED low, then the shape of the SED must be relatively flat, such as that shown by the magenta dashed curve, which requires an M-dwarf with a high accretion rate of 10^{-6} $M_\odot$ yr^{-1}, which would then deplete the disk on a very short timescale.

(2) Recent and historical eclipses must both be the primary eclipse; there is not yet an observed secondary eclipse. If the historical eclipse were interpreted as the secondary eclipse, then one could infer the ratio of $T_{\rm eff}$ from ratio of the eclipse depths. From the full observed light curve (Figure 5.1), we may hypothesize that we are seeing two eclipses, a primary eclipse with a depth of ~5 mag that has just recently occurred, and a secondary eclipse with a depth of ~2 mag that occurred 70 years ago. The durations of the two eclipses are similar (about 4 years long), which would suggest a nearly circular orbit. In that case, the ratio of eclipse depths (in flux units) is approximately the ratio of surface brightnesses of the two bodies. We would have in this case a ratio of 100:6, which would imply a $T_{\rm eff}$ ratio of $\sim 15^{1/4} \approx 2$. This is in fact quite close to the ratio of $T_{\rm eff}$ from the SED fitting above ($8000/3600 \approx 2$).

Another constraint is the ratio of luminosities from the primary eclipse depth. Assuming again that both a primary and secondary eclipse are observed, and that the primary eclipse is near total (which it appears to be from the roughly flat bottom), then the primary eclipse would represent a total blocking of the smaller body by the larger one. The ratio of light lost to light remaining at the bottom of the eclipse is then the ratio of luminosities of the two bodies. In this case, with a primary eclipse depth of ~4.5 mag, we have a

luminosity ratio of ~100.

In order for all of the above to be internally consistent, the fully eclipsed body would have to be both the hotter object *and* the more luminous one. However, as can be seen from the SED (Figure 4.7), the hot component (blue curve) is only more luminous than the red one at UV wavelengths. At visible wavelengths the red giant component dominates by a very large factor. Instead, the observed GALEX fluxes must represent the unobstructed fluxes of the hot component, because it would have to be fully blocked behind the red giant if it is the eclipsed body at primary eclipse. However, in that case GALEX would not have detected the hot component. This then severely limits how luminous the hot component can be relative to the red giant, and implies that it is the red giant that is eclipsed at primary eclipse, and that the data do not show any evidence of a visible secondary eclipse. Indeed, the recently observed eclipse and the historically observed eclipse both phase together nicely (Fig. 5.3), consistent with them representing the same primary eclipse separated by ~69.068 yr.

A possible solution is that the hot component is surrounded by a large, cool disk, and that this is the body that obscures the red giant at primary eclipse. In that case, the red giant would simply become much fainter during eclipse (corresponding to the red curve in Figure 4.7 that matches the APASS SED during eclipse), as a result of being blocked by a large occulting screen. Indeed, in the faint state, the SED appears dominated by the same red giant spectrum as in the bright state, only diminished by a factor of ~50, consistent with the same dominant light source being mostly blocked by a dark screen. Moreover, the occulting screen evidently produces a nearly grey extinction, since the shape of the SED of the red giant component in the faint state is not reddened. We estimate the physical dimensions of the disk surrounding the hot component in Section 5.5.1.

Finally, we can measure the ratio of the stellar radii from the Stefan-Boltzmann law, using the measured ratio of luminosities from the SED fits and the ratio of the best-fit temperatures: $R_{\rm hot}/R_{\rm RG} = \left[(F_{\rm bol,hot}/F_{\rm bol,RG}) \,/\, (T_{\rm eff,hot}/T_{\rm eff,RG})^4 \right]^{1/2}$, where the "hot" and

"RG" subscripts refer to the hot companion and the red giant primary, respectively. The ratio of bolometric fluxes, $F_{\rm bol}$ is obtained simply by integrating the best-fit SEDs over all wavelengths, namely 0.00022. The resulting radius ratio is ≈0.003. Assuming a radius for the red giant primary in the range of 45–170 $R_\odot$ (depending on the assumed mass and age of the red giant; see below), this translates into a range of radii for the hot companion of 0.13–0.51 $R_\odot$. This calculation assumes a thermal, photospheric source and that we are seeing its entire surface (secondary star). It is possible that part of the secondary star is obscured by the disk around it causing us to underestimate its radius. The uncertainty may be as large as a factor of ∼2, given the uncertain $T_{\rm eff}$ from the SED fitting. This estimate for the radius of the hot companion is an order of magnitude smaller than the expected radius for a main-sequence A type star ($T_{\rm eff} \sim 8000$ K, $R \sim 2$ $R_\odot$), and 1–2 orders of magnitude larger than that expected for standard, cooling white dwarfs (≈0.003–0.03 $R_\odot$, depending on mass).

If the companion is actually a cooler star with accretion, then the temperature of the companion is lower than we have estimated here and consequently its radius would be larger, perhaps consistent with a standard main sequence cool dwarf. However we do not consider this likely because of the high accretion rate it would require (see result (1) earlier in this section). The in-eclipse SED (both optical and UV) can also be fit using a solar photosphere with a low accretion value of 3×10^{-8} $M_\odot$ yr^{-1} (magenta dotted curve in Figure 4.7). In this scenario the companion radius would be ∼1 $R_\odot$. In other words, the dotted magenta curve suggests that another possible interpretation of the SED during eclipse is that the red giant primary is 100% extinguished by the disk and that the companion SED is that of a solar-type star accreting at 3×10^{-8} $M_\odot$ yr^{-1} (the magenta dotted curve in Figure 4.7). However, this model does not fit the in-eclipse SED as well as our preferred model, in which the red giant remains partially visible during eclipse (the lower red curve in Figure 4.7) and the UV flux is provided by a small hot source, which fits the UV part of the SED extremely well. We discuss below the likelihood that the hot component is instead a

"stripped red giant" sdB type star.

5.4.2 Orbital Period

From Figure 5.1 and the SED analysis in Section 5.4.1, we interpret the observations of the two eclipses to be the primary eclipse observed twice. Given the depth of the recent event (~4.5 mag), it is possible that TYC 2505-672-1 dimmed below the limiting magnitude of the DASCH plates (B ~15 mag). We can also rule out the possibility that the eclipse happens every ~34.5 years since we would have seen two additional events around ~1908 and ~1979, where we have sufficient coverage to rule out eclipses.

In order to calculate the period, we used a generalized normal distribution to find the midpoint of the event. A generalized normal distribution provides a good functional fit to a transit event without relying on any physical models, and the only physical parameters that are directly measured are the out-of-transit magnitude and the midpoint of transit. For the more recent event, we combined the light curves from AAVSO and CRTS into a single light curve, and then used a least-squares-fit optimization to fit a generalized normal distribution to this data to find that the midpoint of the event is 2456261.12224±2.081 days. We then fit the same function to the DASCH data, allowing only the baseline magnitude and midpoint of transit to be changed and preserving the shape of the transit. For the older event, we found a midpoint of the event of 2431033.91053±4.862 days. Using these two event midpoints, we calculate the event as having a period of 69.068±0.019 years. The initial dimming observed by KELT in mid 2011 does not line up with this symmetric eclipse model fully which might indicate that the eclipse eclipse is not symmetric in shape.

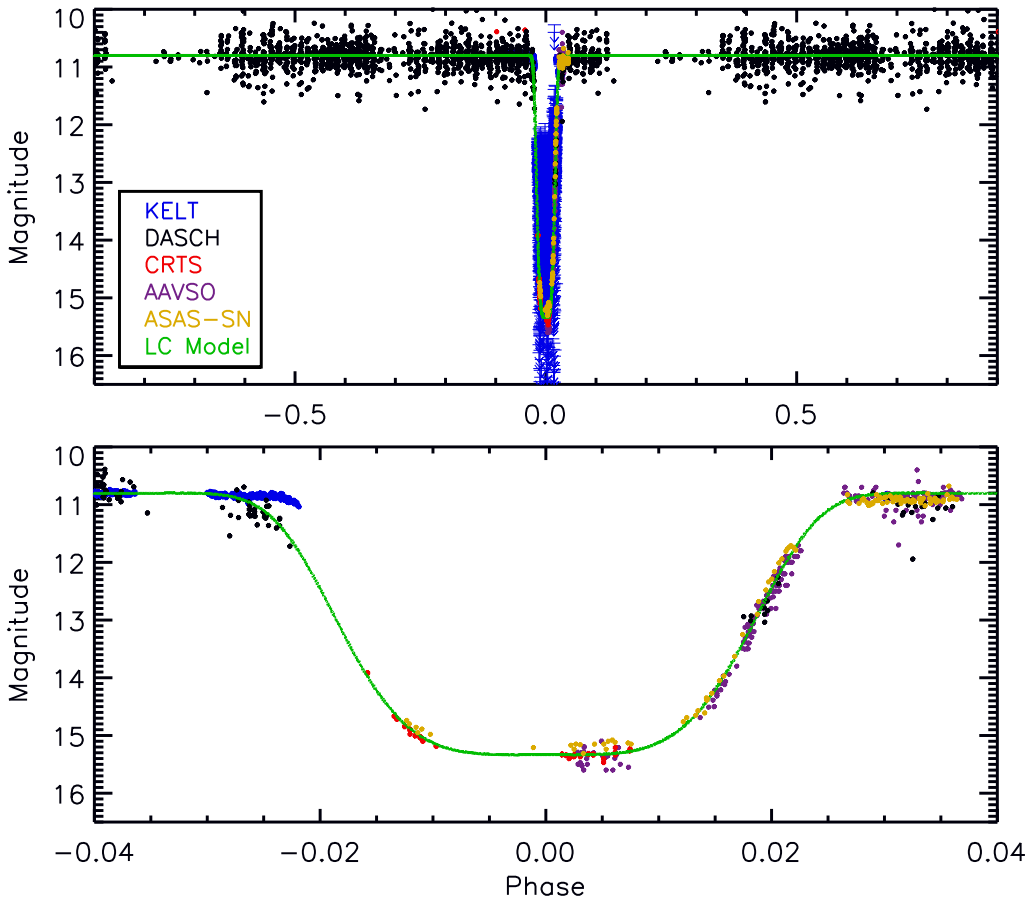

Figure 5.3: (Top) KELT-North (Blue), DASCH (Black), CRTS (Red), AAVSO (Violet), and ASAS-SN (Yellow) lightcurves phased to a period of 69.068 years (Bottom) Zoom in of the eclipse. The green line represents a LC model of the combined photometric data. The KELT-North observations during the eclipse are below the faintness limit of KELT and are therefore only upper limits. For a better visual representation of the in-eclipse structure, the KELT upper limit observations are not included in the bottom figure. Only the AAVSO, CRTS, and ASAS-SN data are in the Visual and V-band magnitudes. We approximate the all observations to the AAVSO V-band to match the quiescent magnitude of the AAVSO data but no attempt has been made to place all the data on the same absolute scale.

5.5 Interpretation and Discussion

5.5.1 Favored Interpretation: A Red Giant Eclipsed by a Pre–Helium-White-Dwarf Companion Surrounded by a Large Opaque Disk

From the SED analysis, we have determined that this system is composed of an M-giant primary star with a hot (T_{eff} ~8000 K) companion that is not contributing a significant

amount of optical light. This secondary component could be a main-sequence A-type star or a cool white dwarf. However, as discussed above, the apparent radius of the hot component is much too large to be a standard dwarf and much too small to be a main-sequence star.

Subdwarf B (sdB) stars are usually interpreted as red giants that been stripped of their hydrogen envelopes, leaving behind an exposed, hot core with an O or B type temperature but with a smaller radius than that of a main-sequence O or B type dwarf and a much larger radius than that of a hot white dwarf. It is expected that these objects eventually become Helium dwarfs (i.e., they are "pre-He-WD"). In this case, however, the temperature is unusually cool for this scenario even if the radius is consistent. We note that Maxted et al. [2014] reported a pre-He-WD system with a cool temperature also of ~8000 K.

Therefore, we suggest that the most plausible interpretation of this system is an eclipsing binary with an M-giant primary and pre-He-WD companion that is surrounded by a large disk. This scenario explains the observed UV excess, the small contribution of the companion to the optical fluxes and the very deep, long-term dimming events in the light curves. Since the dimming events show little to no structure (see Figure 5.3), it is likely the disk around the hot companion is not only large but almost completely opaque. Also, if the secondary component is an sdB star with a large disk, and the M-giant is roughly three orders of magnitude brighter in optical flux than the sdB star (see Figure 4.7), the secondary eclipse would be ~1 mmag in depth, and thus undetectable in any of our data sets.

To determine some of the physical properties of the opaque eclipsing body, we model the 2011–2014 eclipse as an occultation of the M-giant by a large opaque object with a sharp leading knife-edge, perpendicular to its direction of motion. This model requires no knowledge of the orbital eccentricity. Using this simple model, we can calculate a transverse velocity of the occulting body $2\times R_{Star}/T$, where T is the estimated ingress or egress timescale. Afanasiev et al. [2013] measured the spectra of the primary star to be

consistent with an M-giant. The stellar radius of an M-giant ranges from ∼45 $R_{\odot}$(M0 III) to ∼170 $R_{\odot}$(M7/8 III) [Dumm and Schild, 1998]. We estimate the egress of the 2011-2014 eclipse to be ∼315 days. This translates to a range of transverse velocity of 2.3–8.7 km s^{-1}(for the range of stellar radii). Using the total estimated duration of the eclipse to be ∼3.45 years, we also estimate the extent of the occulting body to be V×T(duration) = 1.7–6.3 AU (the disk could be inclined with respect to the companion's orbital motion resulting in a larger disk). Combining the estimated period of the EB (69.068 years) with a mass estimate for the M-giant and the hot companion, we can estimate the semi-major axis of the system, assuming Keplerian motion and a circular orbit. For the hot companion, we adopt a white dwarf mass range of 0.17–1.33 $M_{\odot}$[Kepler et al., 2007, Kilic et al., 2007] and M-giants can range from 0.8 to 5.0 $M_{\odot}$[Bressan et al., 1993, Dumm and Schild, 1998]. Using these mass ranges, this would result in a semi-major axis range of 16.7–31.2 AU. By applying a simple model, we are able to determine that the occulting body is moving 2.3–8.7 km s^{-1}, is 1.7–6.3 AU wide, and is orbiting at a semi-major axis of 16.7–31.2 AU. This would suggest that the hot companion has a few AU diameter disk around it. The 4.5 mag depth of the eclipse implies that the occulter almost completely occults the M-giant. Therefore, if the disk in not inclined to our line-of-sight, the thickness of the disk must be similar to the diameter of the M-giant (45–170 $R_{\odot}$or 0.21–0.8 AU). It is possible that the disk is inclined to our line-of-sight ($\sim 89^{\circ} \pm 1.0^{\circ}$ for ϵ Aur, see Kloppenborg et al. [2015]). If the disk is not edge-on, the thickness of the disk could be significantly thinner (or even thicker) and still cause the eclipse seen. Therefore, we are not able to constrain the disk's thickness. In the case of an edge on disk, the disk thickness-to-diameter ratio would be ∼12%.

5.5.2 Alternate Explanations

We have presented evidence in the previous subsection that the large dimming events of TYC 2505-672-1 are caused by the M-giant primary being eclipsed by a white dwarf with

a large disk surrounding it. We now explore an alternate explanation for these observations.

Another possible explanation for such large dimming events is that the M-giant primary is an RCB star or entering the RCB phase [Denisenko et al., 2013]. These are carbon rich supergiants (usually F or G spectral types) that experience non-periodic, large dimming events (up to ~8 mag in depth) caused by the formation of carbon dust in the stellar atmosphere. The dimmings are typically separated by a few years to a decade and are typically >3 mag in depth. The drop in the RCB star's brightness is very rapid (a few days to weeks) while the recovery is much slower (months to years). These stars also are known to pulsate with amplitudes of ~0.1 mag [Clayton, 2012]. If we were to believe that TYC 2505-672-1 was a unknown RCB star, the UV excess seen in the SED would be from a faint white dwarf orbiting it contributing some UV flux. Since the dimmings are separated by much longer then a few years to a decade, there is no pulsation amplitude observed outside of the most recent dimming (where we have the best photometric precision), the spectra observed by Denisenko et al. [2013] indicate that the primary star is an M-giant (not a supergiant, and the SED analysis supports this), and the most recent dimming show the ingress/egress timescales to be both much longer and more uniform than observed in known RCB stars, we do not believe the RCB scenario to be a plausible explanation for the dimming events observed for TYC 2505-672-1.

5.6 Summary and Conclusions

We have presented new observations of the remarkable eclipsing system TYC 2505-672-1, an M-giant star that has shown two separate dimming events separated by ~69.1 yr over the course of the historical light curve spanning 120 yr. We find that both eclipses phase up nicely with a period of 69.068 years. The most recent event, which was observed by KELT-North, CRTS, AAVSO, and ASAS-SN, show that the eclipse lasts ~3.5 years, has a depth of 4.5 mag in the optical, and shows little to no structure in the lightcurve during the eclipse. Our SED analysis (both in and out of eclipse) indicates to two components, one

with a T_{eff}=3600 K and the other with T_{eff}=8000 K. Combining the SED and photometric analysis, we determine that the system contains an M-giant primary star and a hot, dim companion.

Curiously, however, the hot companion has a radius that is much too small to be a main-sequence dwarf and much too large to be a standard cooling white dwarf. We propose the best solution is that the M-giant is being eclipsed every ~69.1 years by a "stripped red giant" (pre-Helium-white-dwarf, low-mass subdwarf B-type) companion surrounded by a large, opaque disk. This would explain the UV excess in the SED and the near-total occultation seen in the photometry, while also explaining the seemingly strange radius of the hot component.

As with ϵ Aurigae, this system presents a unique laboratory for understanding the disk structure of a companion orbiting an evolved star. At a orbital period of ~69.1 years, this is now the longest period eclipsing system found to date. We encourage continued photometric and spectroscopic follow-up of this system, in particular the measurement of the system's radial velocity motion. Extrapolating from our calculated period and T_C, the next eclipse should begin in early UT 2080 April and end in mid UT 2083 September (T_C = 2480857.48, UT 2081 December 24).

A mystery remains regarding the evolutionary nature of the hot component within the opaque disk. Previous examples of pre-He-WDs [Maxted et al., 2014] are in relatively short-period binary systems (periods of ~1 day), such that the recent stripping of the red giant that produced the currently observed hot source can be reasonably attributed to interactions between the close binary components. In the present case, however, the two stars are evidently very widely separated (semi-major axis ~20 AU). Perhaps the hot component is itself in a tight binary within the surrounding opaque disk, or is the result of a white dwarf merger. It is possible that we are witnessing an object in the very short-lived evolutionary state following the sdB stage leading to the eventual very hot, and then cooling, white dwarf.

Chapter 6

KELT-14b and KELT-15b: An Independent Discovery of WASP-122b and a New Hot Jupiter

6.1 Introduction

The confirmation of over 1000 transiting exoplanets to date is due to the success of ground-based photometric surveys such as HATNet [Bakos et al., 2004], SuperWASP [Pollacco et al., 2006], XO [McCullough et al., 2006], and TrES [Alonso et al., 2004], and the space-based missions CoRoT [Baglin et al., 2006] and Kepler [Borucki et al., 2010]. The field has shifted from pure discovery to understanding the demographics of exoplanets and atmospheric characterization. However, many of the discovered planets are too faint or too small for performing atmospheric characterization with current facilities. To date, there are only 29 giant transiting planets orbiting stars with $V < 11.5$ in the southern hemisphere[1].

It is believed that "hot Jupiters," gas giant planets that orbit extremely close (orbital periods of a few days) to their host stars, must form beyond the "Snow Line." Once formed, the giant planets can migrate inward through various methods [Tanaka et al., 2002, Masset and Papaloizou, 2003, D'Angelo and Lubow, 2008, Jackson et al., 2008, Cloutier and Lin, 2013]. It has been proposed that Jupiter experienced migration early in its lifetime, but did not migrate all the way inward due to the gravitational pull of Saturn [Walsh et al., 2011]. These hot Jupiters, specifically ones orbiting solar-like stars, provide insight into alternate evolutionary scenarios.

The Kilodegree Extremely Little Telescope (KELT) exoplanet survey, operated and owned by Vanderbilt University, Ohio State University, and Lehigh University, has been observing > 60% of the sky with a cadence of 10 to 20 minutes for many years. The project uses two telescopes, KELT-North at Winer Observatory in Sonoita, Arizona and

[1] www.exoplanets.org, as of September 2015

KELT-South at the South African Astronomical Observatory (SAAO) in Sutherland, South Africa. The survey is optimized for high-precision ($\leq$1% RMS) photometry for stars with $8 \leq V \leq 11$ to enable transit discovery of giant planets. Each telescope has a 42 mm aperture, $26^\circ \times 26^\circ$ field of view, and a pixel scale of $23''$/pixel [Pepper et al., 2007, 2012]. The first telescope in the survey, KELT-North, has announced six planets orbiting stars brighter than $V = 11$ [Siverd et al., 2012, Beatty et al., 2012, Pepper et al., 2013, Collins et al., 2014, Bieryla et al., 2015, Fulton et al., 2015]. The younger counterpart in the survey, KELT-South, has already announced one planet, KELT-10b [Kuhn et al., 2015].

In this paper, we present the discovery of a new hot Jupiter by KELT-South, which we name KELT-15b. We also present another hot Jupiter, which we refer to in this paper as KELT-14b. Shortly before the completion of this paper, a draft manuscript was posted to the arXiv [Turner et al., 2015] describing the discovery of three new exoplanets by the SuperWASP survey. One of the planets they name WASP-122b, which is the same planet we designate as KELT-14b. Since the data we present in this paper were collected independently and the analysis performed before the announcement of WASP-122b, we have chosen to discuss our findings as an independent discovery of this planet, and we refer to it here as KELT-14b. However, we acknowledge the prior announcement of it as WASP-122b.

The paper is organized as follows with each section including both discovered systems, KELT-14b and KELT-15b. In §2 we present our discovery and follow-up observations (photometric and spectroscopic). We present our stellar characterization analysis and results in §3. The global modeling and resulting planetary parameters are discussed in §4 with our false positive analysis described in §5. In §6 we describe the evolutionary analysis, long-term follow-up to look for additional companions in each system, and the value each planetary system has for future atmospheric characterization observations. We summarize our results and conclusions in §7.

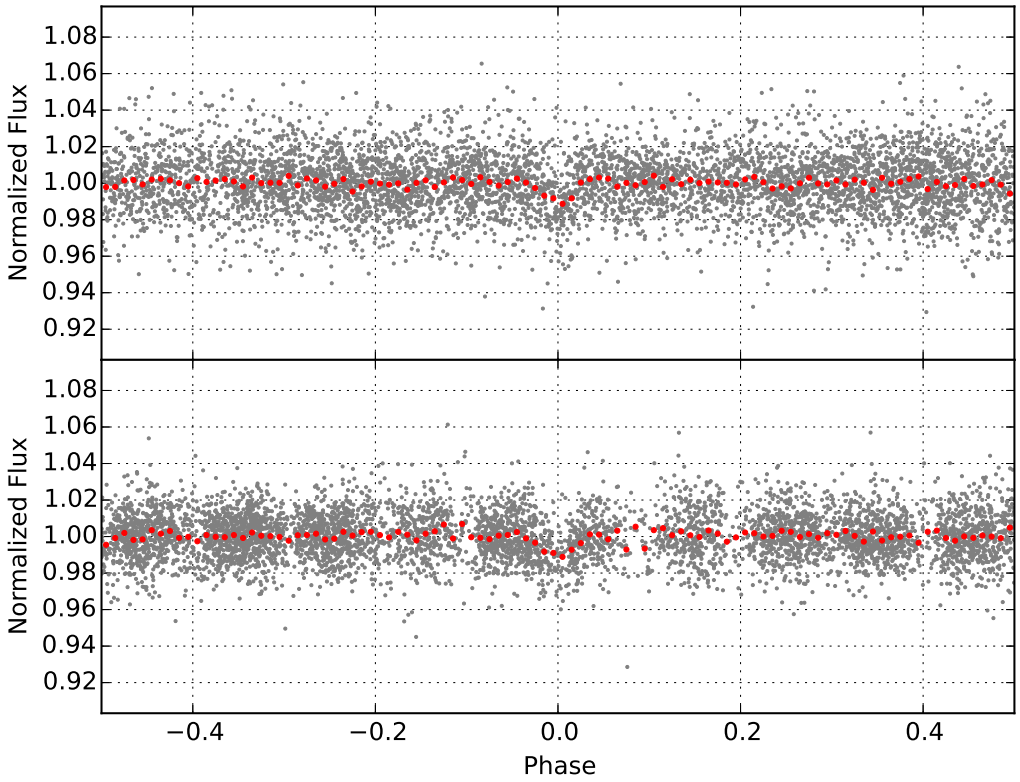

Figure 6.1: Discovery light curve of KELT-14b (Top) and KELT-15b (Bottom) from the KELT-South telescope. The light curves are phase-folded to the discovery periods of P = 1.7100596 and 3.329442 days respectively; the red points show the light curve binned in phase using a bin size of 0.01.

6.2 **Discovery and Follow-Up Observations**

6.2.1 KELT-South

KELT-14 and KELT-15 are located in the KELT-South field 34, which is centered at J2000 α = 08^h 16^m 12^s δ = -54° 00′ 00″. Field 34 was monitored in two separate campaigns: First from UT 2010 January 03 to UT 2010 February 19 as part of the KELT-South commissioning campaign, and then again from UT 2012 September 16 to UT 2014 June 14, acquiring a total of ∼5780 images after post-processing and removal of bad images. Following the strategy described in Kuhn et al. [2015], we reduced the raw images, extracted the light curves, and searched for transit candidates. Two stars emerged as top can-

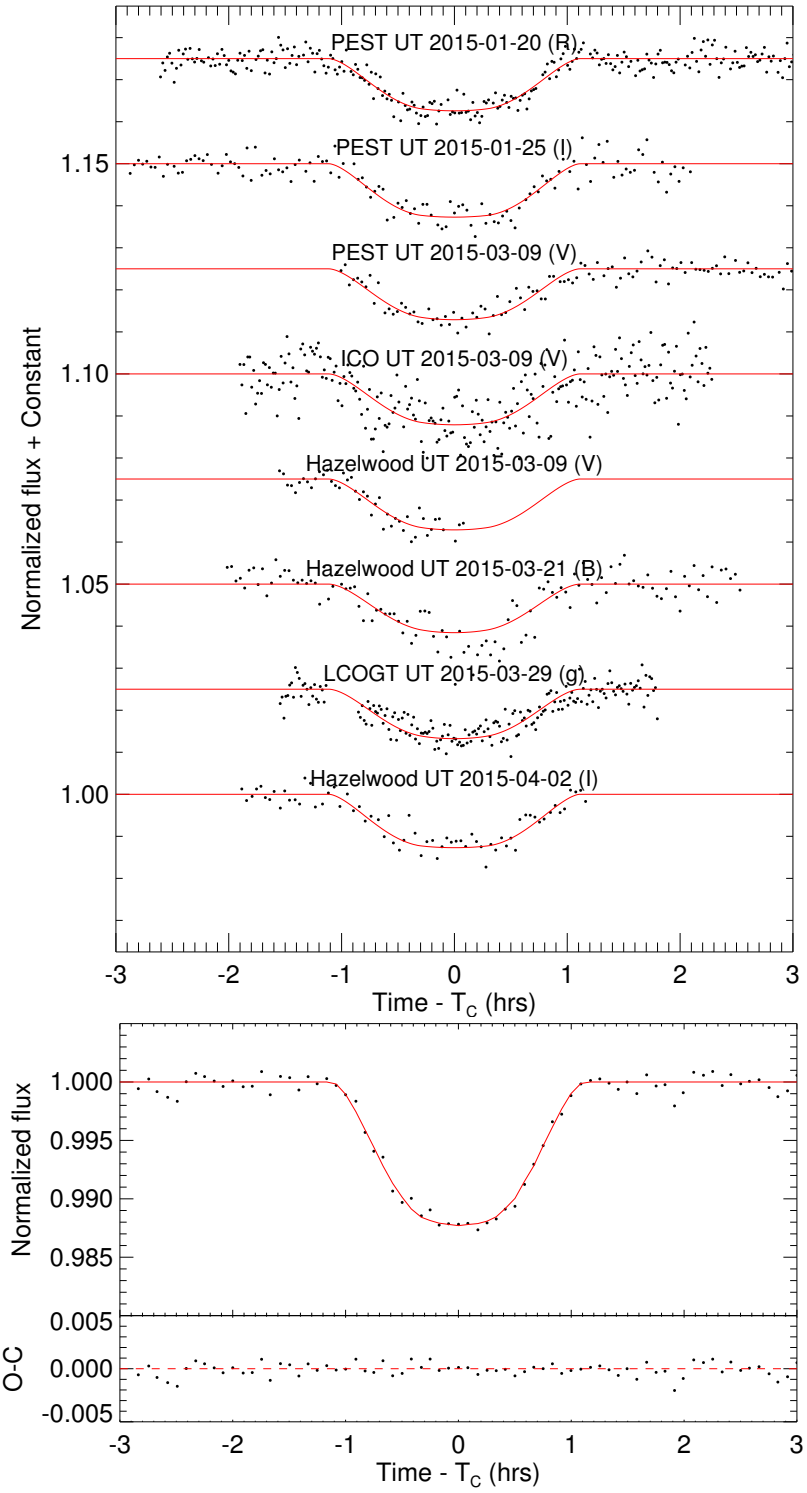

Figure 6.2: (Top) The follow-up photometry of KELT-14b from the KELT follow-up network. The red line is the best model for each follow-up lightcurve. (Bottom) The individual follow-up lightcurves combined and binned in 5 minute intervals. This combined and binned plot represents the true nature of the transit. The combined and binned light curve is for display and is not used in the analysis. The red line represents the combined and binned individual models (red) of each follow-up observation.

Table 6.1: Stellar Properties of KELT-14 and KELT-15 obtained from the literature.

Parameter	Description	KELT-14 Value	KELT-15 Value	Source	Reference(s)
		TYC 7638-981-1 GSC 07638-00981 2MASS J07131235-4224350	TYC 8146-86-1 GSC 08146-00086 2MASS J07493960-5207136		
α_{J2000}	Right Ascension (RA)	07:13:12.347	07:49:39.606	Tycho-2	Høg et al. [2000]
δ_{J2000}	Declination (Dec)	-42:24:35.17	-52:07:13.58	Tycho-2	Høg et al. [2000]
NUV		17.06± 0.1	N/A	GALEX	
B_T	Tycho B_T magnitude	11.963	11.889	Tycho-2	Høg et al. [2000]
V_T	Tycho V_T magnitude	11.088	11.440	Tycho-2	Høg et al. [2000]
Johnson V	APASS magnitude	10.948 ± 0.05	11.189± 0.05	APASS	Henden et al. [2015]
Johnson B	APASS magnitude	11.64 ± 0.05	11.745± 0.05	APASS	Henden et al. [2015]
Sloan g'	APASS magnitude	11.247 ± 0.051	11.438 ± 0.03	APASS	Henden et al. [2015]
Sloan r'	APASS magnitude	10.733 ± 0.053	11.048 ± 0.03	APASS	Henden et al. [2015]
Sloan i'	APASS magnitude	10.631 ± 0.05	10.935 ± 0.05	APASS	Henden et al. [2015]
J	2MASS magnitude	9.808 ± 0.024	10.205 ± 0.024	2MASS	Cutri et al. [2003]
H	2MASS magnitude	9.487 ± 0.024	9.919 ± 0.023	2MASS	Cutri et al. [2003]
K	2MASS magnitude	9.424 ± 0.023	9.854 ± 0.025	2MASS	Cutri et al. [2003]
WISE1	WISE passband	9.369 ± 0.023	9.775 ± 0.023	WISE	Cutri and et al. [2012]
WISE2	WISE passband	9.414 ± 0.021	9.805 ± 0.020	WISE	Cutri and et al. [2012]
WISE3	WISE passband	9.339 ± 0.026	9.919 ± 0.048	WISE	Cutri and et al. [2012]
WISE4	WISE passband	9.442 ± 0.495	<9.580	WISE	Cutri and et al. [2012]
μ_α	Proper Motion in RA (mas yr^{-1})	-13.9 ± 2.2	-3.4 ± 2.3	NOMAD	Zacharias et al. [2004]
μ_δ	Proper Motion in DEC (mas yr^{-1})	-1.3 ± 2.0	-2.0 ± 2.9	NOMAD	Zacharias et al. [2004]
U*	Space motion ($km\,s^{-1}$)	-4.6 ± 1.9	7.8 ± 3.8		This work
V	Space motion ($km\,s^{-1}$)	-14.6 ± 0.9	2.6 ± 0.8		This work
W	Space motion ($km\,s^{-1}$)	-14.0 ± 2.3	-1.5 ± 3.3		This work
Distance	Estimated Distance (pc)	201±19	291±30		This work
RV	Absolute RV ($km\,s^{-1}$)	34.62 ± 0.13	12.20 ± 0.11		This work
$v \sin i_*$	Stellar Rotational Velocity ($km\,s^{-1}$)	7.7±0.4	7.6±0.4		This work

NOTES

Red value correspond to upper limits (S/N < 2)

*U is positive in the direction of the Galactic Center

didates from this process: KS34C030815 (TYC 7638-981-1, GSC 07638-00981, 2MASS J07131235-4224350) located at $\alpha = 07^h\ 13^m\ 12.347^s$ δ = -42°8 24′ 35′′17 J2000, hereafter as KELT-14, and KS34C034621 (TYC 8146-86-1,GSC 08146-00086, 2MASS J07493960-5207136) located at $\alpha = 07^h\ 49^m\ 39.606^s$ δ = -52° 07′ 13′′58 J2000, designated as KELT-15 (see Figure 6.1). The host star properties for both targets are listed in Table 6.1. We used the box-fitting least squares (BLS) algorithm [Kovács et al., 2002, Hartman, 2012] to select these candidates, and the BLS selection criteria and values for both are shown in Table 6.2.

To precisely measure the transits of KELT-14b and KELT-15b, we obtained high-cadence, high-precision photometric follow-up using larger telescopes that cleanly resolve the hosts from their neighbors. These observations better constrain the period, depth, and duration of the transit and also rule out various false positive scenarios. To predict the transits, we use the web interface, TAPIR [Jensen, 2013]. For consistency, all follow-up observations

Table 6.2: KELT-South BLS selection criteria

BLS Statistic	Selection Criteria	KELT-14b KS34C030815	KELT-15b KS34C034621
Signal detection efficiency	SDE > 7.0	7.75403	11.04677
Signal to pink-noise	SPN > 7.0	8.26194	9.78164
Transit depth . . .	$\delta < 0.05$	0.01072	0.00841
χ^2 ratio	$\frac{\Delta\chi^2}{\Delta\chi^2_-} > 1.5$	2.16	2.56
Duty cycle	q < 0.1	0.03333	0.04667

Table 6.3: Photometric follow-up observations and the detrending parameters found by AIJ for the global fit.

Target	Observatory	Date (UT)	Filter	FOV	Pixel Scale	Exposure (s)	FWHM	Detrending parameters for global fit
KELT-14b	PEST	UT 2015 January 20	*R*	$31' \times 21'$	$1.2''$	60	6.04	airmass, *y* coordinates
KELT-14b	PEST	UT 2015 January 25	*I*	$31' \times 21'$	$1.2''$	120	7.48	airmass, *y* coordinates
KELT-14b	PEST	UT 2015 March 09	*V*	$31' \times 21'$	$1.2''$	120	5.56	airmass
KELT-14b	Adelaide	UT 2015 March 09	*V*	$16.6' \times 12.3'$	$0.62''$	60	10.48	airmass, total counts
KELT-14b	Hazelwood	UT 2015 March 09	*V*	$18' \times 12'$	$0.73''$	120	6.10	airmass
KELT-14b	Hazelwood	UT 2015 March 21	*B*	$18' \times 12'$	$0.73''$	120	6.31	airmass
KELT-14b	LCOGT	UT 2015 March 29	g'	$27' \times 27'$	$0.39''$	39	11.24	airmass, pixel width, total counts
KELT-14b	Hazelwood	UT 2015 April 02	*I*	$18' \times 12'$	$0.73''$	120	7.19	airmass
KELT-15b	Adelaide	UT 2014 December 27	*V*	$16.6' \times 12.3'$	$0.62''$	60	9.95	airmass, *y* coordinates, total counts
KELT-15b	Adelaide	UT 2015 January 06	*R*	$16.6' \times 12.3'$	$0.62''$	120	13.8	airmass, *y* coordinates
KELT-15b	PEST	UT 2015 January 16	*I*	$31' \times 21'$	$1.2''$	120	6.35	airmass, sky counts per pixel, total counts

NOTES
All the follow-up photometry presented in this paper is available in machine-readable form in the online journal.

were analyzed using AstroImageJ (AIJ) [Collins and Kielkopf, 2013, Collins, 2015]. This software also provides the best detrending parameters that are included in the global fit (see §6.4.1). The follow-up photometry for KELT-14b and KELT-15b are shown in Figures 6.2 and 6.3 respectively.

6.2.2 Photometric Follow-up

6.2.2.1 LCOGT

We observed a nearly full transit of KELT-14b in the Sloan *g*-band on UT 2015 March 29 from a 1-m telescope in the Las Cumbres Observatory Global Telescope (LCOGT) network[2] located at Cerro Tololo Inter-American Observatory (CTIO) in Chile. The LCOGT

[2]http://lcogt.net/

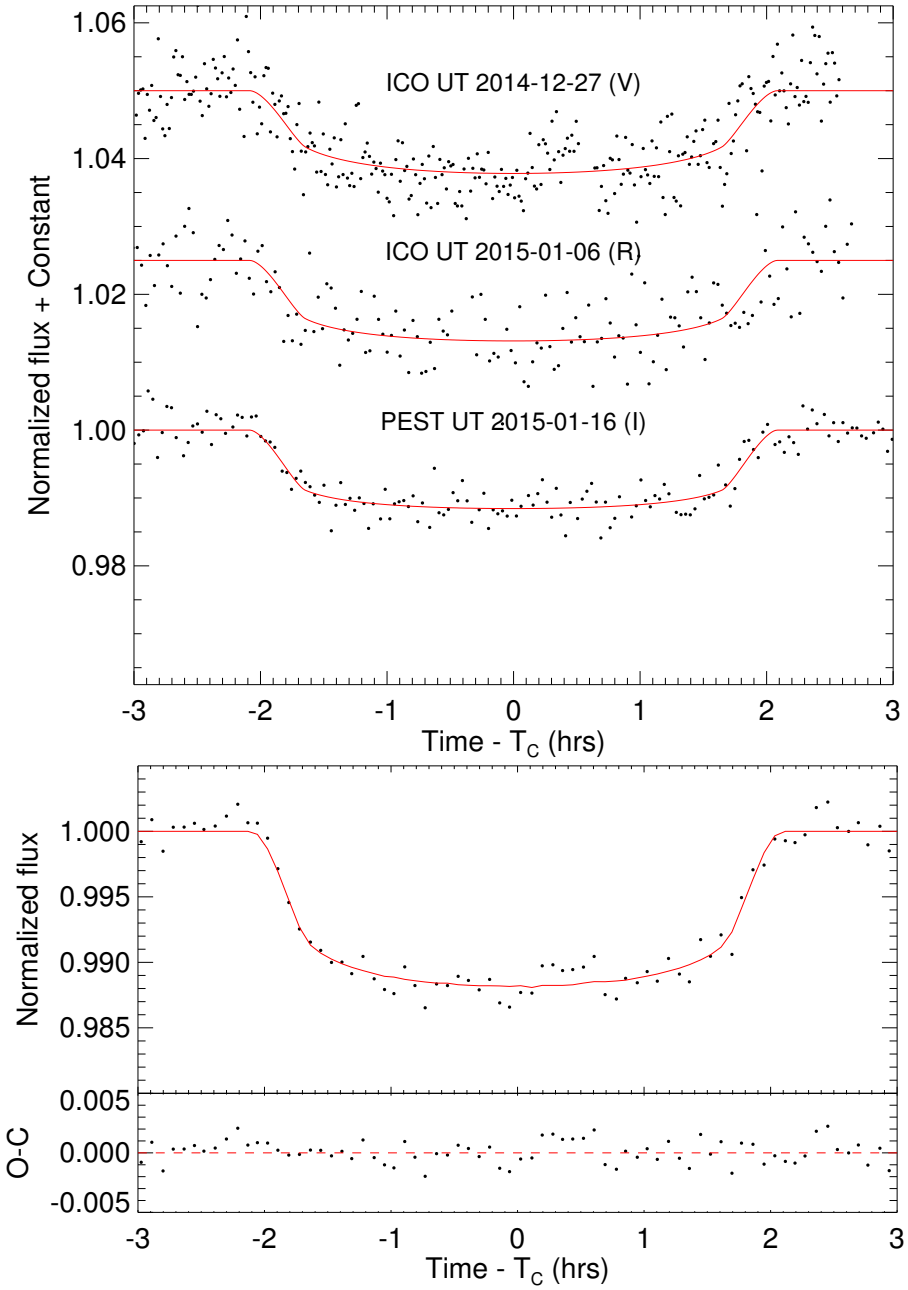

Figure 6.3: (Top) The follow-up photometry of KELT-15b from the KELT follow-up network. The red line is the best model for each follow-up lightcurve. (Bottom) All the follow-up lightcurves combined and binned in 5 minute intervals. This best represents the true nature of the transit. The combined and binned light curve is for display and is not used in the analysis. The red line represents the combined and binned individual models (red) of each follow-up observation.

telescopes at CTIO have a 4K × 4K Sinistro detector with a $27' \times 27'$ field of view and a pixel scale of $0.39''$ per pixel. The typical FWHM of the star in this data set was 11.24 pixels. The reduced data were downloaded from the LCOGT archive and analyzed using the AstroImageJ software. In a portion of the light curve surrounding the transit ingress the target was saturated, therefore we exclude this portion of the data from the global parameter analysis in §6.4.1.

6.2.2.2 PEST Observatory

PEST (Perth Exoplanet Survey Telescope) observatory is a home observatory owned and operated by Thiam-Guan (TG) Tan. It is equipped with a 12-inch Meade LX200 SCT f/10 telescope with focal reducer yielding f/5. The camera is an SBIG ST-8XME with a filter wheel having *B*, *V*, *R*, *I* and Clear filters. The focusing is computer controlled with an Optec TCF-Si focuser. The image scale obtained is 1.2 $''$ per pixel and a full frame image covers $31\ ' \times 21\ '$. For images in focus the usual star FWHM achieved is about 2.5 to 3.5 pixels. The PEST observatory clock is synced on start up to the atomic clock in Bolder, CO and is resynced every 3 hours. PEST observed full transits of KELT-14b on UT 2015 January 20 (*R*) and UT 2015 January 25 (*I*), and a nearly full transit on UT 2015 March 09 (*V*). PEST observed a full transit of KELT-15b on UT 2015 January 16 (*I*).

6.2.2.3 Hazelwood Observatory

The Hazelwood Observatory is a backyard observatory with 0.32 m Planewave CDK telescope working at f/8, a SBIG ST8XME 1.5K × 1K CCD, giving a $18' \times 12'$ field of view and $0.73''$ per pixel. The camera is equipped with Clear, B, V, Rc, and Ic filters (Astrodon Interference). Typical FWHM is $2.4''$ to $2.7''$. The Hazelwood Observatory, operated by Chris Stockdale in Victoria, Australia, obtained an ingress of KELT-14b in *V*-band on UT 2015 March 09, a full transit in the *B*-band on UT 2015 March 21 and a full transit in *I*-band on UT 2015 April 02. The observatory computer clock is synchronised at the start

Table 6.4: Spectroscopic follow-up observations

Target	Telescope/Instrument	Date Range	Type of Observation	Resolution	Wavelength Range	Mean S/N	Epochs
KELT-14	ANU 2.3/WiFes	UT 2015 Feb 02	Reconnaissance	R$\sim$ 3000	3500 – 6000Å	75	1
KELT-14	ANU 2.3/WiFes	UT 2015 Feb 02 – UT 2015 Feb 04	Reconnaissance	R$\sim$ 7000	5200 – 7000Å	85	3
KELT-15	ANU 2.3/WiFes	UT 2014 Dec 29	Reconnaissance	R$\sim$ 3000	3500 – 6000Å	110	1
KELT-15	ANU 2.3/WiFes	UT 2014 Dec 29 – UT 2015 Jan 02	Reconnaissance	R$\sim$ 7000	5200 – 7000Å	80	3
KELT-14	AAT/CYCLOPS2	UT 2015 Feb 26 – UT 2015 May 13	High Resolution	R$\sim$ 70,000	4550 – 7350Å	41.6	15
KELT-15	AAT/CYCLOPS2	UT 2015 Feb 27 – UT 2015 May 15	High Resolution	R$\sim$ 70,000	4550 – 7350Å	41.2	14
KELT-15	Euler/CORALIE	UT 2015 Sep 04 – UT 2015 Sep 13	High Resolution	R$\sim$ 60,000	3900 – 6800Å	28.25	5

of each observing session and then every 15 minutes using NTP protocol to time.nist.gov. ACP, ACP Scheduler and MaximDL are used to acquire the images. The camera shutter latency (0.5s) is allowed for within MaximDL and the adjusted exposure time is recorded within the FITS header. Experience with another project has shown that the exposure start time is recorded in the FITS header to within one second of the actual exposure start time.

6.2.2.4 Adelaide Observations

The Adelaide Observatory, owned and operated by Ivan Curtis is located in Adelaide, Australia (labeled "ICO" in the figures). The observatory is equipped with a 9.25-in Celestron SCT telescope with an Antares 0.63x focal reducer yielding an overall focal ratio of f/6.3. The camera is an Atik 320e, which uses a cooled Sony ICX274 CCD of 1620×1220 pixels. The field of view is $16.6' \times 12.3'$ with a pixel scale of $0.62''$ per pixel and a typical FWHM around 2.5 to 3.1 $''$. The observatory's computer clock is synced with an internet time server before each observation session and has an overall timing uncertainty of a few seconds. The Adelaide Observatory observed a full transit of KELT-14b on UT 2015 March 09 (V) and full transits of KELT-15b on UT 2014 December 27 (R) and UT 2015 January 06 (R).

6.2.3 Spectroscopic Follow-up

6.2.3.1 Reconnaissance Spectroscopy

Since many astrophysical phenomena can create photometric signals that mimic planetary transits, it is important to follow up all candidates carefully to eliminate false positives.

Table 6.5: KELT-14 radial velocity observations with CYCLOPS2.

BJD_{TDB}	RV ($m\,s^{-1}$)	RV error ($m\,s^{-1}$)	Instrument
2457079.939623842	34621.30	16.70	CYCLOPS2
2457079.991772522	34658.60	8.20	CYCLOPS2
2457080.950428010	34456.10	5.20	CYCLOPS2
2457081.937382183	34725.20	5.50	CYCLOPS2
2457083.075531623	34431.30	6.00	CYCLOPS2
2457148.892669835	34776.70	9.80	CYCLOPS2
2457148.924568460	34792.00	12.60	CYCLOPS2
2457149.929456027	34505.50	19.10	CYCLOPS2
2457150.967262368	34528.10	13.10	CYCLOPS2
2457151.873724511	34733.40	14.30	CYCLOPS2
2457153.886260897	34794.20	13.20	CYCLOPS2
2457153.916879608	34729.70	14.90	CYCLOPS2
2457154.898109197	34468.40	8.30	CYCLOPS2
2457155.867229521	34533.50	112.90	CYCLOPS2
2457155.900058155	34560.60	111.50	CYCLOPS2

NOTES
This table is available in its entirety in a machine-readable form in the online journal.

After identifying the targets as planet candidates from the KELT photometry, a first stage of spectroscopic reconnaissance was done using the WiFeS spectrograph mounted on the 2.3m ANU telescope at Siding Spring Observatory [Dopita et al., 2007]. This instrument is an optical dual-beam, image-slicing integral-field spectrograph. The full WiFeS observing strategy and reduction procedure is described in Bayliss et al. [2013].

First, observations of both stars were performed at low resolution (R$\sim$ 3000) in the 3500-6000 Å range to determine their stellar type. Both KELT-14 and KELT-15 were identified with the following parameters: KELT-14 has $T_{eff} = 5572 \pm 200$K, $\log g_* = 3.5 \pm 0.4$ (cgs) and [Fe/H] = 0.0 ± 0.4; KELT-15b has $T_{eff} = 6221 \pm 200$K, $\log g_* = 3.4 \pm 0.4$ (cgs) and [Fe/H] = 0.0 ± 0.4. The low resolution spectra provide poor precision on the $\log g_*$ and therefore, these $\log g_*$ values aren't very reliable.

Additionally, three observations for each target were performed in medium-resolution (R$\sim$ 7000) using the red camera arm of the WiFeS spectrograph (5500-9000 Å) across the

Table 6.6: KELT-15 radial velocity observations with CYCLOPS2 and CORALIE.

BJD_{TDB}	RV ($m\,s^{-1}$)	RV error ($m\,s^{-1}$)	Instrument
2457081.094367965	12320.4	10.8	CYCLOPS2
2457083.091453823	12105.7	17.6	CYCLOPS2
2457148.910598987	12074.4	16.3	CYCLOPS2
2457148.942507928	12247.1	16.6	CYCLOPS2
2457149.947425124	12072.9	25.1	CYCLOPS2
2457150.985251112	12191.4	17.6	CYCLOPS2
2457151.891071429	12281.0	15.0	CYCLOPS2
2457151.953179348	12291.2	12.7	CYCLOPS2
2457153.903635089	12196.2	16.0	CYCLOPS2
2457153.934254059	12188.1	19.9	CYCLOPS2
2457154.912681718	12334.9	13.3	CYCLOPS2
2457154.921681414	12354.9	17.5	CYCLOPS2
2457155.886209486	12085.3	118.0	CYCLOPS2
2457155.918108410	12057.5	114.8	CYCLOPS2
2457269.908610	12096.39	53.81	CORALIE
2457272.903199	12125.96	81.47	CORALIE
2457273.907330	12221.40	57.97	CORALIE
2457276.897042	12216.76	44.60	CORALIE
2457278.894140	12161.43	24.16	CORALIE

NOTES
This table is available in its entirety in a machine-readable form in the online journal.

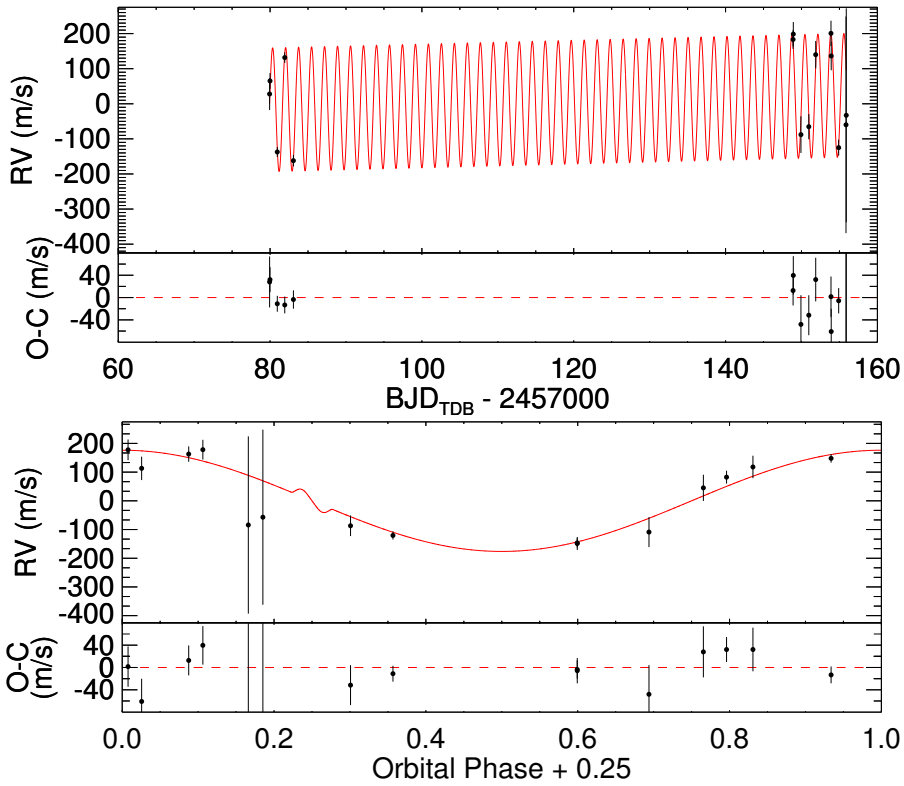

Figure 6.4: (Top) the AAT radial velocity measurements (the median absolute RV has been subtracted off) and residuals for KELT-14. The best-fitting orbit model is shown in red. The residuals of the RV measurements to the best fitting model are shown below. (Bottom) The KELT-14 AAT measurements phase-folded to the final global fit ephemeris.

expected orbital phase based on the photometrically detected period. These observations were aimed at performing multiple radial velocity (RV) measurements of each target to detect signals higher than 5 km/s amplitude, allowing us to identify grazing binary systems or blended eclipsing binaries. The typical RV precision achieved with this instrument is around 1.5 km/s, and both targets showed no significant variations among the three measurements.

6.2.3.2 High Precision Spectroscopic Follow-up

To confirm the planetary nature of the companion, we obtain multi-epoch high-resolution spectroscopy. These spectra allow us to very accurately measure the radial velocity of the host star providing us with a precise measurement of the companion's mass. Also, these

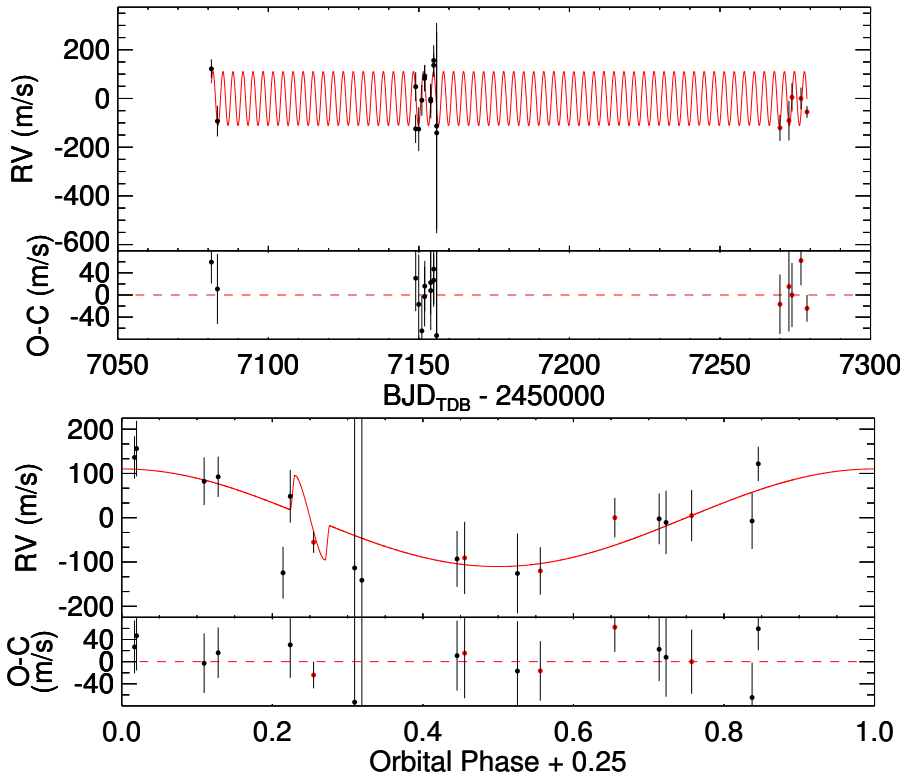

Figure 6.5: (Top) the AAT (black) and CORALIE (red) radial velocity measurements (the median absolute RV has been subtracted off) and residuals for KELT-15. The best-fitting orbit model is shown in red. The residuals of the RV measurements to the best model are shown below. (Bottom) The KELT-15 AAT (black) and CORALIE (red) measurements phase-folded to the final global fit ephemeris.

spectra provide a much better estimate of the stellar properties.

6.2.3.3 CYCLOPS2

Spectroscopic observations of KELT-14 and KELT-15 were carried out using the CYCLOPS2 fibre feed with the UCLES spectrograph instrument on the Anglo-Australian Telescope (AAT) over two observing runs: UT 2015 February 02 - UT 2015 March 01 and UT 2015 May 6 - UT 2015 May 13 (See Figure 6.4 and 6.5). The instrumental set-up and observing strategy for these observations closely follow that described in earlier CYCLOPS radial velocity papers [Addison et al., 2013, 2014].

CYCLOPS2 is a Cassegrain fiber-based integral field unit which reformats a ~2.5”

diameter on-sky aperture into a pseudo-slit of dimensions equivalent to 0.6" wide × 14.5" long [Horton et al., 2012]. CYCLOPS2 has 16 on-sky fibers, plus one fiber illuminated by a ThUXe lamp. Each fiber delivers a spectral resolution of $\lambda/\Delta\lambda \approx 70,000$ over 19 echelle orders in the wavelength range of $4550-7350$Å, when used with the UCLES spectrograph in its 79 line/mm grating configuration.

We use a ThAr calibration lamp to illuminate all of the on-sky fibers at the beginning of observations to create a *reference* ThAr wavelength solution. We then use simultaneous ThUXe data from each exposure to determine low-order distortions which differentially calibrate observations through the night onto the *reference* ThAr solution. These reductions are carried out using custom MATLAB routines (Wright and Tinney, *in prep.*). Calibration precision is estimated from the scatter of fits to the simultaneous ThUXe spectral features and these are tested against velocity standards taken each night. The typical calibration precision is < 10 m s^{-1}. This calibration error is combined with the error from a fit to the cross-correlation profile to give a final uncertainty for each observation.

The cross-correlation profiles are obtained using a weighted cross-correlation [Baranne et al., 1996, Pepe et al., 2002] of a stellar template produced with SYNSPEC [Hubeny and Lanz, 2011]. The velocities are determined from the fit of a generalised normal distribution to the cross-correlation profiles and the errors are estimated from the Jacobian matrix for each fit. We find no correlation between the bisector spans and the measured radial velocities. This provides strong evidence against a blended eclipsing binary scenario.

6.2.3.4 CORALIE

CORALIE is a fibre-fed echelle spectrograph [Queloz et al., 2001] attached to the Swiss 1.2 m Leonard Euler telescope at the ESO La Silla Observatory in Chile. It has a spectral resolution of R∼60000, a wavelength range of $3900-6800$Å, and is able to measure radial velocities of bright stars to a precision of 3 m.s^{-1} or better [Pepe et al., 2002]. In June 2015, the CORALIE spectrograph was equipped with a new Fabry-Peŕot-based calibration

system [Wildi et al., 2011]. This system replaces the ThAr lamp for the simultaneous reference method that determines and corrects for instrumental drift occurring between the calibration and the science exposure [Baranne et al., 1996]. The data-reduction software has been adapted to take into account the new operational mode and take benefit from the higher spectral content, and hence the lower photon noise, on the drift measurement, provided by the Fabry-Peŕot based calibration source. We obtained spectra at five epochs of KELT-15 from UT 2015 September 02 to UT 2015 September 14. All observations were reduced and radial velocities were computed in real time using the standard CORALIE pipeline. The observations from CORALIE are consistent with the CYCLOPS2 measured radial velocities. The results are shown in Figure 6.5. We find no correlation between the bisector spans and the measured radial velocities (see Figure 6.6).

6.3 Analysis and Results

6.3.1 SME Stellar Analysis

In order to determine precise stellar parameters for KELT-14 and KELT-15, we use the available high-resolution, low S/N AAT CYCLOPS2 spectra acquired for radial velocity confirmation of the two planetary systems. For each CYCLOPS2 dataset, we took the flux weighted mean of the individual fibers, continuum normalized each spectral order, and stitched the orders into a single 1-D spectrum. We shifted each resulting spectrum to rest wavelength by accounting for barycentric motion, and median combined all observations into a single spectrum with a S/N $\sim$ 50, sufficient for detailed spectroscopic analysis.

Stellar parameters for KELT-14 and KELT-15 are determined using an implementation of Spectroscopy Made Easy (SME) [Valenti and Piskunov, 1996]. Our Monte Carlo approach to using SME for measuring stellar parameters is detailed in Kuhn et al. [2015]. Briefly, we use a multi-trial minimization of 500 randomly selected initial parameter values, each solving for 5 free parameters: effective temperature ($T_{\rm eff}$), surface gravity ($\log g_*$), iron

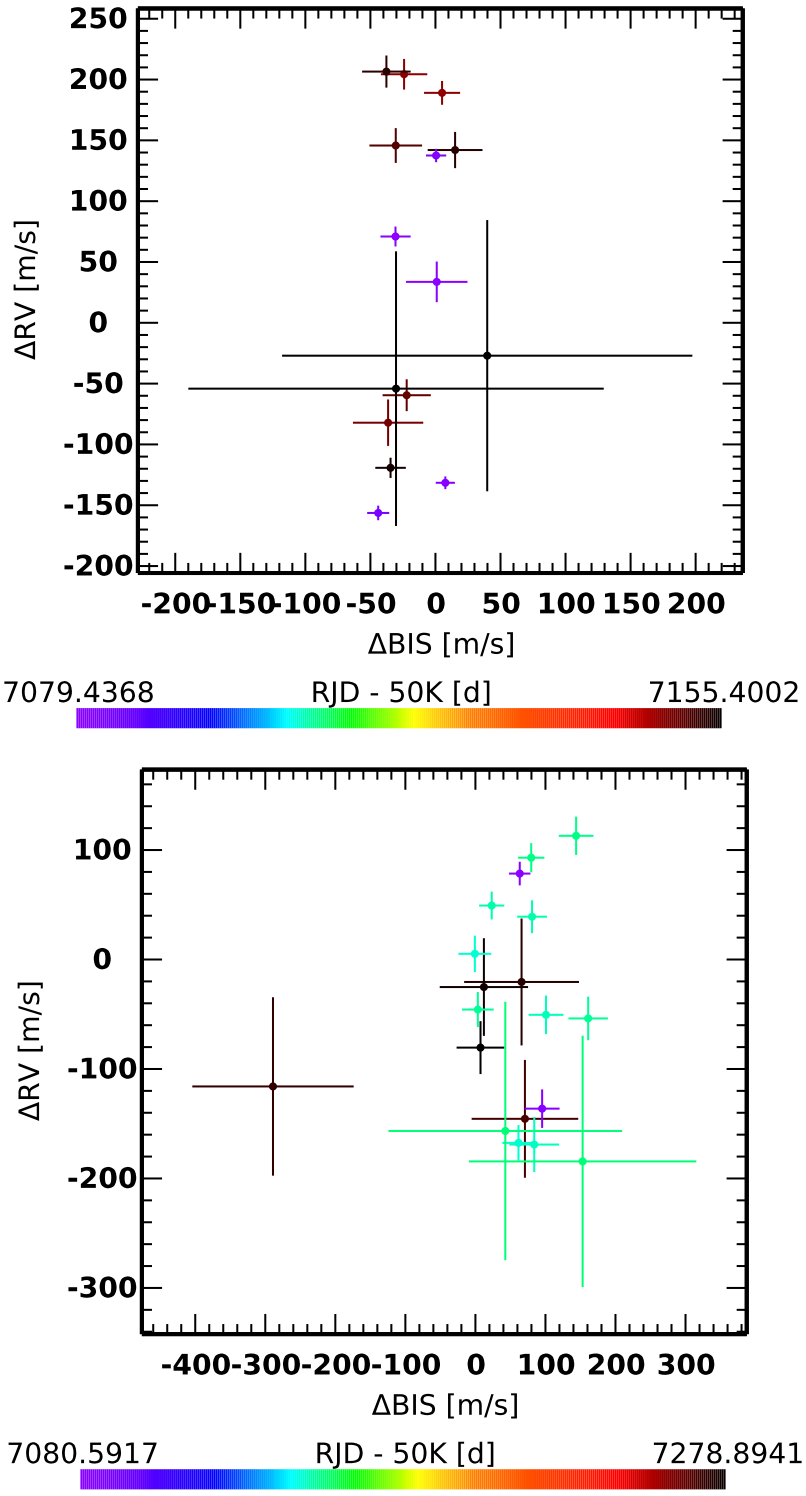

Figure 6.6: The AAT Bisector measurements for the (Top) KELT-14 and the combined AAT and CORALIE bisector measurements for (Bottom) the KELT-15 spectra used for radial velocity measurements. We find no significant correlation between RV and the bisector spans.

abundance ([Fe/H]), metal abundance ([m/H]), and rotational velocity of the star ($v \sin i_*$). We determine our final measured stellar properties by identifying the output parameters that give the optimal SME solution (i.e., the solution with the lowest χ^2). The overall SME measurement uncertainties in the final parameters are calculated by adding in quadrature the internal error determined from the 68.3% confidence region in the χ^2 map, the median absolute deviation of the parameters from the 500 output SME solutions to account for the correlation between the initial guess and the final fit, and an estimate for the systematic errors in our method when compared to other common stellar spectral analysis tools [see Gómez de Castro et al., 2013].

Due to the instrument setup used for measuring high-precision radial velocities, the AAT CYCLOPS2 spectra do not include the full MgB triplet wavelength region, a pressure-broadened set of lines commonly used in spectral synthesis modeling to constrain $\log g_*$ [Valenti and Fischer, 2005]. The available spectra only include one of the three strong Mg lines in this region. In order to investigate the effect of this constraint on our stellar parameters, we run two separate SME runs for both KELT-14 and KELT-15, one with $\log g_*$ as a free parameter and the other with $\log g_*$ fixed from our preliminary global fit of the photometric observations.

Our final SME spectroscopic parameters for KELT-14 are: $T_{\rm eff}$ = 5817±90 K, $\log g_*$ = 4.16±0.12, [m/H] = 0.39±0.03, [Fe/H] = 0.34±0.09 and a projected rotational velocity $v \sin i_*$ =7.7±0.4 km s^{-1}. Similarly, with a fixed $\log g_*$=4.23; $T_{\rm eff}$ = 5834±75 K, [m/H] = 0.39±0.03, [Fe/H] = 0.34±0.09 and $v \sin i_*$ =7.6±0.4 km s^{-1}. For KELT-15 we find: $T_{\rm eff}$ = 6023±61 K, $\log g_*$ = 3.80±0.08, [m/H] = 0.06±0.03, [Fe/H] = 0.05±0.03 and $v \sin i_*$ =11.1±0.5 km s^{-1}. With a fixed $\log g_*$=4.17 we find; $T_{\rm eff}$ = 6102±51 K, [m/H] = 0.02±0.03, [Fe/H] = 0.05±0.03 and $v \sin i_*$ =11.1±0.5 km s^{-1}. We constrain the macro- and microturbulent velocities to the empirically constrained relationship [Gómez de Castro et al., 2013]. However, we do allow them to change during our modelling according to the other stellar parameters. Our best fitting stellar parameters result in $v_{\rm mac}$ = 4.05 km s^{-1} and $v_{\rm mic}$ = 1.00 km s^{-1}for KELT-14,

and for KELT-15 $v_{\rm mac} = 4.37$ km s^{-1} and $v_{\rm mic} = 1.19$ km s^{-1}.

6.3.2 SED Analysis

We construct empirical spectral energy distributions (SEDs) of KELT-14 and KELT-15 using all available broadband photometry in the literature, shown in Figure 6.7. We use the near-UV flux from GALEX [Martin et al., 2005], the B_T and V_T fluxes from the Tycho-2 catalogue, B, V, g', r', and i' fluxes from the AAVSO APASS catalogue, NIR fluxes in the J, H, and K_S bands from the 2MASS Point Source Catalogue [Cutri et al., 2003, Skrutskie et al., 2006], and near-and mid-infrared fluxes in the WISE passbands [Wright et al., 2010].

We fit these fluxes using the Kurucz atmosphere models [Castelli and Kurucz, 2004] by fixing the values of $T_{\rm eff}$, $\log g_*$ and [Fe/H] inferred from the global fit to the lightcurve and RV data as described in §6.4.1 and listed in Table 6.5 and Table 6.6, and then finding the values of the visual extinction A_V and distance d that minimize χ^2, with a maximum permitted A_V based on the full line-of-sight extinction from the dust maps of Schlegel et al. [1998] (maximum $A_V = 0.50$ mag and 0.89 mag for KELT-14 and KELT-15, respectively). Note that while the final best SED fits below are in fact well fit with $A_V \equiv 0$, we did include A_V as a free fit parameter because of the *a priori* likelihood of A_V as large as 0.50–0.89 mag.

For KELT-14 we find $\rm A_V = 0.1 \pm 0.1$ mag and $d = 201 \pm 19$ pc with the best fit model having a reduced $\chi^2 = 1.39$. For KELT-15 we find $\rm A_V = 0.18 \pm 0.12$ and $d = 291 \pm 30$ pc with the best fit model having a reduced $\chi^2 = 0.84$. This implies a very good quality of fit and further corroborates the final derived stellar parameters for the KELT-14 and KELT-15 host stars. We note that the quoted statistical uncertainties on A_V and d are likely to be underestimated because alternate model atmospheres would predict somewhat different SEDs and thus values of extinction and distance, but for stars of the masses and temperatures of KELT-14 and KELT-15 the systematic differences among various model atmospheres are not expected to be large.

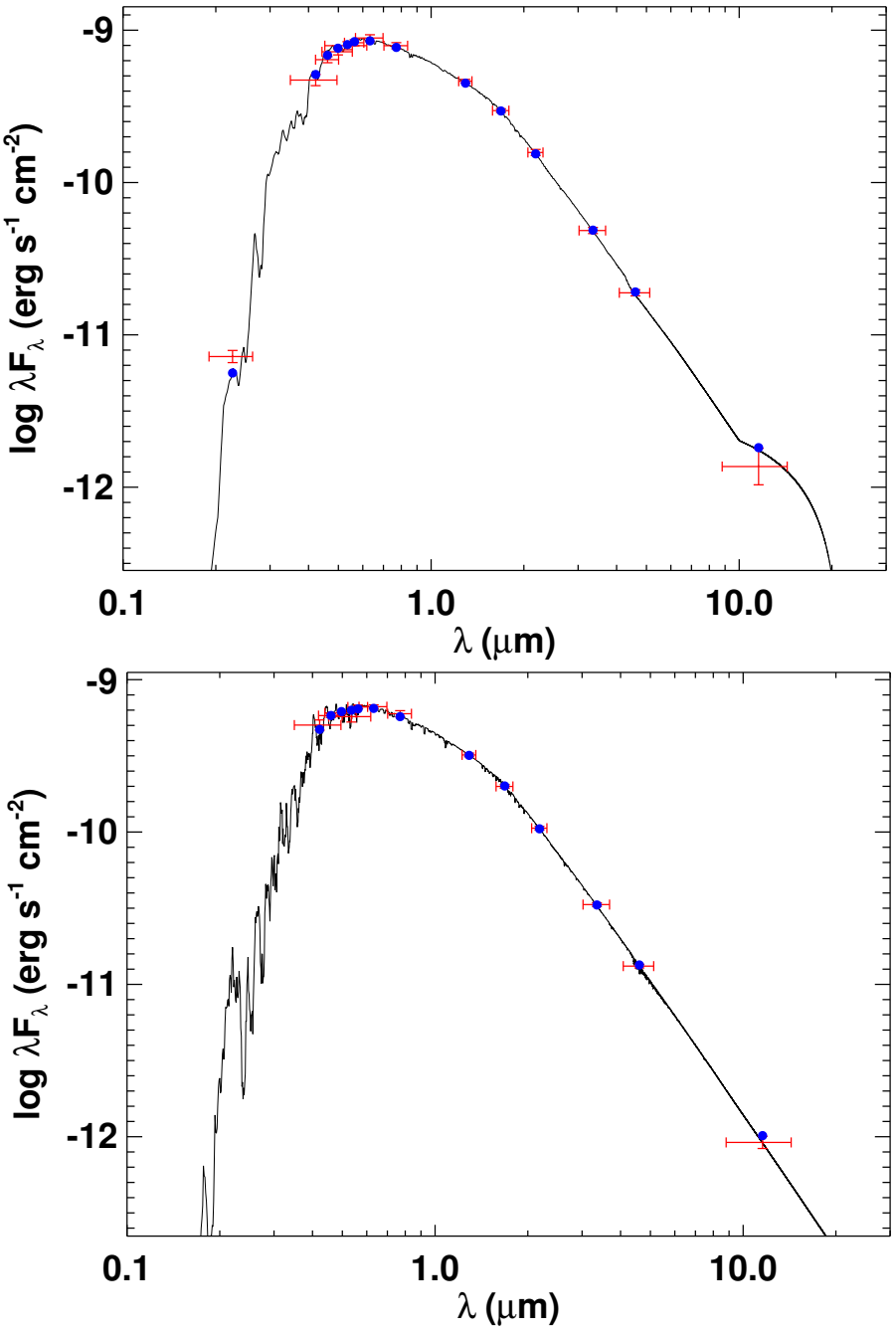

Figure 6.7: The SED fit for (top) KELT-14 and (bottom) KELT-15. The red points show the photometric values and errors given in Table 6.1. The blue points are the predicted integrated fluxes at the corresponding bandpass. The black line represents the best fit stellar atmospheric model.

6.3.3 Evolutionary State

To better place the KELT-14 and KELT-15 systems in context, we show in Figure 6.8 the H-R diagrams for the two systems in the $T_{\rm eff}$ versus $\log g_*$ plane. In each case, we use the Yonsei-Yale stellar evolution model track [Demarque et al., 2004] for a star with the mass and metallicity inferred from the final global fit (this fit used the SME determined [Fe/H]and $T_{\rm eff}$, where $\log g_*$ was not fixed, as priors), where the shaded region represents the mass and [Fe/H] fit uncertainties. The model isochrone ages are indicated as blue points, and the final best global fit $T_{\rm eff}$ and $\log g_*$ values are represented by the red error bars. For comparison, the $T_{\rm eff}$ and $\log g_*$ values determined from spectroscopy alone with $\log g_*$ not fixed are represented by the green error bars while the blue error bars represent when the $\log g_*$ was fixed in the SME analysis (Figure 6.8).

KELT-14 is a G2 type star near the main-sequence turnoff but not yet in the Hertzsprung gap, with an age of $\sim 5.0^{+0.3}_{-0.7}$ Gyr. KELT-15 is a G0 type star with an age of $\sim 4.6^{+0.5}_{-0.4}$ Gyr, on or near the "blue hook" just prior to the Hertzsprung gap. These classifications are also consistent with those reported in the catalogs of Pickles and Depagne [2010] and Ammons et al. [2006]. Note that the observed rotational velocities of the stars (7–11 $\rm km\,s^{-1}$; see Section 6.3.1) are consistent with the 2–15 $\rm km\,s^{-1}$ range observed for solar-type stars with the masses and ages of KELT-14 and KELT-15 [e.g., Soderblom, 1983].

6.3.4 UVW Space motion

To better understand the place of KELT-14 and KELT-15 in the galaxy, we calculate the UVW space motion. This exercise can allow us to determine the membership and possibly the age of a star if it is associated with any known stellar groups. To calculate the UVW space motion, we combine the information presented in Table 6.1 with the determined distance to KELT-14 and KELT-15 from the SED analysis (201±19 pc and 291±30 pc respectively). We also estimated the absolute radial velocity and error by taking the

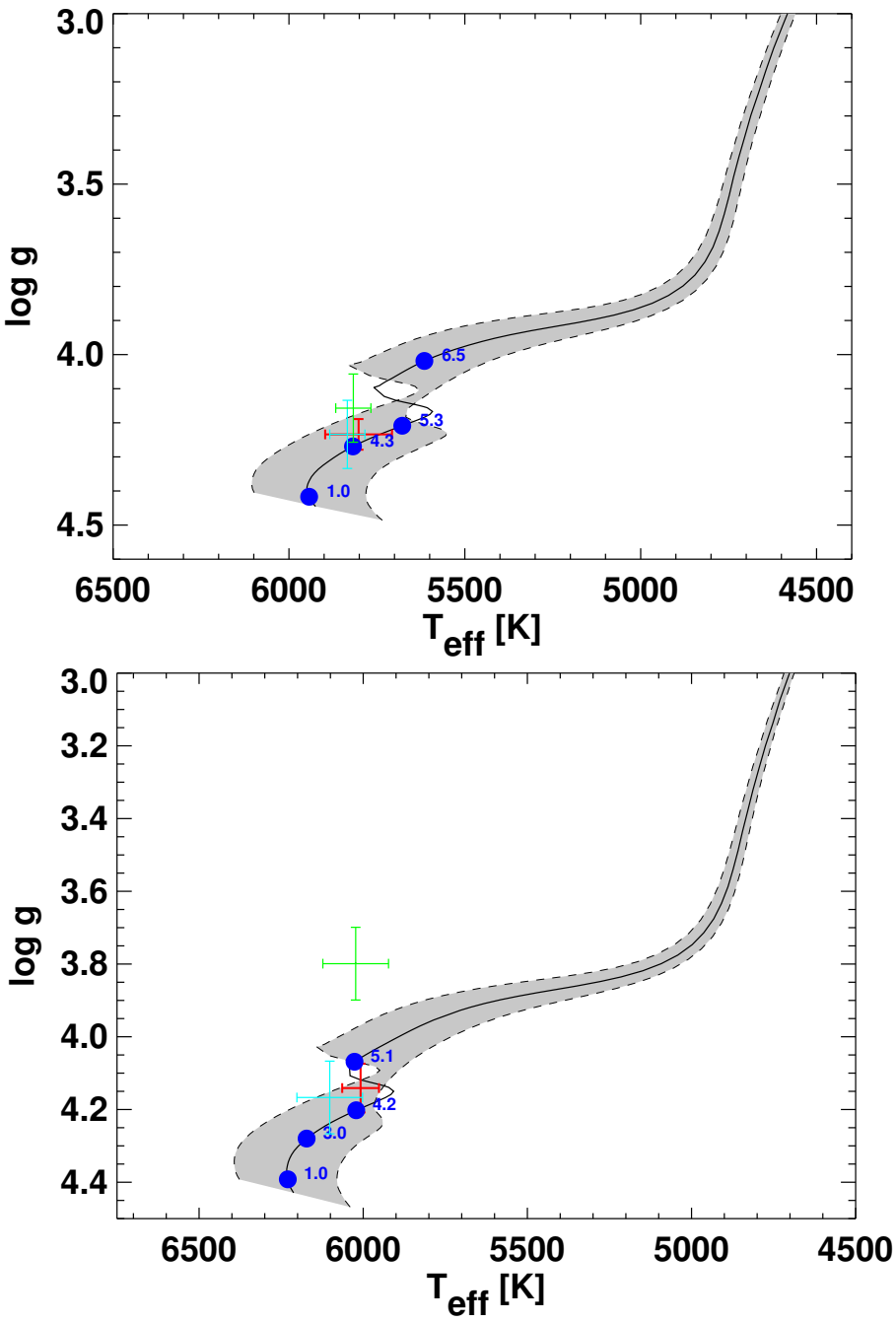

Figure 6.8: The theoretical H-R diagrams for (top) KELT-14 and (bottom) KELT-15 using the Yonsei-Yale stellar evolution models [Demarque et al., 2004]. The $\log g_*$ values are in cgs units. The red cross represents the values from the final global fit. The blue cross is the position and errors of the SME analysis when $\log g_*$ was fixed at the initial global fit value and the green cross is when $\log g_*$ was not fixed. The dashed lines at the edge of the gray shaded region represent the 1σ uncertainties on $M_\star$ and [Fe/H] from the global fit. The various ages along the tracks are represented by the blue points.

average and standard deviation of all the measured radial velocities by AAT. This gave us an estimated absolute radial velocity of 34.62 ± 0.13 $\mathrm{km\,s^{-1}}$and 12.20 ± 0.11 $\mathrm{m\,s^{-1}}$for KELT-14b and KELT-15b, respectively. We calculate the space motion to be U = -4.6 ± 1.9 $\mathrm{km\,s^{-1}}$, V = -14.6 ± 0.9 $\mathrm{km\,s^{-1}}$, W = -14.0 ± 2.3 $\mathrm{km\,s^{-1}}$for KELT-14 and U = 7.8 ± 3.8 $\mathrm{km\,s^{-1}}$, V = 2.6 ± 0.8 $\mathrm{km\,s^{-1}}$, W = -1.5 ± 3.3 $\mathrm{km\,s^{-1}}$for KELT-15 (positive U pointing toward the Galactic center). These space motion values give a 99% chance that both KELT-14 and KELT-15 belong to the thin disk, according to the classification scheme of Bensby et al. [2003]

6.4 Planetary Properties

6.4.1 EXOFAST Global Fit

To perform a global fit of our photometric and spectroscopic data, we use a modified version of the IDL exoplanet fitting tool, EXOFAST [Eastman et al., 2013]. More detailed explanation of the global modeling is provided in Siverd et al. [2012]. To determine a system's final parameters, simultaneous Markov Chain Monte Carlo (MCMC) analysis is performed on the AAT radial velocity measurements and the follow-up photometric observations. To constrain $M_\star$ and $R_\star$ EXOFAST uses either the Yonsei-Yale stellar evolution models [Demarque et al., 2004] or the empirical Torres relations [Torres et al., 2010]. Each photometric observation's raw light curve and the detrending parameters determined from the light curve are inputs for the final fit. We impose a prior on T_{eff} and [Fe/H] using the determined values and errors from the SME analysis of the AAT spectra. From analysis of the KELT-South and follow-up photometric observations, we set a prior on the period. For both KELT-14b and KELT-15b, we perform four global fits: 1) Using the Yonsei-Yale (YY) stellar models with eccentricity fixed at zero. We adopt the system parameters from this globalt fit for all analysis and interpretation for KELT-14b and KELT-15b. 2) Using the YY stellar models with eccentricity as a free parameter. 3) Using the empirical Torres relations

with eccentricity fixed at zero. 4) Using the empirical Torres relations with eccentricity as a free parameter. The results from these four global fits can be seen in Table 6.7 for the KELT-14 system and Table 6.8 for the KELT-15 system. For the parameters shown in solar or jovian units, the values for these constants are $GM_{\odot}$ = 1.3271244 × 10^{20} m^3 s^{-2}, $R_{\odot}$= 6.9566 × 10^8 m, M_J= 0.000954638698 $M_{\odot}$, and R_J= 0.102792236 $R_{\odot}$ [Standish, 1995, Torres et al., 2010, Eastman et al., 2013]. All determined values for the four separate global fits are consistent with each other (within 1σ). We adopt the YY circular fit parameters for each system.

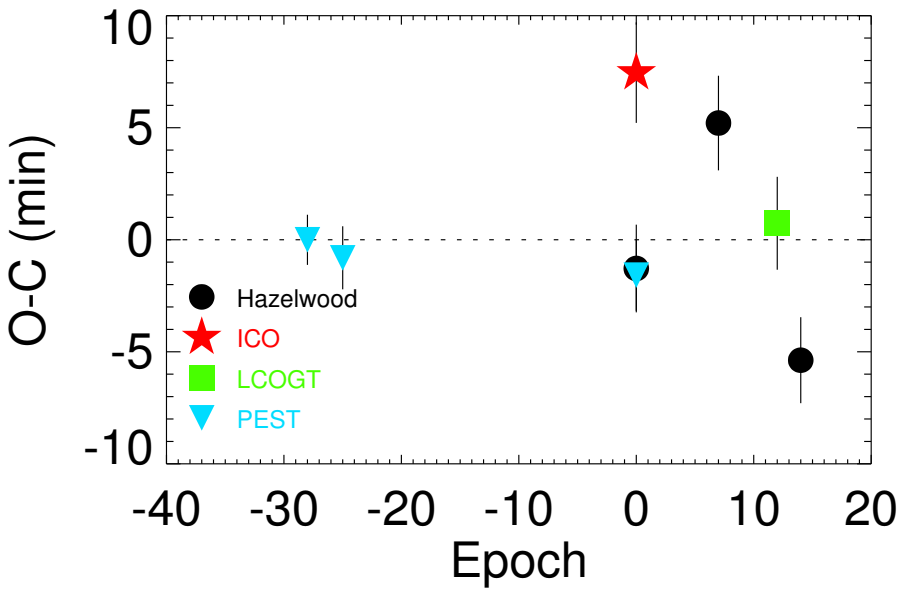

Figure 6.9: Transit time residuals for KELT-14b using our final global fit ephemeris. The times are listed in Table 6.9.

6.4.2 Transit Timing Variation Analysis

We were careful to confirm all observation times are in the BJD_TBD format [Eastman et al., 2010]. All time conversions to BJD_TBD were performed in the AIJ reduction using the timestamps in the image headers. The observatory clocks from our follow-up observers are synchronised at the start of each observing session to a standard clock (atomic clock

Table 6.7: Median values and 68% confidence interval for the physical and orbital parameters of the KELT-14 system

Parameter	Units	**Adopted Value (YY circular)**	Value (YY eccentric)	Value (Torres circular)	Value (Torres eccentric)
Stellar Parameters					
M_*	Mass ($M_\odot$)	$1.178^{+0.052}_{-0.066}$	$1.177^{+0.059}_{-0.066}$	$1.202^{+0.064}_{-0.062}$	$1.203^{+0.066}_{-0.063}$
R_*	Radius ($R_\odot$)	$1.368^{+0.078}_{-0.077}$	$1.378^{+0.10}_{-0.099}$	1.410 ± 0.077	$1.418^{+0.096}_{-0.094}$
L_*	Luminosity ($L_\odot$)	$1.90^{+0.28}_{-0.24}$	$1.93^{+0.34}_{-0.29}$	$2.04^{+0.29}_{-0.26}$	$2.06^{+0.34}_{-0.30}$
ρ_*	Density (cgs)	$0.645^{+0.11}_{-0.087}$	$0.63^{+0.14}_{-0.11}$	$0.604^{+0.096}_{-0.078}$	$0.595^{+0.12}_{-0.094}$
$\log g_*$	Surface gravity (cgs)	$4.234^{+0.045}_{-0.041}$	$4.228^{+0.057}_{-0.054}$	$4.219^{+0.041}_{-0.038}$	$4.215^{+0.051}_{-0.048}$
$T_{\rm eff}$	Effective temperature (K)	5802^{+95}_{-92}	5800^{+96}_{-92}	5815 ± 88	5815 ± 89
[Fe/H]	Metallicity	$0.326^{+0.091}_{-0.089}$	$0.324^{+0.092}_{-0.089}$	$0.338^{+0.087}_{-0.085}$	$0.338^{+0.086}_{-0.085}$
Planet Parameters					
e	Eccentricity	—	$0.041^{+0.036}_{-0.027}$	—	$0.039^{+0.034}_{-0.026}$
ω_*	Argument of periastron (degrees) ..	—	149^{+77}_{-65}	—	156^{+73}_{-69}
P	Period (days)	$1.7100596^{+0.0000074}_{-0.0000075}$	1.7100597 ± 0.0000074	$1.7100596^{+0.0000074}_{-0.0000073}$	1.7100596 ± 0.0000074
a	Semi-major axis (AU)	$0.02956^{+0.00043}_{-0.00057}$	$0.02955^{+0.00048}_{-0.00057}$	0.02976 ± 0.00052	0.02977 ± 0.00053
M_P	Mass (M_J)	1.196 ± 0.072	$1.206^{+0.079}_{-0.076}$	$1.217^{+0.075}_{-0.073}$	$1.226^{+0.081}_{-0.078}$
R_P	Radius (R_J)	$1.52^{+0.12}_{-0.11}$	1.53 ± 0.14	$1.57^{+0.12}_{-0.11}$	$1.57^{+0.14}_{-0.13}$
ρ_P	Density (cgs)	$0.421^{+0.11}_{-0.083}$	$0.414^{+0.12}_{-0.091}$	$0.393^{+0.095}_{-0.076}$	$0.390^{+0.11}_{-0.082}$
$\log g_P$	Surface gravity	$3.107^{+0.066}_{-0.064}$	$3.103^{+0.075}_{-0.071}$	3.089 ± 0.062	$3.088^{+0.068}_{-0.067}$
T_{eq}	Equilibrium temperature (K)	1904 ± 54	1910^{+68}_{-67}	1929^{+55}_{-56}	1934 ± 65
$\langle F \rangle$	Incident flux (10^9 erg s^{-1} cm^{-2}) ...	$2.98^{+0.36}_{-0.33}$	$3.02^{+0.45}_{-0.40}$	$3.15^{+0.38}_{-0.35}$	$3.17^{+0.45}_{-0.41}$
RV Parameters					
T_C	Time of inferior conjunction (BJD$_{\rm TDB}$)	2457111.5484 ± 0.0050	2457111.5497 ± 0.0052	$2457111.5485^{+0.0049}_{-0.0050}$	2457111.5496 ± 0.0051
T_P	Time of periastron (BJD$_{\rm TDB}$)	—	$2457111.81^{+0.36}_{-0.29}$	—	$2457111.84^{+0.35}_{-0.31}$
K	RV semi-amplitude (m/s)	179.8 ± 9.0	181.3 ± 9.3	179.7 ± 8.9	181.2 ± 9.2
$M_P \sin i$ ...	Minimum mass (M_J)	$1.177^{+0.071}_{-0.070}$	$1.185^{+0.076}_{-0.074}$	$1.196^{+0.073}_{-0.072}$&$1.204^{+0.078}_{-0.075}$	
M_P/M_* ...	Mass ratio	$0.000974^{+0.000052}_{-0.000051}$	$0.000981^{+0.000053}_{-0.000052}$	$0.000967^{+0.000051}_{-0.000050}$	0.000973 ± 0.000052
u	RM linear limb darkening	0.668 ± 0.011	0.668 ± 0.011	0.668 ± 0.011	0.668 ± 0.011
γ_{AAT}	m/s	$34590.0^{+6.8}_{-6.7}$	34590.3 ± 6.7	34590.0 ± 6.7	34590.3 ± 6.6
$\dot{\gamma}$	RV slope (m/s/day)	0.53 ± 0.20	0.52 ± 0.23	0.52 ± 0.20	0.53 ± 0.22
$e \cos \omega_*$ ...	.....	—	$-0.019^{+0.021}_{-0.028}$	—	$-0.018^{+0.020}_{-0.028}$
$e \sin \omega_*$	.....	—	$0.005^{+0.045}_{-0.033}$	—	$0.003^{+0.040}_{-0.032}$
Primary Transit					
R_P/R_*	Radius of the planet in stellar radii ..	$0.1143^{+0.0029}_{-0.0026}$	$0.1142^{+0.0029}_{-0.0026}$	$0.1141^{+0.0029}_{-0.0026}$	$0.1141^{+0.0030}_{-0.0026}$
a/R_*	Semi-major axis in stellar radii	$4.64^{+0.25}_{-0.22}$	$4.60^{+0.33}_{-0.28}$	$4.54^{+0.23}_{-0.20}$	$4.51^{+0.28}_{-0.25}$
i	Inclination (degrees)	$79.67^{+0.80}_{-0.77}$	79.5 ± 1.2	79.36 ± 0.75	79.2 ± 1.1
b	Impact parameter	$0.831^{+0.020}_{-0.022}$	$0.831^{+0.020}_{-0.022}$	$0.838^{+0.018}_{-0.020}$	$0.837^{+0.019}_{-0.021}$
δ	Transit depth	$0.01306^{+0.00067}_{-0.00059}$	$0.01305^{+0.00067}_{-0.00059}$	$0.01302^{+0.00067}_{-0.00058}$	$0.01301^{+0.00068}_{-0.00058}$
T_O	Ephemeris from transits (BJD$_{\rm TDB}$) ..	2457091.028632±0.00047	—	—	—
$P_{Transits}$ ...	Ephemeris period from transits (days)	1.7100588±0.0000025	—	—	—
T_{FWHM} ...	FWHM duration (days)	$0.0626^{+0.0018}_{-0.0025}$	$0.0626^{+0.0017}_{-0.0025}$	$0.0625^{+0.0019}_{-0.0028}$	$0.0625^{+0.0019}_{-0.0028}$
τ	Ingress/egress duration (days)	$0.0262^{+0.0046}_{-0.0037}$	$0.0261^{+0.0046}_{-0.0036}$	$0.0274^{+0.0048}_{-0.0037}$	$0.0274^{+0.0049}_{-0.0037}$
T_{14}	Total duration (days)	$0.0889^{+0.0025}_{-0.0026}$	0.0888 ± 0.0026	$0.0900^{+0.0024}_{-0.0025}$	0.0900 ± 0.0025
P_T	A priori non-grazing transit probability	$0.1910^{+0.0089}_{-0.0094}$	$0.194^{+0.020}_{-0.017}$	$0.1952^{+0.0086}_{-0.0089}$	$0.197^{+0.018}_{-0.016}$
$P_{T,G}$	A priori transit probability	$0.240^{+0.012}_{-0.013}$	$0.244^{+0.025}_{-0.022}$	0.246 ± 0.012	$0.248^{+0.023}_{-0.021}$
u_{1B}	Linear Limb-darkening	0.685 ± 0.026	$0.685^{+0.027}_{-0.026}$	$0.684^{+0.026}_{-0.025}$	$0.684^{+0.026}_{-0.025}$
u_{2B}	Quadratic Limb-darkening	$0.134^{+0.020}_{-0.021}$	$0.133^{+0.020}_{-0.021}$	0.135 ± 0.020	0.135 ± 0.020
u_{1I}	Linear Limb-darkening	$0.294^{+0.015}_{-0.014}$	0.294 ± 0.015	0.293 ± 0.014	0.292 ± 0.014
u_{2I}	Quadratic Limb-darkening	$0.2810^{+0.0074}_{-0.0075}$	0.2810 ± 0.0075	$0.2824^{+0.0070}_{-0.0072}$	$0.2825^{+0.0071}_{-0.0073}$
u_{1R}	Linear Limb-darkening	$0.382^{+0.018}_{-0.017}$	0.382 ± 0.018	$0.380^{+0.018}_{-0.017}$	$0.380^{+0.018}_{-0.017}$
u_{2R}	Quadratic Limb-darkening	$0.2777^{+0.0096}_{-0.010}$	$0.2776^{+0.0098}_{-0.010}$	$0.2789^{+0.0094}_{-0.0098}$	$0.2790^{+0.0093}_{-0.0099}$
$u_{1Sloang}$ ...	Linear Limb-darkening	$0.602^{+0.025}_{-0.024}$	$0.602^{+0.026}_{-0.025}$	$0.601^{+0.025}_{-0.024}$	$0.601^{+0.025}_{-0.024}$
$u_{2Sloang}$ ...	Quadratic Limb-darkening	$0.188^{+0.017}_{-0.018}$	$0.188^{+0.018}_{-0.019}$	$0.189^{+0.017}_{-0.018}$	$0.189^{+0.017}_{-0.018}$
u_{1V}	Linear Limb-darkening	0.484 ± 0.021	$0.484^{+0.022}_{-0.021}$	$0.483^{+0.021}_{-0.020}$	$0.483^{+0.021}_{-0.020}$
u_{2V}	Quadratic Limb-darkening	$0.247^{+0.013}_{-0.014}$	$0.247^{+0.013}_{-0.014}$	0.248 ± 0.013	$0.248^{+0.013}_{-0.014}$
Secondary Eclipse					
T_S	Time of eclipse (BJD$_{\rm TDB}$)	2457110.6934 ± 0.0050	$2457112.384^{+0.022}_{-0.029}$	$2457110.6935^{+0.0049}_{-0.0050}$	$2457112.384^{+0.022}_{-0.029}$
b_S	Impact parameter	—	$0.842^{+0.080}_{-0.063}$	—	$0.845^{+0.071}_{-0.059}$
$T_{S,FWHM}$ ..	FWHM duration (days)	—	$0.0609^{+0.0065}_{-0.019}$	—	$0.0612^{+0.0069}_{-0.019}$
τ_S	Ingress/egress duration (days)	—	$0.0275^{+0.013}_{-0.0071}$	—	$0.0286^{+0.013}_{-0.0071}$
$T_{S,14}$	Total duration (days)	—	$0.0872^{+0.0035}_{-0.0048}$	—	$0.0887^{+0.0034}_{-0.0045}$
P_S	A priori non-grazing eclipse probability	—	$0.1910^{+0.0091}_{-0.0094}$	—	$0.1953^{+0.0088}_{-0.0090}$
$P_{S,G}$	A priori eclipse probability	—	0.240 ± 0.013	—	0.246 ± 0.012

Table 6.8: Median values and 68% confidence interval for the physical and orbital parameters of the KELT-15 system

Parameter	Units	**Adopted Value (YY circular)**	Value (YY eccentric)	Value (Torres circular)	Value (Torres eccentric)
Stellar Parameters					
M_*	Mass ($M_\odot$)	$1.181^{+0.051}_{-0.050}$	$1.218^{+0.10}_{-0.071}$	$1.216^{+0.057}_{-0.055}$	$1.244^{+0.092}_{-0.074}$
R_*	Radius ($R_\odot$)	$1.481^{+0.091}_{-0.041}$	$1.63^{+0.34}_{-0.18}$	$1.493^{+0.082}_{-0.042}$	$1.60^{+0.34}_{-0.17}$
L_*	Luminosity ($L_\odot$)	$2.58^{+0.35}_{-0.20}$	$3.11^{+1.3}_{-0.69}$	$2.65^{+0.32}_{-0.20}$	$3.04^{+1.4}_{-0.65}$
ρ_*	Density (cgs)	$0.514^{+0.034}_{-0.076}$	$0.40^{+0.15}_{-0.14}$	$0.518^{+0.032}_{-0.071}$	$0.42^{+0.15}_{-0.17}$
$\log g_*$	Surface gravity (cgs)	$4.168^{+0.019}_{-0.044}$	$4.100^{+0.086}_{-0.11}$	$4.174^{+0.018}_{-0.040}$	$4.120^{+0.084}_{-0.14}$
$T_{\rm eff}$	Effective temperature (K)	6003^{+56}_{-52}	6017^{+58}_{-57}	6021^{+60}_{-61}	6021^{+61}_{-60}
[Fe/H]	Metallicity	0.047 ± 0.032	$0.051^{+0.033}_{-0.032}$	$0.051^{+0.034}_{-0.033}$	0.051 ± 0.033
Planet Parameters					
e	Eccentricity	—	$0.132^{+0.13}_{-0.090}$	—	$0.133^{+0.14}_{-0.091}$
ω_*	Argument of periastron (degrees) ..	—	141^{+71}_{-42}	—	142^{+76}_{-42}
P	Period (days)	3.329441 ± 0.000016	3.329442 ± 0.000016	3.329441 ± 0.000016	3.329442 ± 0.000016
a	Semi-major axis (AU)	0.04613 ± 0.00065	$0.04660^{+0.0013}_{-0.00092}$	0.04657 ± 0.00072	$0.04693^{+0.0011}_{-0.00095}$
M_P	Mass (M_J)	$0.91^{+0.21}_{-0.22}$	$0.94^{+0.26}_{-0.25}$	0.93 ± 0.22	$0.95^{+0.26}_{-0.25}$
R_P	Radius (R_J)	$1.443^{+0.11}_{-0.057}$	$1.59^{+0.31}_{-0.19}$	$1.453^{+0.098}_{-0.057}$	$1.56^{+0.34}_{-0.18}$
ρ_P	Density (cgs)	$0.36^{+0.11}_{-0.10}$	$0.28^{+0.15}_{-0.11}$	$0.363^{+0.11}_{-0.100}$	$0.29^{+0.16}_{-0.13}$
$\log g_P$	Surface gravity	$3.02^{+0.10}_{-0.13}$	$2.95^{+0.14}_{-0.17}$	$3.03^{+0.10}_{-0.12}$	$2.96^{+0.15}_{-0.18}$
T_{eq}	Equilibrium temperature (K)	1642^{+45}_{-25}	1713^{+140}_{-92}	1645^{+41}_{-25}	1699^{+150}_{-87}
$\langle F \rangle$	Incident flux (10^9 erg s^{-1} cm^{-2}) ...	$1.652^{+0.19}_{-0.100}$	$1.92^{+0.58}_{-0.37}$	$1.66^{+0.17}_{-0.10}$	$1.86^{+0.63}_{-0.35}$
RV Parameters					
T_C	Time of inferior conjunction ($\rm BJD_{TDB}$)	$2457029.1663^{+0.0078}_{-0.0073}$	$2457029.1691^{+0.0083}_{-0.0081}$	$2457029.1663^{+0.0079}_{-0.0073}$	$2457029.1688^{+0.0084}_{-0.0080}$
T_P	Time of periastron ($\rm BJD_{TDB}$)	—	$2457029.49^{+0.64}_{-0.29}$	—	$2457029.50^{+0.71}_{-0.29}$
K	RV semi-amplitude (m/s)	110 ± 26	113 ± 30	110 ± 26	113^{+30}_{-29}
$M_P \sin i$ ...	Minimum mass (M_J)	$0.91^{+0.21}_{-0.22}$	$0.94^{+0.26}_{-0.25}$	0.93 ± 0.22	$0.95^{+0.26}_{-0.25}$
M_P/M_* ...	Mass ratio	0.00073 ± 0.00017	0.00073 ± 0.00019	0.00073 ± 0.00017	0.00073 ± 0.00019
u	RM linear limb darkening	$0.6290^{+0.0062}_{-0.0058}$	$0.6275^{+0.0065}_{-0.0059}$	$0.6276^{+0.0066}_{-0.0060}$	$0.6272^{+0.0066}_{-0.0060}$
γ_{AAT}	m/s	12204^{+18}_{-19}	12203 ± 21	12204 ± 19	12204 ± 20
$\gamma_{CORALIE}$ ..	m/s	12216 ± 22	12212 ± 22	12216 ± 21	12211 ± 22
$e \cos \omega_*$ ...	.....	—	$-0.073^{+0.073}_{-0.10}$	—	$-0.074^{+0.074}_{-0.10}$
$e \sin \omega_*$	.....	—	$0.050^{+0.14}_{-0.082}$	—	$0.042^{+0.16}_{-0.085}$
Primary Transit					
R_P/R_*	Radius of the planet in stellar radii ..	$0.1001^{+0.0022}_{-0.0021}$	$0.1005^{+0.0025}_{-0.0023}$	$0.1001^{+0.0021}_{-0.0020}$	$0.1001^{+0.0022}_{-0.0021}$
a/R_*	Semi-major axis in stellar radii	$6.70^{+0.14}_{-0.35}$	$6.16^{+0.68}_{-0.83}$	$6.72^{+0.13}_{-0.32}$	$6.29^{+0.67}_{-0.99}$
i	Inclination (degrees)	$88.3^{+1.2}_{-1.7}$	$87.8^{+1.6}_{-2.3}$	$88.4^{+1.1}_{-1.6}$	$88.1^{+1.3}_{-2.2}$
b	Impact parameter	$0.20^{+0.18}_{-0.14}$	$0.22^{+0.19}_{-0.15}$	$0.19^{+0.17}_{-0.13}$	$0.20^{+0.17}_{-0.13}$
δ	Transit depth	$0.01003^{+0.00044}_{-0.00041}$	$0.01009^{+0.00050}_{-0.00046}$	$0.01001^{+0.00043}_{-0.00040}$	$0.01002^{+0.00044}_{-0.00041}$
T_{FWHM} ...	FWHM duration (days)	$0.1552^{+0.0015}_{-0.0016}$	$0.1552^{+0.0017}_{-0.0018}$	$0.1551^{+0.0015}_{-0.0016}$	0.1550 ± 0.0016
τ	Ingress/egress duration (days)	$0.01635^{+0.0021}_{-0.00079}$	$0.01656^{+0.0026}_{-0.00093}$	$0.01627^{+0.0019}_{-0.00074}$	$0.01631^{+0.0020}_{-0.00076}$
T_{14}	Total duration (days)	$0.1719^{+0.0025}_{-0.0021}$	$0.1722^{+0.0030}_{-0.0024}$	$0.1717^{+0.0024}_{-0.0020}$	$0.1717^{+0.0025}_{-0.0021}$
P_T	A priori non-grazing transit probability	$0.1343^{+0.0072}_{-0.0027}$	$0.155^{+0.058}_{-0.026}$	$0.1340^{+0.0066}_{-0.0026}$	$0.151^{+0.068}_{-0.025}$
$P_{T,G}$	A priori transit probability	$0.1642^{+0.0092}_{-0.0036}$	$0.190^{+0.070}_{-0.032}$	$0.1637^{+0.0084}_{-0.0033}$	$0.185^{+0.084}_{-0.031}$
u_{1I}	Linear Limb-darkening	$0.2500^{+0.0078}_{-0.0069}$	$0.2471^{+0.0086}_{-0.0079}$	$0.2482^{+0.0083}_{-0.0073}$	$0.2468^{+0.0086}_{-0.0077}$
u_{2I}	Quadratic Limb-darkening	$0.2964^{+0.0027}_{-0.0036}$	$0.2980^{+0.0036}_{-0.0040}$	$0.2972^{+0.0028}_{-0.0037}$	$0.2980^{+0.0034}_{-0.0039}$
u_{1R}	Linear Limb-darkening	$0.3259^{+0.0092}_{-0.0080}$	$0.3231^{+0.0098}_{-0.0086}$	$0.3237^{+0.0098}_{-0.0083}$	$0.3227^{+0.0098}_{-0.0085}$
u_{2R}	Quadratic Limb-darkening	$0.3027^{+0.0033}_{-0.0046}$	$0.3042^{+0.0038}_{-0.0048}$	$0.3037^{+0.0035}_{-0.0048}$	$0.3043^{+0.0037}_{-0.0048}$
u_{1V}	Linear Limb-darkening	$0.4158^{+0.011}_{-0.0091}$	$0.4132^{+0.011}_{-0.0092}$	$0.4133^{+0.011}_{-0.0094}$	$0.4127^{+0.011}_{-0.0094}$
u_{2V}	Quadratic Limb-darkening	$0.2858^{+0.0045}_{-0.0061}$	$0.2871^{+0.0044}_{-0.0061}$	$0.2871^{+0.0046}_{-0.0062}$	$0.2874^{+0.0045}_{-0.0061}$
Secondary Eclipse					
T_S	Time of eclipse ($\rm BJD_{TDB}$)	$2457027.5016^{+0.0078}_{-0.0073}$	$2457030.68^{+0.16}_{-0.22}$	$2457027.5015^{+0.0079}_{-0.0073}$	$2457030.68^{+0.16}_{-0.22}$
b_S	Impact parameter	—	$0.25^{+0.22}_{-0.17}$	—	$0.22^{+0.22}_{-0.15}$
$T_{S,FWHM}$ ..	FWHM duration (days)	—	$0.168^{+0.046}_{-0.022}$	—	$0.166^{+0.052}_{-0.024}$
τ_S	Ingress/egress duration (days)	—	$0.0193^{+0.0076}_{-0.0039}$	—	$0.0185^{+0.0085}_{-0.0036}$
$T_{S,14}$	Total duration (days)	—	$0.189^{+0.051}_{-0.026}$	—	$0.186^{+0.060}_{-0.028}$
P_S	A priori non-grazing eclipse probability	—	$0.1394^{+0.011}_{-0.0057}$	—	$0.1383^{+0.011}_{-0.0051}$
$P_{S,G}$	A priori eclipse probability	—	$0.1705^{+0.014}_{-0.0072}$	—	$0.1690^{+0.014}_{-0.0064}$

in Boulder, CO for PEST observatory) and typically the synchronization is redone through out the observing night. From our experience, we have found the time stamp in the image header and the actual start of observations can differ by a few seconds. Using only the transit timing data shown in Table 6.9 and Figure 6.9, we determined a separate ephemeris from our global fit for KELT-14b. To determine an independent ephemeris, we performed a linear fit to the transit center times inferred from the global fit for each follow-up observation. With a χ^2 of 26.9 and 6 degrees of freedom, we get T_0=2457091.028632±0.00046884453 (BJD_{TDB}) and a period of 1.7100588±0.00000247 days. The high χ^2 is likely caused by systematics in the follow-up photometric observations. Although most epochs are consistent with the linear ephemeris listed (see Figure 6.9), we do have a few apparent outliers (<10 minutes). Significant differences in measured transit times can be a result of the differences in the observatory clocks, observing procedures and conditions, and astrophysical red noise [Carter and Winn, 2009]. We do see these outliers as significant. The high χ^2 is likely dominated by the three transits at epoch -1, and specifically the ICO transit which differs from the PEST and Hazelwood transits by 8 minutes. However, we find no evidence of an issue with the observations time stamps and attribute the discrepancy to be a systematic and not astrophysical in nature. Therefore, we are unwilling to claim convincing evidence for significant transit timing variations for KELT-14b. With only three transits of KELT-15b, we do not attempt a TTV analysis.

6.5 False Positive Analysis

A similar signal to a true planetary event can be created by a variety of astrophysical and non-astrophysical scenarios. All spectroscopic observations of both KELT-14 and KELT-15 were thoroughly analyzed to ensure that the observed signal was from the target star. There are no signs of multiple sets of absorption lines. As mentioned in \$6.2.3.2, we find no correlation between the bisector spans and the measured radial velocities (see Figure 6.6). All transit depths across optical band passes are consistent and the global fit $\log g_*$ is

Table 6.9: Transit times for KELT-14b.

Epoch	T_C (BJD$_{\rm TDB}$)	σ_{T_C} (s)	O-C (s)	O-C (σ_{T_C})	Telescope
-29	2457043.146899	67	-5.00	-0.07	PEST
-26	2457048.276707	83	-37.99	-0.45	PEST
-1	2457091.027548	93	-102.01	-1.09	PEST
-1	2457091.033997	134	455.19	3.37	ICO
-1	2457091.027674	121	-91.12	-0.75	Hazelwood
6	2457103.002776	119	311.42	2.60	Hazelwood
11	2457111.550157	169	57.80	0.34	LCOGT
13	2457114.965950	113	-316.62	-2.78	Hazelwood

consistent with the spectroscopic analysis for KELT-14. There is some discrepancy in the KELT-15 $\log g_*$ from the global fit and SME analysis but this is because the AAT spectra do not include the gravity sensitive MgB triplet to provide a better constraint on $\log g_*$. Overall, we find no evidence that KELT-14b and KELT-15b are anything other than transiting exoplanets, but a better estimate of the $\log g_*$ of KELT-15 using a high-resolution spectrum covering the gravity sensitive MgB triplet would help confirm the planetary nature of the companion.

6.6 Discussion

6.6.1 Evolution

As can be seen from the results of the global fit (Table 6.7 and 6.8), KELT-14b and KELT-15b are highly inflated planets, joining the ranks of other hot Jupiters that manifest radii much larger than predicted by standard, non-irradiated models. Several authors [e.g., Demory and Seager, 2011] have suggested an empirical insolation threshold ($\approx 2\times10^8$ erg s^{-1} cm^{-2}) above which hot Jupiters exhibit increasing amounts of radius inflation. KELT-14b and KELT-15b clearly lie above this threshold, with a current estimated insolation of $2.98^{+0.36}_{-0.33}\times10^9$ erg s^{-1} cm^{-2} and $1.652^{+0.19}_{-0.100}\times10^9$ erg s^{-1} cm^{-2}, respectively, from the global fits, and therefore their currently large inflated radii are not surprising. At the same

time, the KELT-14 and KELT-15 host stars are both found to be at present in a state of evolution wherein the stellar radii are expanding as the stars prepare to cross the Hertzsprung gap toward the red giant branch. This means that the stars' surfaces are encroaching on their planets, which presumably is in turn driving up the planets' insolations and also the rate of any tidal interactions between the planets and the stars.

Therefore it is interesting to consider two questions. First, has KELT-14b's and KELT-15b's incident radiation from their host stars been below the empirical radius inflation threshold in the past? If either planet's insolation only recently exceeded the inflation threshold, the system could then serve as an empirical test bed for the different timescales predicted by different inflation mechanisms [see, e.g., Assef et al., 2009, Spiegel and Madhusudhan, 2012]. Second, what is the expected fate of the KELT-14b and KELT-15b planets given the increasingly strong tidal interactions they are experiencing with their encroaching host stars?

To investigate these questions, we follow Penev et al. [2014] to simulate the reverse and forward evolution of the star-planet system, using the measured parameters listed in Table 6.7 and 6.8 as the present-day boundary conditions. This analysis is not intended to examine any type of planet-planet or planet-disk migration effects. Rather, it is a way to investigate (1) the change in insolation of the planet over time due to the changing luminosity of the star and changing star-planet separation, and (2) the change in the planet's orbital semi-major axis due to the changing tidal torque as the star-planet separation changes with the evolving stellar radius. We include the evolution of the star, assumed to follow the Yonsei-Yale stellar model with mass and metallicity. For simplicity we assume that the stellar rotation is negligible and treat the star as a solid body. We also assume a circular orbit aligned with the stellar equator throughout the analysis. The results of our simulations are shown in Figure 6.10. We tested a range of values for the tidal quality factor of the star divided by the love number, $Q'_\star \equiv Q_\star/k_2$, from $\log Q'_\star = 5$ to $\log Q'_\star = 7$ (assuming a constant phase lag between the tidal bulge and the star-planet direction).

We find that although for certain values of $Q'_\star$ the planets may have been initially below the insolation inflation threshold during the first ~100 Myr, in all cases the planets have always received more than enough flux from their hosts to keep the planets irradiated beyond the insolation threshold identified by Demory and Seager [2011].

KELT-15b appears destined to survive for at least the next few Gyr, unless the stellar $Q'_\star$ is very small, in which case it is predicted to experience a rapid in-spiral into its host star. In the case of KELT-14b, the current evolution of the star suggests a concomitant in-spiral of the planet over the next ~1 Gyr, and even faster if the stellar $Q'_\star$ is small. This planet therefore does not appear destined to survive beyond the star's subgiant phase. As additional systems like KELT-14b are discovered and their evolution investigated in detail, it will be interesting to examine the statistics of planet survival and to compare these to predictions such as those shown here in Figure 6.10 to constrain mechanisms of planet-star interaction generally and the values of $Q'_\star$ specifically.

6.6.2 Opportunities for Atmospheric Characterization

Because of its very high equilibrium temperature (1904 K) and its bright K-band magnitude ($K = 9.424$), KELT-14b is an excellent target for detailed atmospheric characterization. Specifically we note that it is an especially ideal target for eclipse observations. Measurements during the secondary eclipse of a hot Jupiter provide a direct measurement of thermal emission from the planet's dayside and allow constraints on the connection between the atmospheric structure and climate and irradiation from the host star. As illustrated in Figure 6.11, KELT-14b has the second largest expected emission signal in the K-band for known transiting planets brighter than $K < 10.5$. We therefore encourage follow up of this planet in eclipse in order to aid comparative studies of exoplanet atmospheres and better understand the connection between irradiation, albedo, and atmospheric circulation.

With an equilibrium temperature of 1642 K, KELT-15b is not as hot as KELT-14b. However, it still has a comparably large expected emission signal in the K band that should

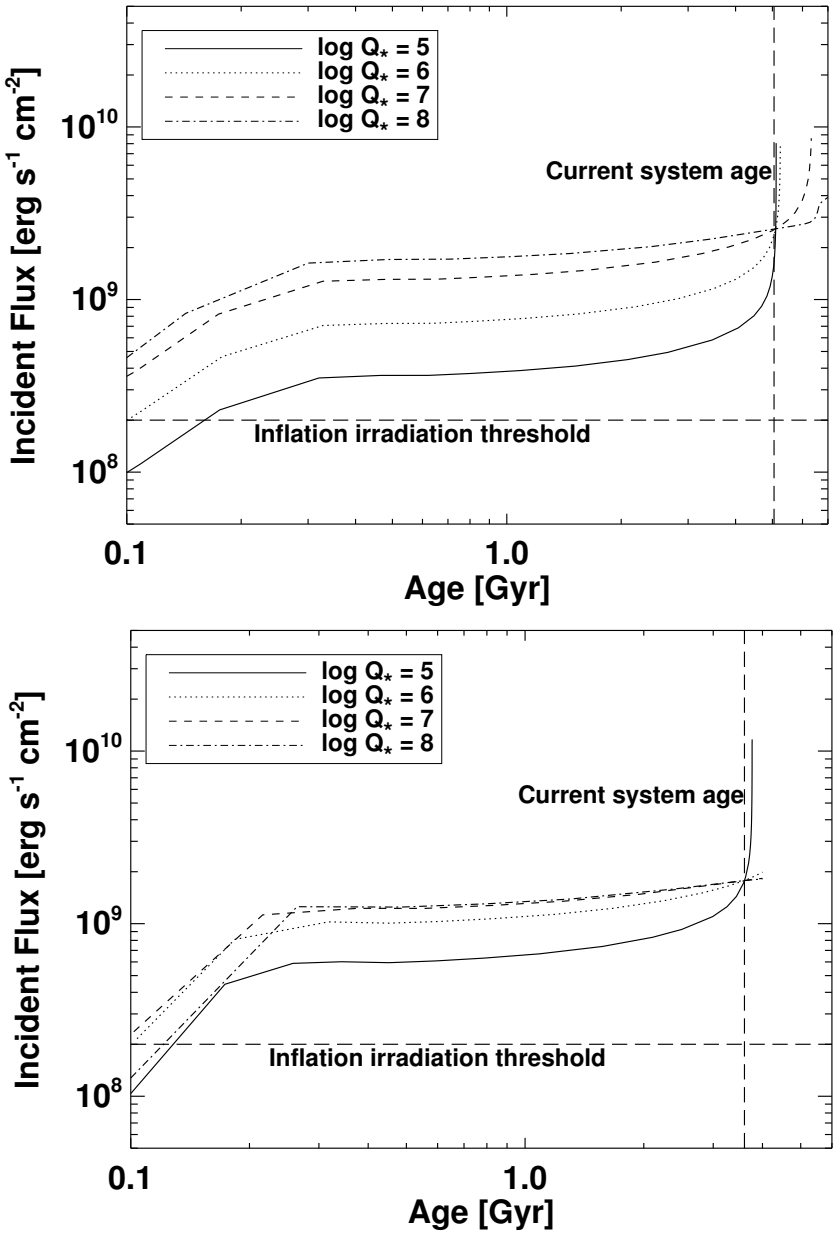

Figure 6.10: The inflation irradiation history for (top) KELT-14 and (bottom) KELT-15 shown for test values of $\log Q'_\star$ of 5 to 8. The model assumes the stellar rotation is negligible and treats the star as a solid body. Also the model assumes a circular orbit aligned with the stellar equator. For both KELT-14b and KELT-15b, we find an the insolation received is above the empirical threshold (horizontal dashed line) determined by Demory and Seager [2011]. The vertical line represents the estimated current age of the system.

be detectable with ground-based telescopes. Observing multiple planets in eclipse that span a range of temperatures and other properties is particularly useful for comparative exoplanetology.

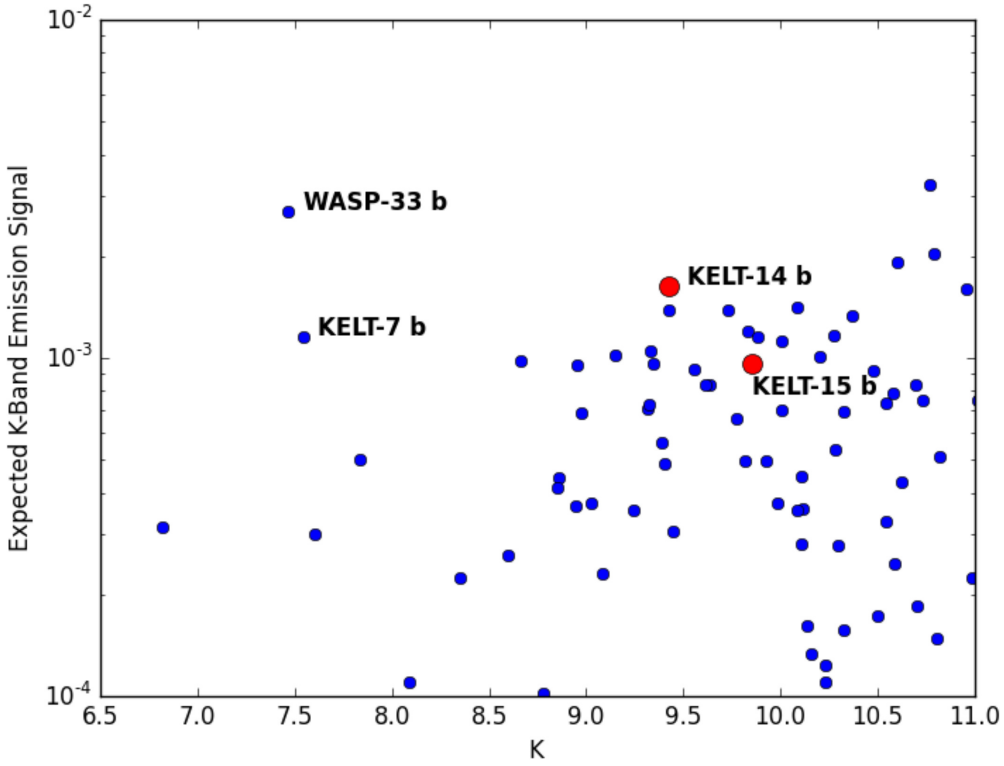

Figure 6.11: The expected day-side thermal emission from the planet in the K-band (assuming no redistribution of heat) for all known transiting planets brighter than a K-band magnitude of 11. Along with KELT-14b and KELT-15b, we highlight WASP-33b, one of the hottest known transiting planets and KELT-7b, another very hot and very bright planet discovered by the northern component of the KELT survey. Data are from this paper and the NASA Exoplanet Archive, accessed on 2015 August 27.

6.6.3 Spectroscopic Follow-up

From our global fit, we find that KELT-14b has a 0.53 ± 0.20 m s^{-1}day^{-1} RV slope. It is possible that this RV trend is from a tertiary component in the system. Another discovery from the KELT survey, KELT-6b, showed a -0.239 ± 0.037 m s^{-1}day^{-1} slope in the RV analysis [Collins et al., 2014]. Recently, the RV slope of KELT-6 has been confirmed to

be the result of KELT-6c, a 3.5 year period companion with a minimum mass of $M_P \sin i = 3.71 \pm 0.21\ M_J$ [Damasso et al., 2015]. We therefore recommend long term spectroscopic follow-up of KELT-14 to try and characterize the long term trend we observed. Also, both KELT-14b and KELT-15b have Rossiter-McLaughlin (R-M) effects that can be detected with current ground−based facilities ($\sim 90\ \mathrm{m\,s^{-1}}$). Two of our radial velocity observations of KELT-15b were taken during the transit and hint at a prograde orbit. However, due to our limited data acquired in transit, we do not claim KELT-15b to be in a prograde orbit but suggest future R−M observations to determine the spin-orbit alignment of the system.

6.7 Summary and Conclusions

We present the discovery of two more transiting inflated hot Jupiter exoplanets from the KELT-South survey, KELT-14b and KELT-15b. KELT-14b, the independent discovery of WASP-122b [Turner et al., 2015] has a period of $1.7100596^{+0.0000074}_{-0.0000075}$ days, a radius of $1.52^{+0.12}_{-0.11}\ R_J$ and a mass of $1.196 \pm 0.072\ M_J$. KELT-15b has a period of 3.329441 ± 0.000016 days, a radius of $1.443^{+0.11}_{-0.057}\ R_J$ and a mass of $0.91^{+0.21}_{-0.22}\ M_J$. Additional follow-up transits are highly desirable for KELT-15b in order to better refine the ephemeris for future follow-up studies. Both KELT-14b and KELT-15b orbit host stars that are bright in the near-IR (K = 9.424 and 9.854, respectively), making them attractive targets for atmospheric characterization through secondary eclipse observations. Both should have large enough emission signals that they can be observed using ground-based observatories. These newly discovered planets increase the number of targets suitable for atmospheric characterization in the southern hemisphere.

Chapter 7

Conclusion

The DESK and KELT exoplanet discoveries afford us the ability to probe a variety of different stages of planet formation and evolution. Specifically, the DESK survey targets the formation of planets in the disks surrounding detected host stars. Although there have only been a few disk eclipsing events, they have already led to such insights as the discovery of dense planet-forming structures within the tidally disrupted disk of a young binary star system [Rodriguez et al., 2013], of Saturn-like rings and gaps in the disk surrounding a young planet [Mamajek et al., 2012], of stratified dust coagulation within a young protoplanetary disk [Bouvier et al., 2013, Rodriguez et al., 2015b], and of an evolved binary star system with remnant planet-building material [Rodriguez et al., 2016]. The discovery and characterization of the KELT exoplanets complements the DESK results by providing insight into the evolution and migration mechanisms once the planets have already formed.

This work has not only already enhanced our knowledge of circumstellar environments and the early stages of stellar and planetary evolution, it will also provide a testbed for the next generation of time domain photometric surveys. Specifically, current and upcoming projects such as PAN-STARRS and LSST will increase the number of stars with long-baseline photometric observations by at least two orders of magnitude. Furthermore, the systems studied by the DESK survey will provide excellent targets for NASA's James Webb Space Telescope, an observatory which will be able to probe the environments of such systems in detail. In addition, the techniques and tools developed from this work will provide a framework to search for these rare systems using data from the Large Synoptic Survey Telescope (LSST) that will observe the entire Southern sky at a cadence of a few days. Given the large number of stars LSST will target and its expected lifetime, it should increase the number of disk eclipsing systems known by an order of magnitude.

BIBLIOGRAPHY

B. C. Addison, C. G. Tinney, D. J. Wright, D. Bayliss, G. Zhou, J. D. Hartman, G. Á. Bakos, and B. Schmidt. A Nearly Polar Orbit for the Extrasolar Hot Jupiter WASP-79b. *The Astrophysical Journal Letters*, 774:L9, September 2013. doi: 10.1088/2041-8205/774/1/L9.

B. C. Addison, C. G. Tinney, D. J. Wright, and D. Bayliss. A Spin-Orbit Alignment for the Hot Jupiter HATS-3b. *The Astrophysical Journal*, 792:112, September 2014. doi: 10.1088/0004-637X/792/2/112.

V. Afanasiev, D. Denisenko, V. Krushinsky, E. Gorbovskoy, V. Lipunov, P. Balanutsa, V. Yecheistov, N. Tiurina, V. Kornilov, A. Belinski, N. Shatskiy, V. Chazov, A. Kuznetsov, D. Zimnukhov, I. Zalozhnih, A. Popov, A. Bourdanov, A. Punanova, K. Ivanov, S. Yazev, N. Budnev, E. Konstantinov, O. Chuvalaev, V. Poleshchuk, O. Gress, A. Parkhomenko, A. Tlatov, D. Dormidontov, V. Senik, V. Yurkov, Y. Sergienko, D. Varda, E. Sinyakov, S. Shurpakov, V. Shumkov, P. Podvorotny, H. Levato, C. Saffe, C. Mallamaci, C. Lopez, and F. Podest. Follow up spectroscopy and photometry of TYC 2505-672-1 (MASTER OT J095310.04+335352.8). *The Astronomer's Telegram*, 4834:1, February 2013.

C. Alard. Image subtraction using a space-varying kernel. *Astronomy and Astrophysics Supplement*, 144:363–370, June 2000. doi: 10.1051/aas:2000214.

C. Alard and R. H. Lupton. A Method for Optimal Image Subtraction. *The Astrophysical Journal*, 503:325–331, August 1998. doi: 10.1086/305984.

R. Alonso, T. M. Brown, G. Torres, D. W. Latham, A. Sozzetti, G. Mandushev, J. A. Belmonte, D. Charbonneau, H. J. Deeg, E. W. Dunham, F. T. O'Donovan, and R. P.

Stefanik. TrES-1: The Transiting Planet of a Bright K0 V Star. *The Astrophysical Journal Letters*, 613:L153–L156, October 2004. doi: 10.1086/425256.

R. Alonso, T. M. Brown, D. Charbonneau, E. W. Dunham, J. A. Belmonte, H. J. Deeg, J. M. Fernández, D. W. Latham, G. Mandushev, F. T. O'Donovan, M. Rabus, and G. Torres. The Transatlantic Exoplanet Survey (TrES): A Review. In C. Afonso, D. Weldrake, and T. Henning, editors, *Transiting Extrapolar Planets Workshop*, volume 366 of *Astronomical Society of the Pacific Conference Series*, page 13, July 2007.

S. M. Ammons, S. E. Robinson, J. Strader, G. Laughlin, D. Fischer, and A. Wolf. The N2K Consortium. IV. New Temperatures and Metallicities for More than 100,000 FGK Dwarfs. *The Astrophysical Journal*, 638:1004–1017, February 2006. doi: 10.1086/498490.

S. M. Andrews, K. A. Rosenfeld, A. L. Kraus, and D. J. Wilner. The Mass Dependence between Protoplanetary Disks and their Stellar Hosts. *The Astrophysical Journal*, 771:129, July 2013. doi: 10.1088/0004-637X/771/2/129.

S. Antipin, A. Belinski, A. Cherepashchuk, D. Cherjasov, A. Dodin, I. Gorbunov, S. Lamzin, M. Kornilov, V. Kornilov, S. Potanin, B. Safonov, V. Senik, N. Shatsky, and O. Voziakova. Resolved photometry of the binary components of RW Aur. *Information Bulletin on Variable Stars*, 6126:1, January 2015.

P. J. Armitage and J. E. Pringle. Radiation-induced Warping of Protostellar Accretions Disks. *The Astrophysical Journal Letters*, 488:L47–L50, October 1997. doi: 10.1086/310907.

R. J. Assef, B. S. Gaudi, and K. Z. Stanek. Detecting Transits of Planetary Companions to Giant Stars. *The Astrophysical Journal*, 701:1616–1626, August 2009. doi: 10.1088/0004-637X/701/2/1616.

A. Baglin, M. Auvergne, L. Boisnard, T. Lam-Trong, P. Barge, C. Catala, M. Deleuil, E. Michel, and W. Weiss. CoRoT: a high precision photometer for stellar ecolution and exoplanet finding. In *36th COSPAR Scientific Assembly*, volume 36 of *COSPAR Meeting*, page 3749, 2006.

G. Bakos, R. W. Noyes, G. Kovács, K. Z. Stanek, D. D. Sasselov, and I. Domsa. Wide-Field Millimagnitude Photometry with the HAT: A Tool for Extrasolar Planet Detection. *Publications of the Astronomical Society of the Pacific*, 116:266–277, March 2004. doi: 10.1086/382735.

I. Baraffe, G. Chabrier, F. Allard, and P. H. Hauschildt. Evolutionary models for solar metallicity low-mass stars: mass-magnitude relationships and color-magnitude diagrams. *Astronomy and Astrophysics*, 337:403–412, September 1998.

A. Baranne, D. Queloz, M. Mayor, G. Adrianzyk, G. Knispel, D. Kohler, D. Lacroix, J.-P. Meunier, G. Rimbaud, and A. Vin. ELODIE: A spectrograph for accurate radial velocity measurements. *Astronomy and Astrophysics Supplement*, 119:373–390, October 1996.

D. Bayliss, G. Zhou, K. Penev, G. Á. Bakos, J. D. Hartman, A. Jordán, L. Mancini, M. Mohler-Fischer, V. Suc, M. Rabus, B. Béky, Z. Csubry, L. Buchhave, T. Henning, N. Nikolov, B. Csák, R. Brahm, N. Espinoza, R. W. Noyes, B. Schmidt, P. Conroy, D. J. Wright, C. G. Tinney, B. C. Addison, P. D. Sackett, D. D. Sasselov, J. Lázár, I. Papp, and P. Sári. HATS-3b: An Inflated Hot Jupiter Transiting an F-type Star. *The Astronomical Journal*, 146:113, November 2013. doi: 10.1088/0004-6256/146/5/113.

T. G. Beatty, J. Pepper, R. J. Siverd, J. D. Eastman, A. Bieryla, D. W. Latham, L. A. Buchhave, E. L. N. Jensen, M. Manner, K. G. Stassun, B. S. Gaudi, P. Berlind, M. L. Calkins, K. Collins, D. L. DePoy, G. A. Esquerdo, B. J. Fulton, G. Fűrész, J. C. Geary, A. Gould, L. Hebb, J. F. Kielkopf, J. L. Marshall, R. Pogge, K. Z. Stanek, R. P. Stefanik, R. Street, A. H. Szentgyorgyi, M. Trueblood, P. Trueblood, and A. M. Stutz. KELT-2Ab:

A Hot Jupiter Transiting the Bright (V = 8.77) Primary Star of a Binary System. *The Astrophysical Journal Letters*, 756:L39, September 2012. doi: 10.1088/2041-8205/756/2/L39.

T. L. Beck and M. Simon. The Variability of T Tauri, RY Tauri, and RW Aurigae from 1899 to 1952. *The Astronomical Journal*, 122:413–417, July 2001. doi: 10.1086/321133.

T. Bensby, S. Feltzing, and I. Lundström. Elemental abundance trends in the Galactic thin and thick disks as traced by nearby F and G dwarf stars. *Astronomy and Astrophysics*, 410:527–551, November 2003. doi: 10.1051/0004-6361:20031213.

L. N. Berdnikov, A. A. Ermash, and S. A. Lamzin. Interpretation of the light curve for the young binary (?) system UY Aur. *Astronomy Letters*, 36:653–663, September 2010. doi: 10.1134/S1063773710090045.

E. Bertin and S. Arnouts. SExtractor: Software for source extraction. *Astronomy and Astrophysics Supplement*, 117:393–404, June 1996. doi: 10.1051/aas:1996164.

C. Bertout. Occultation of young stellar objects by circumstellar disks. I. Theoretical expectations and preliminary comparison with observations. *Astronomy and Astrophysics*, 363:984–990, November 2000.

C. Bertout, G. Basri, and J. Bouvier. Accretion disks around T Tauri stars. *The Astrophysical Journal*, 330:350–373, July 1988. doi: 10.1086/166476.

L. Bianchi, J. Herald, B. Efremova, L. Girardi, A. Zabot, P. Marigo, A. Conti, and B. Shiao. GALEX catalogs of UV sources: statistical properties and sample science applications: hot white dwarfs in the Milky Way. *Astrophysics and Space Science*, 335:161–169, September 2011. doi: 10.1007/s10509-010-0581-x.

E. A. Bibo and P. S. The. The type of variability of Herbig Ae/Be stars. *Astronomy and Astrophysics Supplement*, 89:319–334, August 1991.

A. Bieryla, K. Collins, T. G. Beatty, J. Eastman, R. J. Siverd, J. Pepper, B. S. Gaudi, K. G. Stassun, C. Cañas, D. W. Latham, L. A. Buchhave, R. Sanchis-Ojeda, J. N. Winn, E. L. N. Jensen, J. F. Kielkopf, K. K. McLeod, J. Gregorio, K. D. Colón, R. Street, R. Ross, M. Penny, S. N. Mellon, T. E. Oberst, B. J. Fulton, J. Wang, P. Berlind, M. L. Calkins, G. A. Esquerdo, D. L. DePoy, A. Gould, J. Marshall, R. Pogge, M. Trueblood, and P. Trueblood. KELT-7b: A Hot Jupiter Transiting a Bright V = 8.54 Rapidly Rotating F-star. *The Astronomical Journal*, 150:12, July 2015. doi: 10.1088/0004-6256/150/1/12.

D. V. Bisikalo, A. V. Dodin, P. V. Kaigorodov, S. A. Lamzin, E. V. Malogolovets, and A. M. Fateeva. Reverse rotation of the accretion disk in RW Aur A: Observations and a physical model. *Astronomy Reports*, 56:686–692, September 2012. doi: 10.1134/S1063772912090028.

W. J. Borucki, D. Koch, G. Basri, N. Batalha, T. Brown, D. Caldwell, J. Caldwell, J. Christensen-Dalsgaard, W. D. Cochran, E. DeVore, E. W. Dunham, A. K. Dupree, T. N. Gautier, J. C. Geary, R. Gilliland, A. Gould, S. B. Howell, J. M. Jenkins, Y. Kondo, D. W. Latham, G. W. Marcy, S. Meibom, H. Kjeldsen, J. J. Lissauer, D. G. Monet, D. Morrison, D. Sasselov, J. Tarter, A. Boss, D. Brownlee, T. Owen, D. Buzasi, D. Charbonneau, L. Doyle, J. Fortney, E. B. Ford, M. J. Holman, S. Seager, J. H. Steffen, W. F. Welsh, J. Rowe, H. Anderson, L. Buchhave, D. Ciardi, L. Walkowicz, W. Sherry, E. Horch, H. Isaacson, M. E. Everett, D. Fischer, G. Torres, J. A. Johnson, M. Endl, P. MacQueen, S. T. Bryson, J. Dotson, M. Haas, J. Kolodziejczak, J. Van Cleve, H. Chandrasekaran, J. D. Twicken, E. V. Quintana, B. D. Clarke, C. Allen, J. Li, H. Wu, P. Tenenbaum, E. Verner, F. Bruhweiler, J. Barnes, and A. Prsa. Kepler Planet-Detection Mission: Introduction and First Results. *Science*, 327:977–, February 2010. doi: 10.1126/science.1185402.

J. Bouvier, A. Chelli, S. Allain, L. Carrasco, R. Costero, I. Cruz-Gonzalez, C. Dougados, M. Fernández, E. L. Martín, F. Ménard, C. Mennessier, R. Mujica, E. Recillas, L. Salas,

G. Schmidt, and R. Wichmann. Magnetospheric accretion onto the T Tauri star AA Tauri. I. Constraints from multisite spectrophotometric monitoring. *Astronomy and Astrophysics*, 349:619–635, September 1999.

J. Bouvier, K. N. Grankin, S. H. P. Alencar, C. Dougados, M. Fernández, G. Basri, C. Batalha, E. Guenther, M. A. Ibrahimov, T. Y. Magakian, S. Y. Melnikov, P. P. Petrov, M. V. Rud, and M. R. Zapatero Osorio. Eclipses by circumstellar material in the T Tauri star AA Tau. II. Evidence for non-stationary magnetospheric accretion. *Astronomy and Astrophysics*, 409:169–192, October 2003. doi: 10.1051/0004-6361:20030938.

J. Bouvier, S. H. P. Alencar, T. Boutelier, C. Dougados, Z. Balog, K. Grankin, S. T. Hodgkin, M. A. Ibrahimov, M. Kun, T. Y. Magakian, and C. Pinte. Magnetospheric accretion-ejection processes in the classical T Tauri star AA Tauri. *Astronomy and Astrophysics*, 463:1017–1028, March 2007. doi: 10.1051/0004-6361:20066021.

J. Bouvier, K. Grankin, L. E. Ellerbroek, H. Bouy, and D. Barrado. AA Tauri's sudden and long-lasting deepening: enhanced extinction by its circumstellar disk. *Astronomy and Astrophysics*, 557:A77, September 2013. doi: 10.1051/0004-6361/201321389.

A. Bressan, F. Fagotto, G. Bertelli, and C. Chiosi. Evolutionary sequences of stellar models with new radiative opacities. II - Z = 0.02. *Astronomy and Astrophysics, Supplement*, 100:647–664, September 1993.

C. J. Burrows, J. E. Krist, K. R. Stapelfeldt, and WFPC2 Investigation Definition Team. HST Observations of the Beta Pictoris Circumstellar Disk. In *American Astronomical Society Meeting Abstracts*, volume 27 of *Bulletin of the American Astronomical Society*, page 1329, December 1995.

C. J. Burrows, K. R. Stapelfeldt, A. M. Watson, J. E. Krist, G. E. Ballester, J. T. Clarke, D. Crisp, J. S. Gallagher, III, R. E. Griffiths, J. J. Hester, J. G. Hoessel, J. A. Holtzman, J. R. Mould, P. A. Scowen, J. T. Trauger, and J. A. Westphal. Hubble Space Telescope

Observations of the Disk and Jet of HH 30. *The Astrophysical Journal*, 473:437, December 1996. doi: 10.1086/178156.

O. W. Butters, R. G. West, D. R. Anderson, A. Collier Cameron, W. I. Clarkson, B. Enoch, C. A. Haswell, C. Hellier, K. Horne, Y. Joshi, S. R. Kane, T. A. Lister, P. F. L. Maxted, N. Parley, D. Pollacco, B. Smalley, R. A. Street, I. Todd, P. J. Wheatley, and D. M. Wilson. The first WASP public data release. *Astronomy and Astrophysics*, 520:L10, September 2010. doi: 10.1051/0004-6361/201015655.

S. Cabrit, J. Pety, N. Pesenti, and C. Dougados. Tidal stripping and disk kinematics in the RW Aurigae system. *Astronomy and Astrophysics*, 452:897–906, June 2006. doi: 10.1051/0004-6361:20054047.

S. M. Carroll, E. F. Guinan, G. P. McCook, and R. A. Donahue. Interpreting Epsilon Aurigae. *The Astrophysical Journal*, 367:278–287, January 1991. doi: 10.1086/169626.

J. A. Carter and J. N. Winn. Parameter Estimation from Time-series Data with Correlated Errors: A Wavelet-based Method and its Application to Transit Light Curves. *The Astrophysical Journal*, 704:51–67, October 2009. doi: 10.1088/0004-637X/704/1/51.

F. Castelli and R. L. Kurucz. New Grids of ATLAS9 Model Atmospheres. *ArXiv Astrophysics e-prints*, May 2004.

A. Chelli, L. Carrasco, R. Mújica, E. Recillas, and J. Bouvier. Periodic changes of veiling and circumstellar grey extinction in DF Tauri. I. Dust clouds spiraling into a T Tauri star? *Astronomy and Astrophysics*, 345:L9–L13, May 1999.

E. I. Chiang and R. A. Murray-Clay. The Circumbinary Ring of KH 15D. *The Astrophysical Journal*, 607:913–920, June 2004. doi: 10.1086/383522.

M.-Y. Chou, M. Takami, N. Manset, T. Beck, T.-S. Pyo, W.-P. Chen, N. Panwar, J. L. Karr, H. Shang, and H. B. Liu. Time Variability of Emission Lines for Four Active T Tauri

Stars. I. October-December in 2010. *The Astronomical Journal*, 145:108, April 2013. doi: 10.1088/0004-6256/145/4/108.

C. J. Clarke and J. E. Pringle. Accretion disc response to a stellar fly-by. *Monthly Notices of the Royal Astronomical Society*, 261:190–202, March 1993.

G. C. Clayton. What Are the R Coronae Borealis Stars? *Journal of the American Association of Variable Star Observers (JAAVSO)*, 40:539, June 2012.

R. Cloutier and M.-K. Lin. Orbital migration of giant planets induced by gravitationally unstable gaps: the effect of planet mass. *Monthly Notices of the Royal Astronomical Society*, 434:621–632, September 2013. doi: 10.1093/mnras/stt1047.

K. Collins and J. Kielkopf. AstroImageJ: ImageJ for Astronomy. Astrophysics Source Code Library, September 2013.

K. A. Collins. High-precision time-series photometry for the discovery and characterization of transiting exoplanets. Electronic Theses and Dissertations, University of Louisville, May 2015.

K. A. Collins, J. D. Eastman, T. G. Beatty, R. J. Siverd, B. S. Gaudi, J. Pepper, J. F. Kielkopf, J. A. Johnson, A. W. Howard, D. A. Fischer, M. Manner, A. Bieryla, D. W. Latham, B. J. Fulton, J. Gregorio, L. A. Buchhave, E. L. N. Jensen, K. G. Stassun, K. Penev, J. R. Crepp, S. Hinkley, R. A. Street, P. Cargile, C. E. Mack, T. E. Oberst, R. L. Avril, S. N. Mellon, K. K. McLeod, M. T. Penny, R. P. Stefanik, P. Berlind, M. L. Calkins, Q. Mao, A. J. W. Richert, D. L. DePoy, G. A. Esquerdo, A. Gould, J. L. Marshall, R. J. Oelkers, R. W. Pogge, M. Trueblood, and P. Trueblood. KELT-6b: A P ˜ 7.9 Day Hot Saturn Transiting a Metal-poor Star with a Long-period Companion. *The Astronomical Journal*, 147:39, February 2014. doi: 10.1088/0004-6256/147/2/39.

A. W. Cox, C. A. Grady, H. B. Hammel, J. Hornbeck, R. W. Russell, M. L. Sitko, and

B. E. Woodgate. Imaging the Disk and Jet of the Classical T Tauri Star AA Tau. *The Astrophysical Journal*, 762:40, January 2013. doi: 10.1088/0004-637X/762/1/40.

R. M. Cutri and et al. VizieR Online Data Catalog: WISE All-Sky Data Release (Cutri+ 2012). *VizieR Online Data Catalog*, 2311:0, 2012.

R. M. Cutri and et al. VizieR Online Data Catalog: AllWISE Data Release (Cutri+ 2013). *VizieR Online Data Catalog*, 2328:0, January 2014.

R. M. Cutri, M. F. Skrutskie, S. van Dyk, C. A. Beichman, J. M. Carpenter, T. Chester, L. Cambresy, T. Evans, J. Fowler, J. Gizis, E. Howard, J. Huchra, T. Jarrett, E. L. Kopan, J. D. Kirkpatrick, R. M. Light, K. A. Marsh, H. McCallon, S. Schneider, R. Stiening, M. Sykes, M. Weinberg, W. A. Wheaton, S. Wheelock, and N. Zacarias. VizieR Online Data Catalog: 2MASS All-Sky Catalog of Point Sources (Cutri+ 2003). *VizieR Online Data Catalog*, 2246:0, June 2003.

F. Dai, S. Facchini, C. J. Clarke, and T. J. Haworth. A tidal encounter caught in the act: modelling a star-disc fly-by in the young RW Aurigae system. *Monthly Notices of the Royal Astronomical Society*, 449:1996–2009, May 2015. doi: 10.1093/mnras/stv403.

M. Damasso, M. Esposito, V. Nascimbeni, S. Desidera, A. S. Bonomo, A. Bieryla, L. Malavolta, K. Biazzo, A. Sozzetti, E. Covino, D. W. Latham, D. Gandolfi, M. Rainer, C. Petrovich, K. A. Collins, C. Boccato, R. U. Claudi, R. Cosentino, R. Gratton, A. F. Lanza, A. Maggio, G. Micela, E. Molinari, I. Pagano, G. Piotto, E. Poretti, R. Smareglia, L. Di Fabrizio, P. Giacobbe, M. Gomez-Jimenez, S. Murabito, M. Molinaro, L. Affer, M. Barbieri, L. R. Bedin, S. Benatti, F. Borsa, J. Maldonado, L. Mancini, G. Scandariato, J. Southworth, and R. Zanmar Sanchez. The GAPS programme with HARPS-N at TNG. IX. The multi-planet system KELT-6: Detection of the planet KELT-6 c and measurement of the Rossiter-McLaughlin effect for KELT-6 b. *Astronomy and Astrophysics*, 581:L6, September 2015. doi: 10.1051/0004-6361/201526995.

G. D'Angelo and S. H. Lubow. Evolution of Migrating Planets Undergoing Gas Accretion. *The Astrophysical Journal*, 685:560–583, September 2008. doi: 10.1086/590904.

F. D'Antona and I. Mazzitelli. Evolution of low mass stars. *Memorie della Societ Astronomica Italiana*, 68:807, 1997.

P. Demarque, J.-H. Woo, Y.-C. Kim, and S. K. Yi. Y^2 Isochrones with an Improved Core Overshoot Treatment. *The Astrophysical Journal Supplement*, 155:667–674, December 2004. doi: 10.1086/424966.

B.-O. Demory and S. Seager. Lack of Inflated Radii for Kepler Giant Planet Candidates Receiving Modest Stellar Irradiation. *The Astrophysical Journal Supplement*, 197:12, November 2011. doi: 10.1088/0067-0049/197/1/12.

D. Denisenko, E. Gorbovskoy, V. Lipunov, P. Balanutsa, V. Yecheistov, N. Tiurina, V. Kornilov, A. Belinski, N. Shatskiy, V. Chazov, A. Kuznetsov, D. Zimnukhov, V. Krushinsky, I. Zalozhnih, A. Popov, A. Bourdanov, A. Punanova, K. Ivanov, S. Yazev, N. Budnev, E. Konstantinov, O. Chuvalaev, V. Poleshchuk, O. Gress, A. Parkhomenko, A. Tlatov, D. Dormidontov, V. Senik, V. Yurkov, Y. Sergienko, D. Varda, E. Sinyakov, S. Shurpakov, V. Shumkov, P. Podvorotny, H. Levato, C. Saffe, C. Mallamaci, C. Lopez, and F. Podest. Optical "anti-transient" detected by MASTER. *The Astronomer's Telegram*, 4784:1, February 2013.

S. D'Odorico, H. Dekker, R. Mazzoleni, J. Vernet, I. Guinouard, P. Groot, F. Hammer, P. K. Rasmussen, L. Kaper, R. Navarro, R. Pallavicini, C. Peroux, and F. M. Zerbi. X-shooter UV- to K-band intermediate-resolution high-efficiency spectrograph for the VLT: status report at the final design review. In *Society of Photo-Optical Instrumentation Engineers (SPIE) Conference Series*, volume 6269 of *Society of Photo-Optical Instrumentation Engineers (SPIE) Conference Series*, page 33, June 2006. doi: 10.1117/12.672969.

M. Dopita, J. Hart, P. McGregor, P. Oates, G. Bloxham, and D. Jones. The Wide Field

Spectrograph (WiFeS). *Astrophysics and Space Science*, 310:255–268, August 2007. doi: 10.1007/s10509-007-9510-z.

V. D'Orazi, K. Biazzo, and S. Randich. Chemical composition of the Taurus-Auriga association. *Astronomy and Astrophysics*, 526:A103, February 2011. doi: 10.1051/0004-6361/201015616.

A. Dotter, B. Chaboyer, D. Jevremović, V. Kostov, E. Baron, and J. W. Ferguson. The Dartmouth Stellar Evolution Database. *The Astrophysical Journal Supplement*, 178:89–101, September 2008. doi: 10.1086/589654.

A. J. Drake, S. G. Djorgovski, A. Mahabal, E. Beshore, S. Larson, M. J. Graham, R. Williams, E. Christensen, M. Catelan, A. Boattini, A. Gibbs, R. Hill, and R. Kowalski. First Results from the Catalina Real-Time Transient Survey. *The Astrophysical Journal*, 696:870–884, May 2009. doi: 10.1088/0004-637X/696/1/870.

G. Duchêne, J.-L. Monin, J. Bouvier, and F. Ménard. Accretion in Taurus PMS binaries: a spectroscopic study. *Astronomy and Astrophysics*, 351:954–962, November 1999.

C. P. Dullemond, M. E. van den Ancker, B. Acke, and R. van Boekel. Explaining UX Orionis Star Variability with Self-shadowed Disks. *Astrophysical Journal Letters*, 594: L47–L50, September 2003. doi: 10.1086/378400.

T. Dumm and H. Schild. Stellar radii of M giants. *NA*, 3:137–156, April 1998. doi: 10.1016/S1384-1076(98)00003-7.

J. Eastman, R. Siverd, and B. S. Gaudi. Achieving Better Than 1 Minute Accuracy in the Heliocentric and Barycentric Julian Dates. *Publications of the Astronomical Society of the Pacific*, 122:935–946, August 2010. doi: 10.1086/655938.

J. Eastman, B. S. Gaudi, and E. Agol. EXOFAST: A Fast Exoplanetary Fitting Suite in

IDL. *Publications of the Astronomical Society of the Pacific*, 125:83–112, January 2013. doi: 10.1086/669497.

J. D. Eastman, T. G. Beatty, R. J. Siverd, J. M. O. Antognini, M. T. Penny, E. J. Gonzales, J. R. Crepp, A. W. Howard, R. L. Avril, A. Bieryla, K. Collins, B. J. Fulton, J. Ge, J. Gregorio, B. Ma, S. N. Mellon, T. E. Oberst, J. Wang, B. S. Gaudi, J. Pepper, K. G. Stassun, L. A. Buchhave, E. L. N. Jensen, D. W. Latham, P. Berlind, M. L. Calkins, P. A. Cargile, K. D. Colon, S. Dhital, G. A. Esquerdo, J. A. Johnson, J. F. Kielkopf, M. Manner, Q. Mao, K. K. McLeod, K. Penev, R. P. Stefanik, R. Street, R. Zambelli, D. L. DePoy, A. Gould, J. L. Marshall, R. W. Pogge, M. Trueblood, and P. Trueblood. KELT-4Ab: An inflated Hot Jupiter transiting the bright (V˜10) component of a hierarchical triple. *ArXiv e-prints*, September 2015.

N. L. Eaton and W. Herbst. An Ultraviolet and Optical Study of Accreting Pre-Main-Sequence Stars: Uxors. *The Astronomical Journal*, 110:2369, November 1995. doi: 10.1086/117695.

J. A. Eisner, L. A. Hillenbrand, R. J. White, J. S. Bloom, R. L. Akeson, and C. H. Blake. Near-Infrared Interferometric, Spectroscopic, and Photometric Monitoring of T Tauri Inner Disks. *The Astrophysical Journal*, 669:1072–1084, November 2007. doi: 10.1086/521874.

J. H. Elias. A study of the Taurus dark cloud complex. *The Astrophysical Journal*, 224: 857–872, September 1978. doi: 10.1086/156436.

C. Espaillat, P. D'Alessio, J. Hernández, E. Nagel, K. L. Luhman, D. M. Watson, N. Calvet, J. Muzerolle, and M. McClure. Unveiling the Structure of Pre-transitional Disks. *The Astrophysical Journal*, 717:441–457, July 2010. doi: 10.1088/0004-637X/717/1/441.

S. Fromang. The effect of MHD turbulence on massive protoplanetary disk fragmenta-

tion. *Astronomy and Astrophysics*, 441:1–8, October 2005. doi: 10.1051/0004-6361:20053080.

B. J. Fulton, K. A. Collins, B. S. Gaudi, K. G. Stassun, J. Pepper, T. G. Beatty, R. J. Siverd, K. Penev, A. W. Howard, C. Baranec, G. Corfini, J. D. Eastman, J. Gregorio, N. M. Law, M. B. Lund, T. E. Oberst, M. T. Penny, R. Riddle, J. E. Rodriguez, D. J. Stevens, R. Zambelli, C. Ziegler, A. Bieryla, G. D'Ago, D. L. DePoy, E. L. N. Jensen, J. F. Kielkopf, D. W. Latham, M. Manner, J. Marshall, K. K. McLeod, and P. A. Reed. KELT-8b: A Highly Inflated Transiting Hot Jupiter and a New Technique for Extracting High-precision Radial Velocities from Noisy Spectra. *The Astrophysical Journal*, 810:30, September 2015. doi: 10.1088/0004-637X/810/1/30.

G. F. Gahm, P. P. Petrov, R. Duemmler, J. F. Gameiro, and M. T. V. T. Lago. RW Aur A, a close binary? *Astronomy and Astrophysics*, 352:L95–L98, December 1999.

A. M. Ghez, G. Neugebauer, and K. Matthews. The multiplicity of T Tauri stars in the star forming regions Taurus-Auriga and Ophiuchus-Scorpius: A 2.2 micron speckle imaging survey. *The Astronomical Journal*, 106:2005–2023, November 1993. doi: 10.1086/116782.

A. M. Ghez, D. W. McCarthy, J. L. Patience, and T. L. Beck. The Multiplicity of Pre-Main-Sequence Stars in Southern Star-forming Regions. *The Astrophysical Journal*, 481:378–385, May 1997a.

A. M. Ghez, R. J. White, and M. Simon. High Spatial Resolution Imaging of Pre-Main-Sequence Binary Stars: Resolving the Relationship between Disks and Close Companions. *The Astrophysical Journal*, 490:353–367, November 1997b.

A. I. Gómez de Castro, J. López-Santiago, A. Talavera, A. Y. Sytov, and D. Bisikalo. XMM-Newton Monitoring of the Close Pre-main-sequence Binary AK Sco. Evidence

of Tide-driven Filling of the Inner Gap in the Circumbinary Disk. *The Astrophysical Journal*, 766:62, March 2013. doi: 10.1088/0004-637X/766/1/62.

N. A. Gorynja. New variable star in Taurus SVS 1578. *Astronomicheskij Tsirkulyar*, 474: 7–7, 1968.

C. A. Grady, M. L. Sitko, R. W. Russell, D. K. Lynch, M. S. Hanner, M. R. Perez, K. S. Bjorkman, and D. de Winter. Infalling Planetesimals in Pre-Main Stellar Systems. *Protostars and Planets IV*, page 613, May 2000.

K. N. Grankin, S. Y. Melnikov, J. Bouvier, W. Herbst, and V. S. Shevchenko. Results of the ROTOR-program. I. The long-term photometric variability of classical T Tauri stars. *Astronomy and Astrophysics*, 461:183–195, January 2007. doi: 10.1051/0004-6361:20065489.

J. Grindlay, S. Tang, E. Los, and M. Servillat. Opening the 100-Year Window for Time-Domain Astronomy. In E. Griffin, R. Hanisch, and R. Seaman, editors, *IAU Symposium*, volume 285 of *IAU Symposium*, pages 29–34, April 2012. doi: 10.1017/S1743921312000166.

V. Grinin, H. C. Stempels, G. F. Gahm, S. Sergeev, A. Arkharov, O. Barsunova, and L. Tambovtseva. The unusual pre-main-sequence star V718 Persei (HMW 15). Photometry and spectroscopy across the eclipse. *Astronomy and Astrophysics*, 489:1233–1238, October 2008. doi: 10.1051/0004-6361:200810349.

V. P. Grinin. On the Blue Emission Visible during Deep Minima of Young Irregular Variables. *Soviet Astronomy Letters*, 14:27, February 1988.

V. P. Grinin and A. N. Rostopchina. Orientation of circumstellar disks and the statistics of H_{alpha} profiles of Ae/Be Herbig stars. *Astronomy Reports*, 40:171–178, March 1996.

V. P. Grinin, N. N. Kiselev, G. P. Chernova, N. K. Minikulov, and N. V. Voshchinnikov. The investigations of 'zodiacal light' of isolated AE-Herbig stars with nonperiodic algol-type minima. *Astrophysics and Space Science*, 186:283–298, December 1991. doi: 10.1007/BF02111202.

V. P. Grinin, A. N. Rostopchina, and D. N. Shakhovskoi. On the nature of cyclic light variations in UX Ori stars. *Astronomy Letters*, 24:802–807, November 1998.

V. P. Grinin, L. V. Tambovtseva, and N. Y. Sotnikova. Disk Wind in Young Binaries and the Origin of the Cyclic Activity of Young Stars. *Astronomy Letters*, 30:694–706, October 2004. doi: 10.1134/1.1808056.

K. E. Haisch, Jr., E. A. Lada, and C. J. Lada. Disk Frequencies and Lifetimes in Young Clusters. *The Astrophysical Journal Letters*, 553:L153–L156, June 2001. doi: 10.1086/320685.

P. Hartigan, S. Edwards, and L. Ghandour. Disk Accretion and Mass Loss from Young Stars. *The Astrophysical Journal*, 452:736, October 1995. doi: 10.1086/176344.

J. Hartman. VARTOOLS: Light Curve Analysis Program. Astrophysics Source Code Library, August 2012.

A. A. Henden, S. Levine, D. Terrell, and D. L. Welch. APASS - The Latest Data Release. In *American Astronomical Society Meeting Abstracts*, volume 225 of *American Astronomical Society Meeting Abstracts*, page 336.16, January 2015.

G. H. Herbig and K. R. Bell. *Third Catalog of Emission-Line Stars of the Orion Population : 3 : 1988*. 1988.

W. Herbst and V. S. Shevchenko. A Photometric Catalog of Herbig AE/BE Stars and Discussion of the Nature and Cause of the Variations of UX Orionis Stars. *The Astronomical Journal*, 118:1043–1060, August 1999. doi: 10.1086/300966.

W. Herbst, J. A. Holtzman, and B. E. Phelps. Optical monitoring of Orion population stars. I - Results for some T Tauri and Herbig Ae/Be stars. *The Astronomical Journal*, 87: 1710–1729, December 1982. doi: 10.1086/113262.

W. Herbst, D. K. Herbst, E. J. Grossman, and D. Weinstein. Catalogue of UBVRI photometry of T Tauri stars and analysis of the causes of their variability. *The Astronomical Journal*, 108:1906–1923, November 1994. doi: 10.1086/117204.

D. W. Hoard, S. B. Howell, and R. E. Stencel. Taming the Invisible Monster: System Parameter Constraints for epsilon Aurigae from the Far-ultraviolet to the Mid-infrared. *The Astrophysical Journal*, 714:549–560, May 2010. doi: 10.1088/0004-637X/714/1/549.

E. Hog, A. Kuzmin, U. Bastian, C. Fabricius, K. Kuimov, L. Lindegren, V. V. Makarov, and S. Roeser. The TYCHO Reference Catalogue. *Astronomy and Astrophysics*, 335: L65–L68, July 1998.

E. Høg, C. Fabricius, V. V. Makarov, S. Urban, T. Corbin, G. Wycoff, U. Bastian, P. Schwekendiek, and A. Wicenec. The Tycho-2 catalogue of the 2.5 million brightest stars. *Astronomy and Astrophysics*, 355:L27–L30, March 2000.

A. Horton, C. G. Tinney, S. Case, T. Farrell, L. Gers, D. Jones, J. Lawrence, S. Miziarski, N. Staszak, D. Orr, M. Vuong, L. Waller, and R. Zhelem. CYCLOPS2: the fibre image slicer upgrade for the UCLES high resolution spectrograph. In *Society of Photo-Optical Instrumentation Engineers (SPIE) Conference Series*, volume 8446 of *Society of Photo-Optical Instrumentation Engineers (SPIE) Conference Series*, page 3, September 2012. doi: 10.1117/12.924945.

I. Hubeny and T. Lanz. Synspec: General Spectrum Synthesis Program. Astrophysics Source Code Library, September 2011.

B. Jackson, R. Greenberg, and R. Barnes. Tidal Evolution of Close-in Extrasolar Planets. *The Astrophysical Journal*, 678:1396–1406, May 2008. doi: 10.1086/529187.

E. Jensen. Tapir: A web interface for transit/eclipse observability. Astrophysics Source Code Library, June 2013.

K. E. Kearns and W. Herbst. Additional Periodic Variables in NGC 2264. *The Astronomical Journal*, 116:261–265, July 1998. doi: 10.1086/300426.

S. J. Kenyon, D. Dobrzycka, and L. Hartmann. A new optical extinction law and distance estimate for the Taurus-Auriga molecular cloud. *The Astronomical Journal*, 108:1872–1880, November 1994. doi: 10.1086/117200.

S. O. Kepler, S. J. Kleinman, A. Nitta, D. Koester, B. G. Castanheira, O. Giovannini, A. F. M. Costa, and L. Althaus. White dwarf mass distribution in the SDSS. *Monthly Notices of the Royal Astronomical Society*, 375:1315–1324, March 2007. doi: 10.1111/j.1365-2966.2006.11388.x.

M. Kilic, C. Allende Prieto, W. R. Brown, and D. Koester. The Lowest Mass White Dwarf. *The Astrophysical Journal*, 660:1451–1461, May 2007. doi: 10.1086/514327.

Y. Kitamura, M. Momose, S. Yokogawa, R. Kawabe, M. Tamura, and S. Ida. Investigation of the Physical Properties of Protoplanetary Disks around T Tauri Stars by a 1 Arcsecond Imaging Survey: Evolution and Diversity of the Disks in Their Accretion Stage. *The Astrophysical Journal*, 581:357–380, December 2002. doi: 10.1086/344223.

B. Kloppenborg, R. Stencel, J. D. Monnier, G. Schaefer, M. Zhao, F. Baron, H. McAlister, T. ten Brummelaar, X. Che, C. Farrington, E. Pedretti, P. J. Sallave-Goldfinger, J. Sturmann, L. Sturmann, N. Thureau, N. Turner, and S. M. Carroll. Infrared images of the transiting disk in the ϵ Aurigae system. *Nature*, 464:870–872, April 2010. doi: 10.1038/nature08968.

B. K. Kloppenborg, R. E. Stencel, J. D. Monnier, G. H. Schaefer, F. Baron, C. Tycner, R. T. Zavala, D. Hutter, M. Zhao, X. Che, T. A. ten Brummelaar, C. D. Farrington, R. Parks, H. A. McAlister, J. Sturmann, L. Sturmann, P. J. Sallave-Goldfinger, N. Turner, E. Pedretti, and N. Thureau. Interferometry of ϵ Aurigae: Characterization of the Asymmetric Eclipsing Disk. *The Astrophysical Journal Supplement*, 220:14, September 2015. doi: 10.1088/0067-0049/220/1/14.

G. Kovács, S. Zucker, and T. Mazeh. A box-fitting algorithm in the search for periodic transits. *Astronomy and Astrophysics*, 391:369–377, August 2002. doi: 10.1051/0004-6361:20020802.

R. B. Kuhn, J. E. Rodriguez, K. A. Collins, M. B. Lund, R. J. Siverd, K. D. Colón, J. Pepper, K. G. Stassun, P. A. Cargile, D. J. James, K. Penev, G. Zhou, D. Bayliss, T. G. Tan, I. A. Curtis, S. Udry, D. Segransan, D. Mawet, J. Soutter, R. Hart, B. Carter, B. S. Gaudi, G. Myers, T. G. Beatty, J. D. Eastman, D. E. Reichart, J. B. Haislip, J. Kielkopf, A. Bieryla, D. W. Latham, E. L. N. Jensen, T. E. Oberst, and D. J. Stevens. KELT-10b: The First Transiting Exoplanet from the KELT-South Survey – A Hot Sub-Jupiter Transiting a V = 10.7 Early G-Star. *ArXiv e-prints*, September 2015.

C. Leinert, H. Zinnecker, N. Weitzel, J. Christou, S. T. Ridgway, R. Jameson, M. Haas, and R. Lenzen. A systematic approach for young binaries in Taurus. *Astronomy and Astrophysics*, 278:129–149, October 1993.

V. Lipunov, V. Kornilov, E. Gorbovskoy, N. Shatskij, D. Kuvshinov, N. Tyurina, A. Belinski, A. Krylov, P. Balanutsa, V. Chazov, A. Kuznetsov, P. Kortunov, A. Sankovich, A. Tlatov, A. Parkhomenko, V. Krushinsky, I. Zalozhnyh, A. Popov, T. Kopytova, K. Ivanov, S. Yazev, and V. Yurkov. Master Robotic Net. *Advances in Astronomy*, 2010:349171, 2010. doi: 10.1155/2010/349171.

C.-F. Liu and H. Shang. RW Aur A from the X-Wind Point of View: General Features. *The Astrophysical Journal*, 761:94, December 2012. doi: 10.1088/0004-637X/761/2/94.

N. R. Lomb. Least-squares frequency analysis of unequally spaced data. *Astrophysics and Space Science*, 39:447–462, February 1976. doi: 10.1007/BF00648343.

L. López-Martín, S. Cabrit, and C. Dougados. Proper motions and velocity asymmetries in the RW Aur jet. *Astronomy and Astrophysics*, 405:L1–L4, July 2003. doi: 10.1051/0004-6361:20030758.

K. L. Luhman, E. E. Mamajek, P. R. Allen, and K. L. Cruz. An Infrared/X-Ray Survey for New Members of the Taurus Star-Forming Region. *The Astrophysical Journal*, 703:399–419, September 2009. doi: 10.1088/0004-637X/703/1/399.

E. E. Mamajek, A. C. Quillen, M. J. Pecaut, F. Moolekamp, E. L. Scott, M. A. Kenworthy, A. Collier Cameron, and N. R. Parley. Planetary Construction Zones in Occultation: Discovery of an Extrasolar Ring System Transiting a Young Sun-like Star and Future Prospects for Detecting Eclipses by Circumsecondary and Circumplanetary Disks. *The Astronomical Journal*, 143:72, March 2012. doi: 10.1088/0004-6256/143/3/72.

D. C. Martin, J. Fanson, D. Schiminovich, P. Morrissey, P. G. Friedman, T. A. Barlow, T. Conrow, R. Grange, P. N. Jelinsky, B. Milliard, O. H. W. Siegmund, L. Bianchi, Y.-I. Byun, J. Donas, K. Forster, T. M. Heckman, Y.-W. Lee, B. F. Madore, R. F. Malina, S. G. Neff, R. M. Rich, T. Small, F. Surber, A. S. Szalay, B. Welsh, and T. K. Wyder. The Galaxy Evolution Explorer: A Space Ultraviolet Survey Mission. *The Astrophysical Journal Letters*, 619:L1–L6, January 2005. doi: 10.1086/426387.

F. S. Masset and J. C. B. Papaloizou. Runaway Migration and the Formation of Hot Jupiters. *The Astrophysical Journal*, 588:494–508, May 2003. doi: 10.1086/373892.

P. F. L. Maxted, A. M. Serenelli, T. R. Marsh, S. Catalán, D. P. Mahtani, and V. S. Dhillon. WASP 1628+10 - an EL CVn-type binary with a very low mass stripped red giant star

and multiperiodic pulsations. *Monthly Notices of the Royal Astronomical Society*, 444: 208–216, October 2014. doi: 10.1093/mnras/stu1465.

P. R. McCullough, J. E. Stys, J. A. Valenti, C. M. Johns-Krull, K. A. Janes, J. N. Heasley, B. A. Bye, C. Dodd, S. W. Fleming, A. Pinnick, R. Bissinger, B. L. Gary, P. J. Howell, and T. Vanmunster. A Transiting Planet of a Sun-like Star. *The Astrophysical Journal*, 648:1228–1238, September 2006. doi: 10.1086/505651.

F. Ménard and P. Bastien. A polarization outburst in the T Tauri star UY Aurigae. In I. Appenzeller and C. Jordan, editors, *Circumstellar Matter*, volume 122 of *IAU Symposium*, pages 133–134, 1987.

D. Mouillet, J. D. Larwood, J. C. B. Papaloizou, and A. M. Lagrange. A planet on an inclined orbit as an explanation of the warp in the Beta Pictoris disc. *Monthly Notices of the Royal Astronomical Society*, 292:896, December 1997. doi: 10.1093/mnras/292.4.896.

R. Mundt and J. Eislöffel. T Tauri Stars Associated with Herbig-Haro Objects and Jets. *The Astronomical Journal*, 116:860–867, August 1998. doi: 10.1086/300461.

A. Natta and B. A. Whitney. Models of scattered light in UXORs. *Astronomy and Astrophysics*, 364:633–640, December 2000.

A. F. Nelson, W. Benz, and T. V. Ruzmaikina. Dynamics of Circumstellar Disks. II. Heating and Cooling. *The Astrophysical Journal*, 529:357–390, January 2000. doi: 10.1086/308238.

R. D. Oudmaijer, J. Palacios, C. Eiroa, J. K. Davies, D. de Winter, R. Ferlet, F. Garzón, C. A. Grady, A. Collier Cameron, H. J. Deeg, A. W. Harris, K. Horne, B. Merín, L. F. Miranda, B. Montesinos, A. Mora, A. Penny, A. Quirrenbach, H. Rauer, J. Schneider, E. Solano, Y. Tsapras, and P. R. Wesselius. EXPORT: Optical photometry and polarime-

try of Vega-type and pre-main sequence stars. *Astronomy and Astrophysics*, 379:564–578, November 2001. doi: 10.1051/0004-6361:20011331.

F. Palla and S. W. Stahler. Star Formation in Space and Time: Taurus-Auriga. *The Astrophysical Journal*, 581:1194–1203, December 2002. doi: 10.1086/344293.

K. Penev, M. Zhang, and B. Jackson. POET: A Model for Planetary Orbital Evolution Due to Tides on Evolving Stars. *Publications of the Astronomical Society of the Pacific*, 126: 553–564, June 2014. doi: 10.1086/677042.

F. Pepe, M. Mayor, F. Galland, D. Naef, D. Queloz, N. C. Santos, S. Udry, and M. Burnet. The CORALIE survey for southern extra-solar planets VII. Two short-period Saturnian companions to ¡ASTROBJ¿HD 108147¡/ASTROBJ¿ and ¡ASTROBJ¿HD 168746¡/ASTROBJ¿. *Astronomy and Astrophysics*, 388:632–638, June 2002. doi: 10.1051/0004-6361:20020433.

J. Pepper, R. W. Pogge, D. L. DePoy, J. L. Marshall, K. Z. Stanek, A. M. Stutz, S. Poindexter, R. Siverd, T. P. O'Brien, M. Trueblood, and P. Trueblood. The Kilodegree Extremely Little Telescope (KELT): A Small Robotic Telescope for Large-Area Synoptic Surveys. *Publications of the Astronomical Society of the Pacific*, 119:923–935, August 2007. doi: 10.1086/521836.

J. Pepper, R. B. Kuhn, R. Siverd, D. James, and K. Stassun. The KELT-South Telescope. *Publications of the Astronomical Society of the Pacific*, 124:230–241, March 2012. doi: 10.1086/665044.

J. Pepper, R. J. Siverd, T. G. Beatty, B. S. Gaudi, K. G. Stassun, J. Eastman, K. Collins, D. W. Latham, A. Bieryla, L. A. Buchhave, E. L. N. Jensen, M. Manner, K. Penev, J. R. Crepp, P. A. Cargile, S. Dhital, M. L. Calkins, G. A. Esquerdo, P. Berlind, B. J. Fulton, R. Street, B. Ma, J. Ge, J. Wang, Q. Mao, A. J. W. Richert, A. Gould, D. L. DePoy, J. F. Kielkopf, J. L. Marshall, R. W. Pogge, R. P. Stefanik, M. Trueblood, and P. Trueblood.

KELT-3b: A Hot Jupiter Transiting a V = 9.8 Late-F Star. *The Astrophysical Journal*, 773:64, August 2013. doi: 10.1088/0004-637X/773/1/64.

P. P. Petrov and B. S. Kozack. The origin of the photometric and spectral variability of RW Aur. *Astronomy Reports*, 51:500–511, June 2007. doi: 10.1134/S1063772907060091.

P. P. Petrov, J. Pelt, and I. Tuominen. Periodic variations in the colours of the classical T Tauri star RW Aur A. *Astronomy and Astrophysics*, 375:977–981, September 2001. doi: 10.1051/0004-6361:20010883.

P. P. Petrov, G. F. Gahm, A. A. Djupvik, E. V. Babina, S. A. Artemenko, and K. N. Grankin. Another deep dimming of the classical T Tauri star RW Aurigae A. *Astronomy and Astrophysics*, 577:A73, May 2015. doi: 10.1051/0004-6361/201525845.

A. Pickles and É. Depagne. All-Sky Spectrally Matched UBVRI-ZY and u'g'r'i'z' Magnitudes for Stars in the Tycho2 Catalog. *Publications of the Astronomical Society of the Pacific*, 122:1437–1464, December 2010. doi: 10.1086/657947.

P. Plavchan, A. H. Gee, K. Stapelfeldt, and A. Becker. The Peculiar Periodic YSO WL 4 in ρ Ophiuchus. *Astrophysical Journal Letters*, 684:L37–L40, September 2008. doi: 10.1086/592107.

G. Pojmanski. The All Sky Automated Survey. *Acta Astronomica*, 47:467–481, October 1997.

G. Pojmanski. The All Sky Automated Survey. Catalog of Variable Stars. I. 0 h - 6 hQuarter of the Southern Hemisphere. *Acta Astronomica*, 52:397–427, December 2002.

D. L. Pollacco, I. Skillen, A. Collier Cameron, D. J. Christian, C. Hellier, J. Irwin, T. A. Lister, R. A. Street, R. G. West, D. R. Anderson, W. I. Clarkson, H. Deeg, B. Enoch, A. Evans, A. Fitzsimmons, C. A. Haswell, S. Hodgkin, K. Horne, S. R. Kane, F. P.

Keenan, P. F. L. Maxted, A. J. Norton, J. Osborne, N. R. Parley, R. S. I. Ryans, B. Smalley, P. J. Wheatley, and D. M. Wilson. The WASP Project and the SuperWASP Cameras. *Publications of the Astronomical Society of the Pacific*, 118:1407–1418, October 2006. doi: 10.1086/508556.

W. H. Press and G. B. Rybicki. Fast algorithm for spectral analysis of unevenly sampled data. *The Astrophysical Journal*, 338:277–280, March 1989. doi: 10.1086/167197.

D. Queloz, M. Mayor, S. Udry, M. Burnet, F. Carrier, A. Eggenberger, D. Naef, N. Santos, F. Pepe, G. Rupprecht, G. Avila, F. Baeza, W. Benz, J.-L. Bertaux, F. Bouchy, C. Cavadore, B. Delabre, W. Eckert, J. Fischer, M. Fleury, A. Gilliotte, D. Goyak, J. C. Guzman, D. Kohler, D. Lacroix, J.-L. Lizon, D. Megevand, J.-P. Sivan, D. Sosnowska, and U. Weilenmann. From CORALIE to HARPS. The way towards 1 m s^{-1} precision Doppler measurements. *The Messenger*, 105:1–7, September 2001.

N. J. Rattenbury, Ł. Wyrzykowski, Z. Kostrzewa-Rutkowska, A. Udalski, S. Kozłowski, M. K. Szymański, G. Pietrzyński, I. Soszyński, R. Poleski, K. Ulaczyk, J. Skowron, P. Pietrukowicz, P. Mróz, and D. Skowron. OGLE-BLG182.1.162852: An Eclipsing Binary with a Circumstellar Disk. *ArXiv e-prints*, October 2014.

T. S. Rice, B. Reipurth, S. J. Wolk, L. P. Vaz, and N. J. G. Cross. Near-Infrared Variability in the Orion Nebula Cluster. *ArXiv e-prints*, May 2015.

A. Richichi, C. Leinert, R. Jameson, and H. Zinnecker. New binary young stars in the Taurus and Ophiuchus star-forming regions. *Astronomy and Astrophysics*, 287:145–153, July 1994.

T. P. Robitaille, B. A. Whitney, R. Indebetouw, K. Wood, and P. Denzmore. Interpreting Spectral Energy Distributions from Young Stellar Objects. I. A Grid of 200,000 YSO Model SEDs. *The Astrophysical Journal Supplement*, 167:256–285, December 2006a. doi: 10.1086/508424.

T. P. Robitaille, B. A. Whitney, R. Indebetouw, K. Wood, and P. Denzmore. Interpreting Spectral Energy Distributions from Young Stellar Objects. I. A Grid of 200,000 YSO Model SEDs. *The Astrophysical Journal Supplement*, 167:256–285, December 2006b. doi: 10.1086/508424.

T. P. Robitaille, B. A. Whitney, R. Indebetouw, and K. Wood. Interpreting Spectral Energy Distributions from Young Stellar Objects. II. Fitting Observed SEDs Using a Large Grid of Precomputed Models. *The Astrophysical Journal Supplement*, 169:328–352, April 2007. doi: 10.1086/512039.

J. E. Rodriguez, J. Pepper, K. G. Stassun, R. J. Siverd, P. Cargile, T. G. Beatty, and B. S. Gaudi. Occultation of the T Tauri Star RW Aurigae A by its Tidally Disrupted Disk. *AJ*, 146:112, November 2013. doi: 10.1088/0004-6256/146/5/112.

J. E. Rodriguez, J. Pepper, and K. G. Stassun. First Results from the Disk Eclipse Search with KELT (DESK) Survey. *ArXiv e-prints*, September 2015a.

J. E. Rodriguez, J. Pepper, K. G. Stassun, R. J. Siverd, P. Cargile, D. A. Weintraub, T. G. Beatty, B. S. Gaudi, E. E. Mamajek, and N. N. Sanchez. V409 Tau as Another AA Tau: Photometric Observations of Stellar Occultations by the Circumstellar Disk. *The Astronomical Journal*, 150:32, July 2015b. doi: 10.1088/0004-6256/150/1/32.

J. E. Rodriguez, P. A. Reed, R. J. Siverd, J. Pepper, K. G. Stassun, B. S. Gaudi, D. A. Weintraub, T. G. Beatty, M. B. Lund, and D. J. Stevens. Recurring Occultations of RW Aurigae by Coagulated Dust in the Tidally Disrupted Circumstellar Disk. *ArXiv e-prints*, December 2015c.

J. E. Rodriguez, K. G. Stassun, M. B. Lund, R. J. Siverd, J. Pepper, S. Tang, S. Kafka, S. Gaudi, K. E. Conroy, T. G. Beatty, D. J. Stevens, B. J. Shappee, and C. S. Kochanek. An Extreme Analogue of ϵ Aurigae: An M-giant Eclipsed Every 69 Years by a Large Opaque Disk Surrounding a Small Hot Source. *ArXiv e-prints*, January 2016.

G. Romano. Observations of T Tauri stars and related objects in Taurus dark cloud. *Memorie della Societ Astronomica Italiana*, 46:81–95, February 1975.

A. N. Rostopchina, V. P. Grinin, and D. N. Shakhovskoi. Cyclic variability of UX Ori Stars: UX Ori, SV Cep, and RZ Psc. *Astronomy Letters*, 25:243–249, April 1999.

R. J. Sault, P. J. Teuben, and M. C. H. Wright. A Retrospective View of MIRIAD. In R. A. Shaw, H. E. Payne, and J. J. E. Hayes, editors, *Astronomical Data Analysis Software and Systems IV*, volume 77 of *Astronomical Society of the Pacific Conference Series*, page 433, 1995.

J. D. Scargle. Studies in astronomical time series analysis. II - Statistical aspects of spectral analysis of unevenly spaced data. *The Astrophysical Journal*, 263:835–853, December 1982. doi: 10.1086/160554.

D. J. Schlegel, D. P. Finkbeiner, and M. Davis. Maps of Dust Infrared Emission for Use in Estimation of Reddening and Cosmic Microwave Background Radiation Foregrounds. *The Astrophysical Journal*, 500:525–553, June 1998. doi: 10.1086/305772.

P. C. Schneider, H. M. Günther, J. Robrade, S. Facchini, K. W. Hodapp, C. F. Manara, V. Perdelwitz, J. H. M. M. Schmitt, S. Skinner, and S. J. Wolk. The nature of the 2014-2015 dim state of RW Aurigae revealed by X-ray, optical, and near-IR observations. *Astronomy and Astrophysics*, 584:L9, December 2015. doi: 10.1051/0004-6361/201527237.

B. J. Shappee, J. L. Prieto, D. Grupe, C. S. Kochanek, K. Z. Stanek, G. De Rosa, S. Mathur, Y. Zu, B. M. Peterson, R. W. Pogge, S. Komossa, M. Im, J. Jencson, T. W.-S. Holoien, U. Basu, J. F. Beacom, D. M. Szczygieł, J. Brimacombe, S. Adams, A. Campillay, C. Choi, C. Contreras, M. Dietrich, M. Dubberley, M. Elphick, S. Foale, M. Giustini, C. Gonzalez, E. Hawkins, D. A. Howell, E. Y. Hsiao, M. Koss, K. M. Leighly,

N. Morrell, D. Mudd, D. Mullins, J. M. Nugent, J. Parrent, M. M. Phillips, G. Pojmanski, W. Rosing, R. Ross, D. Sand, D. M. Terndrup, S. Valenti, Z. Walker, and Y. Yoon. The Man behind the Curtain: X-Rays Drive the UV through NIR Variability in the 2013 Active Galactic Nucleus Outburst in NGC 2617. *The Astrophysical Journal*, 788:48, June 2014. doi: 10.1088/0004-637X/788/1/48.

L. Siess, E. Dufour, and M. Forestini. An internet server for pre-main sequence tracks of low- and intermediate-mass stars. *Astronomy and Astrophysics*, 358:593–599, June 2000.

M. Simon, A. M. Ghez, C. Leinert, L. Cassar, W. P. Chen, R. R. Howell, R. F. Jameson, K. Matthews, G. Neugebauer, and A. Richichi. A lunar occultation and direct imaging survey of multiplicity in the Ophiuchus and Taurus star-forming regions. *The Astrophysical Journal*, 443:625–637, April 1995. doi: 10.1086/175554.

R. J. Siverd, T. G. Beatty, J. Pepper, J. D. Eastman, K. Collins, A. Bieryla, D. W. Latham, L. A. Buchhave, E. L. N. Jensen, J. R. Crepp, R. Street, K. G. Stassun, B. S. Gaudi, P. Berlind, M. L. Calkins, D. L. DePoy, G. A. Esquerdo, B. J. Fulton, G. Fűrész, J. C. Geary, A. Gould, L. Hebb, J. F. Kielkopf, J. L. Marshall, R. Pogge, K. Z. Stanek, R. P. Stefanik, A. H. Szentgyorgyi, M. Trueblood, P. Trueblood, A. M. Stutz, and J. L. van Saders. KELT-1b: A Strongly Irradiated, Highly Inflated, Short Period, 27 Jupiter-mass Companion Transiting a Mid-F Star. *The Astrophysical Journal*, 761:123, December 2012. doi: 10.1088/0004-637X/761/2/123.

M. F. Skrutskie, R. M. Cutri, R. Stiening, M. D. Weinberg, S. Schneider, J. M. Carpenter, C. Beichman, R. Capps, T. Chester, J. Elias, J. Huchra, J. Liebert, C. Lonsdale, D. G. Monet, S. Price, P. Seitzer, T. Jarrett, J. D. Kirkpatrick, J. E. Gizis, E. Howard, T. Evans, J. Fowler, L. Fullmer, R. Hurt, R. Light, E. L. Kopan, K. A. Marsh, H. L. McCallon, R. Tam, S. Van Dyk, and S. Wheelock. The Two Micron All Sky Survey (2MASS). *The Astronomical Journal*, 131:1163–1183, February 2006. doi: 10.1086/498708.

D. R. Soderblom. Rotational studies of late-type stars. II - Ages of solar-type stars and the rotational history of the sun. *The Astrophysical Journal Supplement*, 53:1–15, September 1983. doi: 10.1086/190880.

D. S. Spiegel and N. Madhusudhan. Jupiter will Become a Hot Jupiter: Consequences of Post-main-sequence Stellar Evolution on Gas Giant Planets. *The Astrophysical Journal*, 756:132, September 2012. doi: 10.1088/0004-637X/756/2/132.

E. M. Standish. Report of the IAU WGAS Sub-group on Numerical Standards. *Highlights of Astronomy*, 10:180, 1995.

A. Y. Sytov, P. V. Kaigorodov, A. M. Fateeva, and D. V. Bisikalo. Structure of the circumbinary envelopes of young binary stars with elliptical orbits. *Astronomy Reports*, 55:793–800, September 2011. doi: 10.1134/S1063772911090071.

S. Tackett, W. Herbst, and E. Williams. Periodic Variability in the Pre-Main-Sequence Object CB 34V. *The Astronomical Journal*, 126:348–352, July 2003. doi: 10.1086/375756.

H. Tanaka, T. Takeuchi, and W. R. Ward. Three-Dimensional Interaction between a Planet and an Isothermal Gaseous Disk. I. Corotation and Lindblad Torques and Planet Migration. *The Astrophysical Journal*, 565:1257–1274, February 2002. doi: 10.1086/324713.

S. Tang, J. E. Grindlay, L. Bildsten, and m. collaborators. A Mysterious Twin of Epsilon-Aurigae. In *Giants of Eclipse*, page 20302, July 2013.

G. Torres, J. Andersen, and A. Giménez. Accurate masses and radii of normal stars: modern results and applications. *Astronomy and Astrophysics Reviews*, 18:67–126, February 2010. doi: 10.1007/s00159-009-0025-1.

O. D. Turner, D. R. Anderson, A. Collier Cameron, L. Delrez, M. Gillon, C. Hellier, E. Jehin, M. Lendl, P. F. L. Maxted, F. Pepe, D. Pollacco, D. Queloz, D. Sègransan, B. Smal-

ley, A. M. S. Smith, A. H. M. J. Triaud, S. Udry, and R. G. West. WASP-120b, WASP-122b and WASP-123b: Three newly discovered planets from the WASP-South survey. *ArXiv e-prints*, September 2015.

Y. C. Unruh, J.-F. Donati, J. M. Oliveira, A. Collier Cameron, C. Catala, H. F. Henrichs, C. M. Johns-Krull, B. Foing, J. Hao, H. Cao, J. D. Landstreet, H. C. Stempels, J. A. de Jong, J. Telting, N. Walton, P. Ehrenfreund, A. P. Hatzes, J. E. Neff, T. Böhm, T. Simon, L. Kaper, K. G. Strassmeier, and T. Granzer. Multisite observations of SU Aurigae. *Monthly Notices of the Royal Astronomical Society*, 348:1301–1320, March 2004. doi: 10.1111/j.1365-2966.2004.07445.x.

J. A. Valenti and D. A. Fischer. Spectroscopic Properties of Cool Stars (SPOCS). I. 1040 F, G, and K Dwarfs from Keck, Lick, and AAT Planet Search Programs. *The Astrophysical Journal Supplement*, 159:141–166, July 2005. doi: 10.1086/430500.

J. A. Valenti and N. Piskunov. Spectroscopy made easy: A new tool for fitting observations with synthetic spectra. *Astronomy and Astrophysics Supplement*, 118:595–603, September 1996.

J. Vernet, H. Dekker, S. D'Odorico, L. Kaper, P. Kjaergaard, F. Hammer, S. Randich, F. Zerbi, P. J. Groot, J. Hjorth, I. Guinouard, R. Navarro, T. Adolfse, P. W. Albers, J.-P. Amans, J. J. Andersen, M. I. Andersen, P. Binetruy, P. Bristow, R. Castillo, F. Chemla, L. Christensen, P. Conconi, R. Conzelmann, J. Dam, V. de Caprio, A. de Ugarte Postigo, B. Delabre, P. di Marcantonio, M. Downing, E. Elswijk, G. Finger, G. Fischer, H. Flores, P. François, P. Goldoni, L. Guglielmi, R. Haigron, H. Hanenburg, I. Hendriks, M. Horrobin, D. Horville, N. C. Jessen, F. Kerber, L. Kern, M. Kiekebusch, P. Kleszcz, J. Klougart, J. Kragt, H. H. Larsen, J.-L. Lizon, C. Lucuix, V. Mainieri, R. Manuputy, C. Martayan, E. Mason, R. Mazzoleni, N. Michaelsen, A. Modigliani, S. Moehler, P. Møller, A. Norup Sørensen, P. Nørregaard, C. Péroux, F. Patat, E. Pena, J. Pragt, C. Reinero, F. Rigal, M. Riva, R. Roelfsema, F. Royer, G. Sacco, P. Santin, T. Schoen-

maker, P. Spano, E. Sweers, R. Ter Horst, M. Tintori, N. Tromp, P. van Dael, H. van der Vliet, L. Venema, M. Vidali, J. Vinther, P. Vola, R. Winters, D. Wistisen, G. Wulterkens, and A. Zacchei. X-shooter, the new wide band intermediate resolution spectrograph at the ESO Very Large Telescope. *Astronomy & Astrophysics*, 536:A105, December 2011. doi: 10.1051/0004-6361/201117752.

N. V. Voshchinnikov. Dust around young stars. Model of Algol-type minima of UX Orionis stars. *Astrophysics*, 30:313–321, May 1989. doi: 10.1007/BF01003892.

F. J. Vrba, P. F. Chugainov, W. B. Weaver, and J. S. Stauffer. Photometric and spectroscopic monitoring of AA Tau, DN Tau, UX Tau A, T Tau, RY Tau, LK CA 4, and LK CA 7. *The Astronomical Journal*, 106:1608–1626, October 1993. doi: 10.1086/116751.

K. J. Walsh, A. Morbidelli, S. N. Raymond, D. P. O'Brien, and A. M. Mandell. A low mass for Mars from Jupiter's early gas-driven migration. *Nature*, 475:206–209, July 2011. doi: 10.1038/nature10201.

F. M. Walter. X-ray sources in regions of star formation. I - The naked T Tauri stars. *The Astrophysical Journal*, 306:573–586, July 1986. doi: 10.1086/164367.

L. B. F. M. Waters and C. Waelkens. Herbig Ae/Be Stars. *Annual Review of Astronomy and Astrophysics*, 36:233–266, 1998. doi: 10.1146/annurev.astro.36.1.233.

W. Wenzel. Photoelektrische Beobachtungen an SV Cephei. *Zentralinstitut fuer Astrophysik Sternwarte Sonneberg Mitteilungen ueber Veraenderliche Sterne*, 5:75–82, 1969.

R. J. White and A. M. Ghez. Observational Constraints on the Formation and Evolution of Binary Stars. *The Astrophysical Journal*, 556:265–295, July 2001. doi: 10.1086/321542.

R. J. White and L. A. Hillenbrand. On the Evolutionary Status of Class I Stars and Herbig-Haro Energy Sources in Taurus-Auriga. *The Astrophysical Journal*, 616:998–1032, December 2004. doi: 10.1086/425115.

B. A. Whitney, K. Wood, J. E. Bjorkman, and M. Cohen. Two-dimensional Radiative Transfer in Protostellar Envelopes. II. An Evolutionary Sequence. *The Astrophysical Journal*, 598:1079–1099, December 2003a. doi: 10.1086/379068.

B. A. Whitney, K. Wood, J. E. Bjorkman, and M. J. Wolff. Two-dimensional Radiative Transfer in Protostellar Envelopes. I. Effects of Geometry on Class I Sources. *The Astrophysical Journal*, 591:1049–1063, July 2003b. doi: 10.1086/375415.

R. Wichmann, U. Bastian, J. Krautter, I. Jankovics, and S. M. Rucinski. HIPPARCOS observations of pre-main-sequence stars. *Monthly Notices of the Royal Astronomical Society*, 301:39L–43L, December 1998.

F. Wildi, F. Pepe, B. Chazelas, G. Lo Curto, and C. Lovis. The performance of the new Fabry-Perot calibration system of the radial velocity spectrograph HARPS. In *Society of Photo-Optical Instrumentation Engineers (SPIE) Conference Series*, volume 8151 of *Society of Photo-Optical Instrumentation Engineers (SPIE) Conference Series*, page 1, October 2011. doi: 10.1117/12.901550.

J. P. Williams and S. M. Andrews. The Dust Properties of Eight Debris Disk Candidates as Determined by Submillimeter Photometry. *The Astrophysical Journal*, 653:1480–1485, December 2006. doi: 10.1086/508919.

J. N. Winn, M. J. Holman, J. A. Johnson, K. Z. Stanek, and P. M. Garnavich. KH 15D: Gradual Occultation of a Pre-Main-Sequence Binary. *Astrophysical Journal Letters*, 603:L45–L48, March 2004. doi: 10.1086/383089.

J. N. Winn, D. Fabrycky, S. Albrecht, and J. A. Johnson. Hot Stars with Hot Jupiters Have High Obliquities. *The Astrophysical Journal Letters*, 718:L145–L149, August 2010. doi: 10.1088/2041-8205/718/2/L145.

J. Woitas, C. Leinert, and R. Köhler. Mass ratios of the components in T Tauri binary

systems and implications for multiple star formation. *Astronomy and Astrophysics*, 376: 982–996, September 2001. doi: 10.1051/0004-6361:20011034.

J. Woitas, T. P. Ray, F. Bacciotti, C. J. Davis, and J. Eislöffel. Hubble Space Telescope Space Telescope Imaging Spectrograph Observations of the Bipolar Jet from RW Aurigae: Tracing Outflow Asymmetries Close to the Source. *The Astrophysical Journal*, 580:336–342, November 2002. doi: 10.1086/343124.

J. Woitas, F. Bacciotti, T. P. Ray, A. Marconi, D. Coffey, and J. Eislöffel. Jet rotation: Launching region, angular momentum balance and magnetic properties in the bipolar outflow from RW Aur. *Astronomy and Astrophysics*, 432:149–160, March 2005. doi: 10.1051/0004-6361:20034439.

E. L. Wright, P. R. M. Eisenhardt, A. K. Mainzer, M. E. Ressler, R. M. Cutri, T. Jarrett, J. D. Kirkpatrick, D. Padgett, R. S. McMillan, M. Skrutskie, S. A. Stanford, M. Cohen, R. G. Walker, J. C. Mather, D. Leisawitz, T. N. Gautier, III, I. McLean, D. Benford, C. J. Lonsdale, A. Blain, B. Mendez, W. R. Irace, V. Duval, F. Liu, D. Royer, I. Heinrichsen, J. Howard, M. Shannon, M. Kendall, A. L. Walsh, M. Larsen, J. G. Cardon, S. Schick, M. Schwalm, M. Abid, B. Fabinsky, L. Naes, and C.-W. Tsai. The Wide-field Infrared Survey Explorer (WISE): Mission Description and Initial On-orbit Performance. *The Astronomical Journal*, 140:1868, December 2010. doi: 10.1088/0004-6256/140/6/1868.

H. Y. Xiao, K. R. Covey, L. Rebull, D. Charbonneau, G. Mandushev, F. O'Donovan, C. Slesnick, and J. P. Lloyd. A Census of Rotation and Variability in L1495: A Uniform Analysis of Trans-atlantic Exoplanet Survey Light Curves for Pre-main-sequence Stars in Taurus. *The Astrophysical Journal Supplement*, 202:7, September 2012. doi: 10.1088/0067-0049/202/1/7.

N. Zacharias, D. G. Monet, S. E. Levine, S. E. Urban, R. Gaume, and G. L. Wycoff. The Naval Observatory Merged Astrometric Dataset (NOMAD). In *American Astronomical*

Society Meeting Abstracts, volume 36 of *Bulletin of the American Astronomical Society*, page 1418, December 2004.

N. Zacharias, C. T. Finch, T. M. Girard, A. Henden, J. L. Bartlett, D. G. Monet, and M. I. Zacharias. VizieR Online Data Catalog: UCAC4 Catalogue (Zacharias+, 2012). *VizieR Online Data Catalog*, 1322:0, July 2012.